UNIVERSITÀ DEGLI STUDI DI NAPOLI
FEDERICO II

Facoltà di Scienze Matematiche Fisiche e Naturali
Dipartimento di Fisica

Complesso Universitario di Monte S.Angelo
via Cintia - I-80126 Napoli Italia

Tesi di dottorato in Fisica

Dario Bercioux

Spin-dependent transport in nanostructures

Candidato

Dr. Dario Bercioux

Coordinatore del ciclo

Prof. Arturo Tagliacozzo

XVII Ciclo di dottorato

ii

Contents

List of Figures

Ad Antonio

x

Introduction

Generalities

In the recent years the field of *mesoscopic* physics has caught both theoretical and experimental physics communities attention. The main motivation is related to the fact this field has permitted to well understand quantum phenomena in the crossover region between microscopic and macroscopic physical system. Moreover, it is very interesting to note how mesoscopic physics is nowadays considered for its technological application, *quantum electronics*.

Mesoscopic systems are in the middle between the classical world and the atomic one. They are characterized by dimensions within nanometer (nm) and micrometer (μm). A mesoscopic system is much larger than just a few atoms or molecules and small enough for being distinguished from classical objects. It is necessary to introduce several length-scales that define and characterize the different regimes of transport for a mesoscopic system. Electrons in mesoscopic system are characterized by the *de Broglie wave length* λ, which goes from few Angstrom ($\text{Å} = 10^{-10}$m) in metals to the order of 50 nm in semiconductors. The *mean free path* l_e is the distance that an electron travels before its initial momentum is destroyed in elastic collisions with impurities creating a disordered potential. The third relevant one is the *phase-relaxation length* l_φ. This is the distance over which the electrons lose their initial phase, usually through inelastic scattering events.

A conductor of size L, held at sufficiently low temperature, appear to be ohmic (or classical) when its dimensions are much larger than the former λ, l_φ and l_e. On the contrary, it is considered mesoscopic when shows coherence, that is $L \leq l_\varphi$. In the former case, the conductance G is not determined by the Ohm's law but depends on the number of *channels* or *transverse modes* in the conductor. This regime is governed by the *Landauer* formula $G = (e^2/h)T$ that relates the conductance with the quantum probability of an electron to be transmitted through the conductor. The transmission T represents the sum of the probabilities over all possible channels. The quantity $e^2/h \sim (25.8 \ k\Omega)^{-1}$, represent in mesoscopic system, the quantum conductance associated with a single channel. Then it is important to take account of the disorder effects. A disordered mesoscopic conductors such that $l_e \ll L$ is called *diffusive*, in this category are present the metals. In the opposite limit $L \ll l_e$ the impurity scattering events are strongly reduced and

in this case the conductor is called *ballistic*. In this situation the geometrical shape of the system plays an important role and it is important to consider specular reflection to the boundary of the system.

In the last twenty years it has been possible to realize structures that present characteristic dimensions smaller than the mean free path l_e. This kind of structures are usually realized in GaAs/GaAlAs (gallium arsenide/ aluminium gallium arsenide) semiconductor heterostructures. In the simplest situation these consist in an abrupt interface between two semiconductors with different doping levels. At the interface a thin layer due to the accumulation of charge carriers is formed. This thin layer is known as two-dimensional electron gas (2DEG). The presence of the bulk structure of the semiconductors forming the heterostructure considered by means of the effective mass. These heterostructures at sufficiently low temperature, present mobilities of 10^6cm^2/Vs that corresponds to a mean free path of 10 μm and a phase-relaxation length even longer. In this limit it clear that the transport is governed by the Landauer formula instead than the Boltzman equation. Furthermore for typically large electron densities and low temperature the single-particle picture applies.

Until recently, the spin degree of freedom of the electron was been ignored in mainstream charge-based electronics decides. A new technology, called *spintronics*, is developing. Here it is not the electron charge but the electron spin that carries information, and this offers opportunities for a new generation of devices combining standard microelectronics with spin-dependent effects that arise from the interaction between spin of the carrier and the magnetic properties of the materials. Traditional approaches to using spin are base on the alignment of a spin relative to a reference, for example an external magnetic field. Than the device operations proceed with some quantity that depends in a predictable way on the degree of alignment. Adding the spin degree of freedom to conventional semiconductor charge-based electronics or using the spin degree of freedom alone will add substantially more capability and performance to electronics products.

Therefore it is important to have a way to manipulate the spin degree of freedom. One possibility is the to use the so called *Rashba effect*. This is a spin-orbit interaction present in two-dimensional electron gas realized in heterostructures and it is due to the lack of symmetry in growth direction. It is usually important in small-gap zinc–blende–type semiconductors. It induces a spin precession in the carriers moving in the gas and, very important thing, the strength of this interaction can be tuned through an electric field perpendicular to the gas. A lot of devices based on the Rashba effect have been proposed. The spin-field effect transistor, proposed by Datta and Das in the 1990, is the most famous and represent the prototypical spintronics

device scheme. This is based on spin injection and spin detection by a ferromagnetic source and drain, and spin precession due to the Rashba effect in the quasi-one-dimensional channel of an ordinary field effect transistor.

The Rashba effect is also important because it can give a signature of the *Aharonov-Casher* effect. This is the dual of the *Aharonov-Bohm* effect, where the carrier charge is replaced by the magnetic moment and the magnetic field is replaced by the electric field. This has been demonstrated both theoretically and experimentally through the transport properties of mesoscopic system with a ring geometry.

This work explores the wide physics of the spin dynamics in quantum transport through mesoscopic systems. In the following the objectives and the methods are summarized.

Purpose of this work

The thesis treats two main aspects related to spintronics: the first is the attempt to realize a spin-field effect transistor working without ferromagnetic source and drain, and the second is to study the Aharonov-Casher effect in lattice structures.

The present thesis is organized as follow. In the first chapter it is reported a wide introduction to spin-orbit interactions in semiconductor heterostructures: Rashba and Dresselhaus effect. The main differences between them is introduces and it is shown how it is possible to detect them experimentally. After that it is analyzed in detail the spin-field effect transistor proposed by Datta and Das and it discussed why it is not realized yet. Finally the Chapter ends with an introduction to the Aharonov-Casher effect in comparison with the Aharonov-Bohm effect.

In the Chapter 2 it is studied the phenomenon of the spin-double refraction. This is observed in two-dimensional electron gas when electrons are inject with an angle out of the normal on an interface separating a region without Rashba SO coupling from a region with it. The behavior of electron spin in such scattering events is analogous to the polarization of the light in a biaxial crystal: the incident ray splits, within the crystal, in two rays (ordinary and extraordinary) whose polarizations are orthogonal. The transmission properties of the system are analyzed into details showing that in the case of normal incidence the interface is not able to distinguish spin up and spin down electrons. Instead, the oblique scattering, due to the spin-double refraction, gives rise to an output spin up probability different from the spin down probability. This effect of polarization survives also when all the injection angles are taken into account. It is shown that in this case the

conductance of the system is different for spin up and spin down electron.

The third Chapter is devoted to the proposal for a spin-field effect transistor without ferromagnetic source and drain. This is based on the spin-double refraction. This is realized in a two-dimensional electron gas where a region in which the Rashba SO coupling is present. The source and the drain could be realized using n^+-semiconductors. The novel feature of this setup is the transmission double step that is accompanied by the appearance of a spin polarization. It is shown how, fixed the injection angle for the electrons, varying the Rashba effect strength over a fixed threshold the transmission and the polarization of the system behave in the same oscillating way. This modulation of the output current is obtained with a spin-unpolarized input current, whereas in the original Datta and Das proposal the current oscillation stems out from the difference of phase accumulated along a path by the two spin propagating modes.

The Chapter 4 is devoted to the study of the Rashba effect in quantum networks. These are graphs of one-dimensional wires connected at nodes. In this chapter is developer a formalism to study quantum networks of generic shape in presence of Rashba effect and magnetic field. Here it is shown that in particular quantum network extending in only one-dimension (chain of square loops connected at one vertex), Rashba effect gives rise to a electron localization phenomena. This localization effect can be attributed to the spin precession due to the Rashba effect. Similar localization phenomena are observed in presence of magnetic field. Both the effects are due to the strong interplay between the external fields and the geometry of the network. Here these effect are presented in one- and two-dimensional cases showing that in special situation the interplay of magnetic field and Rashba effect completely destroys the localization effect.

The thesis ends with wide conclusions and with a discussion on future development.

Not everything that can be counted counts, and not everything that counts can be counted.

Albert Einstein (1879-1955)

1

Rashba Spin-Orbit Interaction

Introduction

In this chapter I will present a brief introduction of the theoretical and experimental issue related to the *Rashba* Spin-Orbit interaction (SO) [1].

This kind of SO interaction has been introduced by Rashba in the 1960 to describe the absorption of radio waves in semiconductors with a wurtzite lattice. He showed that the presence of the SO term, gives rise to transitions involving a change in spin due to the Lorentz force.

Only during the eighty the interest in this kind of SO interaction takes new life. In fact in that time a set of experimental data on the combined resonance (i.e., electric dipole spin resonance) and the cyclotron resonance of two-dimensional electron gas (2DEG) at the interfaces of GaAs-Al$_x$Ga$_{1-x}$As heterojunctions, reported in the papers of Stein *et al.* [2] and Stormer *et al.* [3], shown that the spin degeneracy was lifted in the inversion layer. The theory developed by Rashba in the 1960 enabled Bychkov and Rashba [4] to describe this experimental data in term of SO interaction. The theory that they proposed was based on the following expression for a SO Hamiltonian:

$$\mathcal{H}_{\text{SO}} = \frac{\alpha}{\hbar}(\vec{\sigma} \times \vec{k}) \cdot \hat{\nu}. \tag{1.1}$$

where $\vec{\sigma}$ are the Pauli matrices, α is the SO coupling constant and $\hat{\nu}$ is a unit vector perpendicular to the layer. This operator lifts the twofold spin degeneracy at $\vec{k} \neq 0$ and determines the SO band slitting near $\vec{k} = 0$.

1.1   Two-Dimensional Electron Gas

In the context of semiconductor materials and fabrication based on planar integrated circuit technology, quantum confinement can be mainly realized in two different way: a) through the growth of inhomogeneous layer structures resulting in quantization perpendicular to the substrate surface, b) through lateral patterning using ultrafine lithography techniques. Historically, the development of quantum confined system was realized in heterolayer structures grown on semiconducting substrates. The first demonstration of quantization of semiconductor states due to the artificial confinement was in the inversion layer of SiMOS structures [5]. In this system, quantization of the carrier motion is due to the confining potential of the Si/SiO_2 interface barrier and the potential well in the other direction due to band bending. Later, with the development of precision epitaxial growth techniques such as molecular beam epitaxy (MBE) and metal organic chemical vapor deposition (MOCVD), high-quality lattice-matched heterojunction systems could be realized. These systems exhibits quantum confinement effects bigger than those in the SiMOS system due to several reasons, including the low surface state density at the interface of the lattice-matched materials such as GaAs and $Al_xGa_{1-x}As$, and the lower conduction band mass of III-V compound materials.

To understand why this layer is formed consider the conduction and the valence band line-up in the z direction before to *join* the two kinds of semiconductors (Fig. 1.1a). The Fermi energy E_f in the widegap AlGaAs layer is higher than in the narrowgap GaAs layer. Consequently electrons come out from the n-AlGaAs leaving behind positively charged donors. This space charge gives rise to an electrostatic potential that causes the bands to bend as shown in Fig. 1.1b. At the equilibrium the Fermi energy is constant in the sample and inside the conduction band. The electron density is sharply peaked near the GaAs-AlGaAs interface forming a thin conduction layer that is the two-dimensional electron gas. The carrier concentration in a 2DEG typically ranges from $2 \cdot 10^{11} cm^{-2}$ to $2 \cdot 10^{12} cm^{-2}$ and can be varied by applying a negative voltage to a metallic gate deposited on the surface. Usually the 2DEG is confined in layers of thickness of about 100Å, this corresponds to a bulk concentration of 10^{18} cm^{-3}. In structures of this kind usually the mobility is high up to 10^6 cm^2/V s. This value is due to the spatial separation between the donor atoms in the AlGaAs layer and the conduction electrons in the GaAs layer: the low scattering cross-section due to the impurities, leads to a weaker scattering.

(a)

Surface

x

z

y

n–AlGaAs

i–GaAs

E_c

E

E_f

z

E_v

2DEG

(b)

E

E_f

z

E_c

E_v
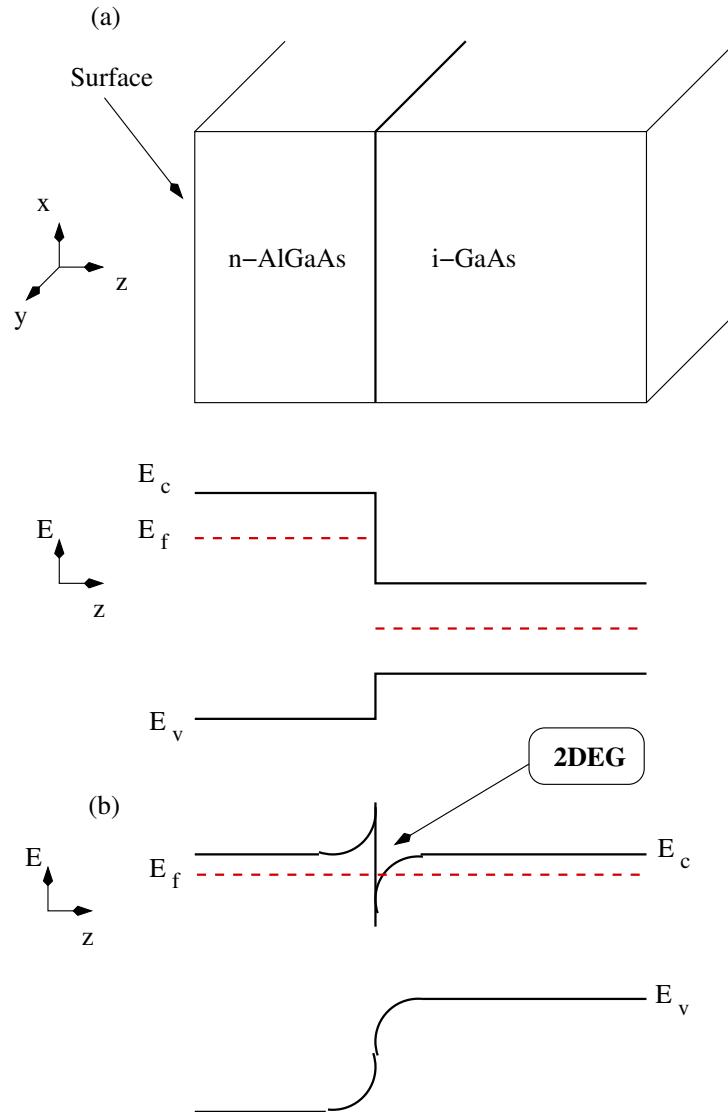
Figure 1.1: Conduction and valence band line-up at a junction between an n-type AlGaAs and intrinsic GaAs, (a) before and (b) after charge transfer has taken place. Note that this is a cross-sectional view.

1.2 Rashba effect in 2DEG

It is well known that the spin splitting in the 2DEG presents two distinct contributions. One contribution is due to the inversion asymmetry of the zinc-blende crystal structure of the bulk host material. In the lowest order in the momentum k, this splitting is described in the bulk by a term of the form [6–8]

$$\mathcal{H}_{k^3} = \frac{\gamma}{\hbar} \left[\sigma_x p_x \left(k_y^2 - k_z^2 \right) + \sigma_y p_y \left(k_z^2 - k_x^2 \right) + \sigma_z p_z \left(k_x^2 - k_y^2 \right) \right], \qquad (1.2)$$

where σ_i stands for the Pauli matrices, γ is a material constant, and the coordinated axis are now assumed parallel to the crystallographic cubic axis. In a sufficiently narrow quantum well grown along the [001] direction, it is possible to approximate the operator p_z and p_z^2 by their expectation values $\langle p_z \rangle$, $\langle p_z^2 \rangle$. This leads to the following two contributions to SO coupling resulting from the bulk inversion asymmetry: the Dresselhaus term

$$\mathcal{H}_D = \frac{\beta}{\hbar} \left(\sigma_x p_x - \sigma_y p_y \right) \qquad (1.3)$$

liner in the momenta with $\beta = \gamma \langle p_z^2 \rangle$ and the trilinear term

$$\mathcal{H}_D^{(3)} = \frac{\gamma}{\hbar} \left(\sigma_x p_x p_y^2 - \sigma_y p_y p_x^2 \right). \qquad (1.4)$$
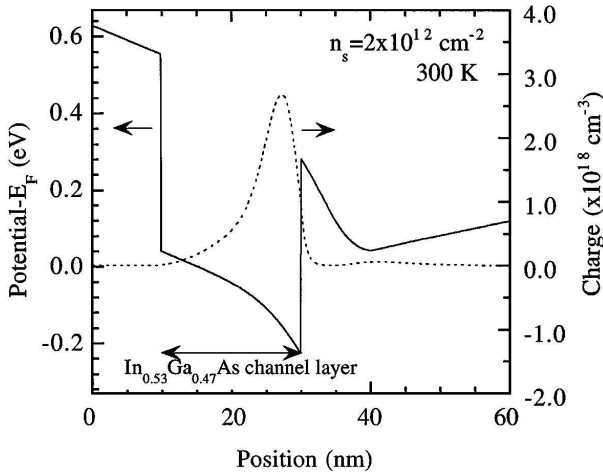
Figure 1.2: Calculated conduction band diagram and electron distribution [9].

Clearly the typical magnitude of $\mathcal{H}_D^{(3)}$ compared to the linear term $\mathcal{H}_D$ is given by the ratio of the Fermi energy $\mathcal{E}_F$ of the in-plane motion to the kinetic energy of the quantized degree of freedom in the growth direction. For typical values of $\mathcal{E}_F$ of about 10 meV and not too broad quantum wells this ratio is small, therefore is the Dresselhaus trilinear term is usually neglected.

The other kind of SO coupling present in 2DEG is due to the Rashba effect. Contrary to the Dresselhaus effect, the Rashba SO interaction is not due to bulk properties. In fact it has been demonstrated by de Andrada e Silva *et al.* [10] that it is

present only in semiconductor heretostructures where there is a lack of inversion symmetry in the growth direction.

So far those two models of SO interaction in semiconductor heterostructures have been introduced, in the following their essential difference is underlined. The Dresselhaus term is due to bulk properties of the semiconductors so that its coupling constant β is fixed and cannot be tuned. Instead the Rashba term depends of the shape of the confining potential and the coupling constant α can be tuned by means metallic gate since the confining potential can be modified using electric field (see Fig. 1.2).

This feature can be verified experimentally. One way is to study the beating pattern in the Shubnikov-de Haas (SdH) oscillations [9, 11, 12]. The basic idea is that the magnetoconductance of a 2DEG at $T = 0$ is given by

$$\sigma_{xx} \propto \sum_{n\pm} \left(n \pm \frac{1}{2} \right) \exp \left\{ -\frac{(E_F - E_n^{\pm})^2}{\Gamma^2} \right\}, \tag{1.5}$$

where E_F is the Fermi energy, $E_n^{\pm}$ is the energy of the nth Landau level with spin up $(+)$ and spin down $(-)$ and Γ is the Landau level broadening that is assumed constant. In a magnetic field B, the energy spectrum for the nth Landau level is described by

$$E_0 = \frac{1}{2}\hbar\omega_c \quad \text{when } n = 0, \tag{1.6}$$

$$E_n^{\pm} = \hbar\omega_c \left[n + \frac{1}{2}\sqrt{\left(1 - \frac{gm^*}{2} \right)^2 + n\frac{\Delta_R^2}{E_F\hbar\omega_c}} \right], \tag{1.7}$$

where ω_c is the cyclotron frequency which is given by $\omega_c = eB/m^*$, and g is the effective g factor. In the last equation the information relative to the spin-splitting is taken in account through the factor $\Delta_R = 2k_F\alpha$ with α Rashba SO coupling constant.

In Fig. 1.3 are shown the SdH oscillations as function of the gate voltages in a sample of $In_{0.53}Ga_{0.47}As/ In_{0.52}Al_{0.48}As$ at a temperature of 0.4 K. It is evident the presence of beating pattern because the existence of two closely spaced SdH oscillation frequency components with similar amplitudes. By increasing the positive gate voltage from $V_g = 0V$ to $V_g = 0.3V$, the beat pattern enhance. Above $V_g = 0.5V$, a clearly different low SdH oscillation frequency component becomes visible due to the occupation of the second subband. Taking more negative value of V_g the oscillation frequency becomes lower because of the decrease in the carrier concentration. Using the data of this experiment [9] it has been obtained a variation of α in the range from $0.6 \cdot 10^{-11}$ to $0.95 \cdot 10^{-11}$ eV m.
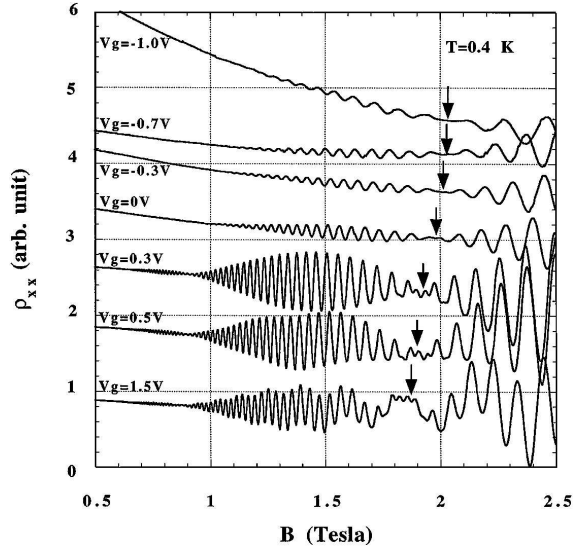
Figure 1.3: Schubnikov-de Haas oscillations as function of the gate voltages. [9].

The other way to measure the tunability of the Rashba SO interaction takes in account that the conductivity of low-dimensional system shows signature of quantum interference that depend on magnetic field and SO coupling [13]. In particular, constructive backscattering associated with pairs of time-reversed closed-loop electron trajectories in the absence of significant SO interaction leads to negative magnetoresistance measurement known as weak localization. On the contrary, when it is present a significant SO interaction the backscattering becomes destructive and the positive magnetoresistance changes is known as anti-weak localization.

It has been demonstrated by Miller *et al.* [14] that controlling the SO coupling in a moderately high-mobility GaAs/AlGaAs 2DEG through the applications of top-gate voltage it is possible to induce a crossover from weak localization to anti-localization (see Fig. 1.4).

So far I have introduced two techniques that are not able to distinguish the relative contributions of Rashba and Dresselhaus terms to the SO coupling. This can be measured studying the angular dependence on the spin-galvanic photocurrent [15]. This is induced by a non-equilibrium, but uniform population of electron spin. The microscopic origin for this effect is that the two electronic sub-bands for spin-up and spin-down electrons are shifted in the momentum space and, although the electron distribution in each sub-band is symmetric, there is an inherent asymmetry in the spin-flip scattering
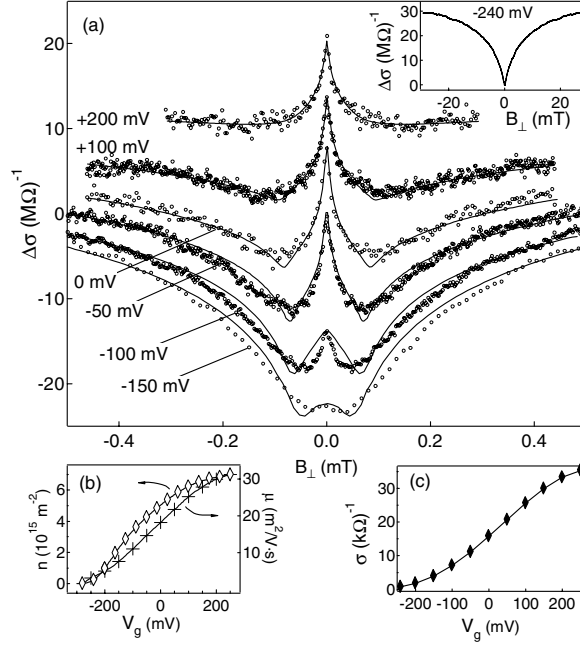
Figure 1.4: (a) Experimental magnetoconductance, $\Delta\sigma = \sigma(B) - \sigma(0)$ (circles), offset for clarity, along with three-parameter fits (solid line) for several gate voltages. Inset: Experimental magnetoconductance data for the most negative gate voltage, showing pure weak localization. (b) Density and mobility as function of V_g, extracted from longitudinal and Hall voltage measurements. (c) Experimental conductivity, showing strong dependence on V_g [14].

events between the two sub-bands. In this case it is possible to measure the anisotropic orientation of spins in the momentum space and hence the different contribution of the Rashba and the Dresselhaus terms [16]. The spin-galvanic current is driven by the electron in-plane average spin $\vec{S}_\parallel$ according to

$$\vec{j}_{\mathrm{SGE}} \propto \begin{pmatrix} \beta & -\alpha \\ \alpha & -\beta \end{pmatrix} \vec{S}_\parallel. \tag{1.8}$$

Therefore, the spin-galvanic current $\vec{j}_{\mathrm{SGE}}$ for a certain direction of $\vec{S}_\parallel$ consists of Rashba and Dresselhaus coupling induced currents, $\vec{j}_{\mathrm{R}}$ and $\vec{j}_{\mathrm{D}}$. Their magnitudes are $j_{\mathrm{R}} \propto \alpha|\vec{S}_\parallel|$ and $j_{\mathrm{D}} \propto \beta|\vec{S}_\parallel|$, and their ratio is

$$\frac{j_{\mathrm{R}}}{j_{\mathrm{D}}} = \frac{\alpha}{\beta}. \tag{1.9}$$
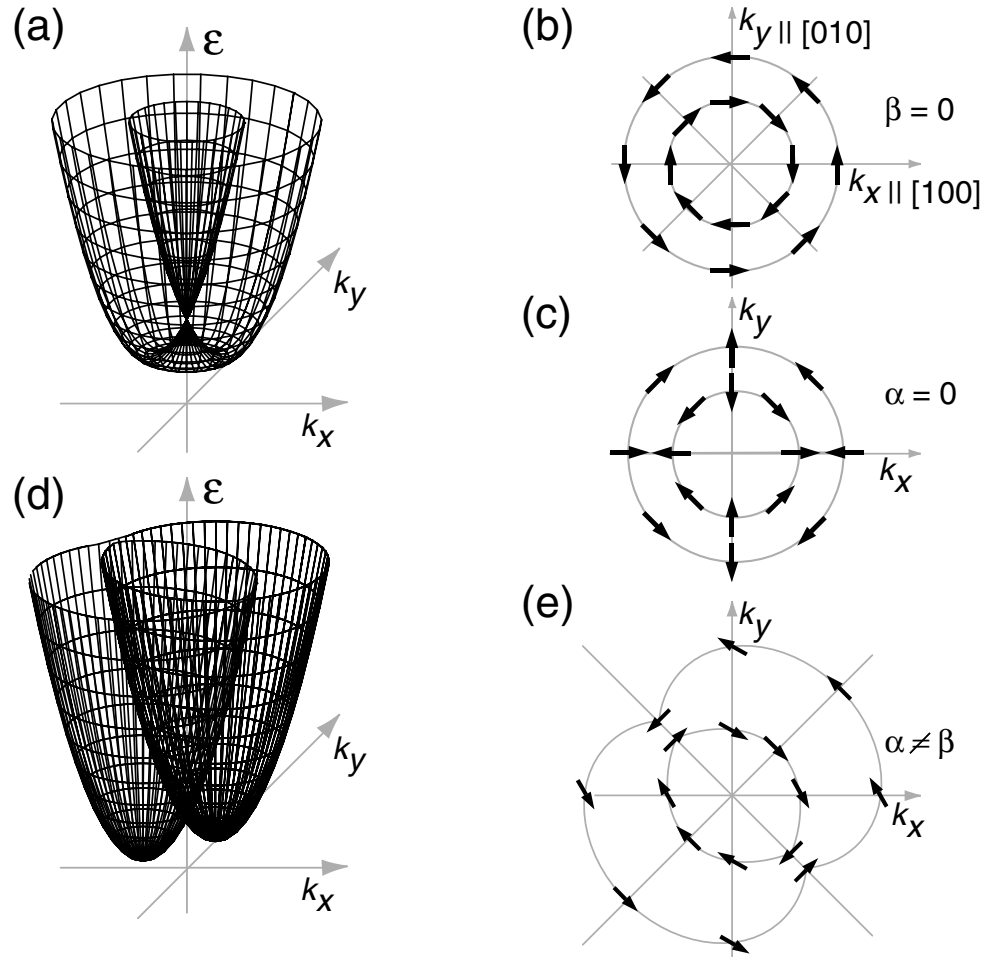
Figure 1.5: Schematic 2D band structure with $\vec{k}$-linear terms for C_2v symmetry for different relative strength of the Rashba and Dresselhaus terms and the distribution of the spin orientations at the 2D Fermi energy: (a) The case of the only Rashba or Dresselhaus spin-orbit coupling. (d) The case of the simultaneous presence of both contributions. Arrows indicate the orientation of spins.
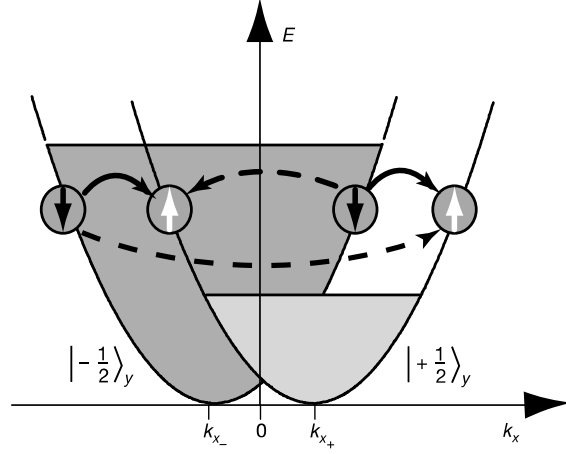
Figure 1.6: Microscopic origin of the spin-galvanic current in presence of the $\vec{k}$-linear terms in the electron Hamiltonian. If one spin sub-band is preferentially occupied, for example, by spin injection asymmetric spin-flip scattering results in a current in the x direction. The transitions sketched by dashed arrows yield an asymmetric occupation of both sub-bands and hence a current flow.

For $\vec{S}_\parallel$ oriented along one of the cubic axes it follows from Eq. (1.8) that the currents flowing along and perpendicular to $\vec{S}_\parallel$ are equal to j_R and j_D, respectively, yielding experimental access to determine α/β.

The experiment of Ganichev *et. al.* [16] are been performed in (001)-oriented n-type heterostructures of $InAs/Al_{0.3}Ga_{0.7}Sb$ having a C_{2V} point symmetry. The width of the quantum well is of 15 nm with a free carrier density of about $1.3 \cdot 10^{12}$ cm^{-2} and a mobility at room temperature of $\sim 2 \cdot 10^4$ cm^2/(V s). The ratio of Rashba and Dresslhaus currents has been evaluated equal to $j_R/j_D = 2.14 \pm 0.25$. This corresponds to the value of the ratio α/β, that agrees with theoretical results, which predict a dominant Rashba SO coupling in InAs quantum wells.
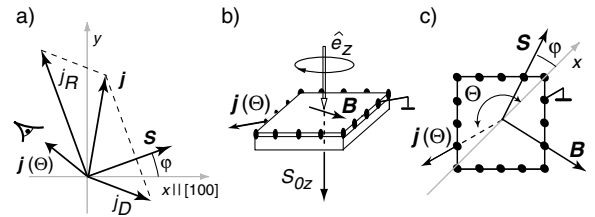
Figure 1.7: Angular dependence of the spin-galvanic current (a) and the geometry of the experiment (b),(c).

1.3   Properties of the Rashba Hamiltonian

I consider a 2DEG in the plane (x, y) in presence of the Rashba SO term
(1.1), the Hamiltonian of the system is

$$\mathcal{H} = \frac{\vec{p}}{2m} + \frac{\alpha}{\hbar}(\vec{\sigma} \times \vec{p}) \cdot \hat{z}. \tag{1.10}$$

where $\vec{p} \equiv (p_x, p_y)$ is the in plane momentum and $\hat{z}$ is a unitary vector
perpendicular to the 2DEG. The eigenvalues of the Hamiltonian (1.10) are

$$\mathcal{E}_{\pm}(\vec{k}) = \frac{\hbar^2 k^2}{2m} \pm \alpha k = \frac{\hbar^2}{2m}(k \pm k_{\mathrm{SO}})^2 - \Delta_{\mathrm{SO}}, \tag{1.11}$$

where $k = \sqrt{k_x^2 + k_y^2}$ is the modulus of the electron momentum, $k_{\mathrm{SO}} = \alpha m / \hbar^2$
is a recast form of the SO coupling constant and $\Delta_{\mathrm{SO}} = (\alpha m / \hbar)^2$. Usually
the last term of (1.11) is neglected because the SO coupling α is small. The
eigenvecorts of the Hamiltonian (1.10) relative to the spectrum (1.11) are
plane waves function of the momentum $\vec{k}$

$$\Psi_{+}(x, y) = e^{i(k_x x + k_y y)} \frac{1}{\sqrt{2}} \begin{pmatrix} 1 \\ i e^{-i\theta} \end{pmatrix}, \tag{1.12}$$

$$\Psi_{-}(x, y) = e^{i(k_x x + k_y y)} \frac{1}{\sqrt{2}} \begin{pmatrix} 1 \\ -i e^{-i\theta} \end{pmatrix} \tag{1.13}$$

where $\theta = \arctan(k_y / k_x)$ is the angle between the momentum vector and
the k_x direction. It is important to note that the spin states (1.12-1.13) are
always perpendicular to the motion direction. In fact, if the electron moves
along x direction the spinor part of the eigenvectors become $\begin{pmatrix} 1 \\ i \end{pmatrix}$ and $\begin{pmatrix} 1 \\ -i \end{pmatrix}$
that is the spin up and spin down in the y direction, on the contrary if the
electron moves along the y direction the eigenvectors become $\begin{pmatrix} 1 \\ 1 \end{pmatrix}$ and $\begin{pmatrix} 1 \\ -1 \end{pmatrix}$
that is the spin up and spin down state in the x direction (see Fig. 1.8 Panel
b).

In Fig. 1.8 Panel c),d) and e) are reported the k_y-section of the energy
spectra as function of the momentum for a 2DEG is different physical situa-
tion. The Panel c) is relative to a free electron of a 2DEG. In this case the
spin degeneracy is present. In the presence of a magnetic field $\vec{B}$ (Panel d),
the spin degeneracy is lifted out by the *Zeeman* effect and the gap separating
spin up and spin down is equal to $g^* \mu_{\mathrm{B}} B$ where g^* is the effective gyromag-
netic ratio and μ_{B} is the Bohr's magneton. When the Rashba SO interaction
is present (Panel e), the spin degeneracy is lifted out but for $\vec{k} = 0$. In this
situation the degeneracy is removed without the opening of gaps.
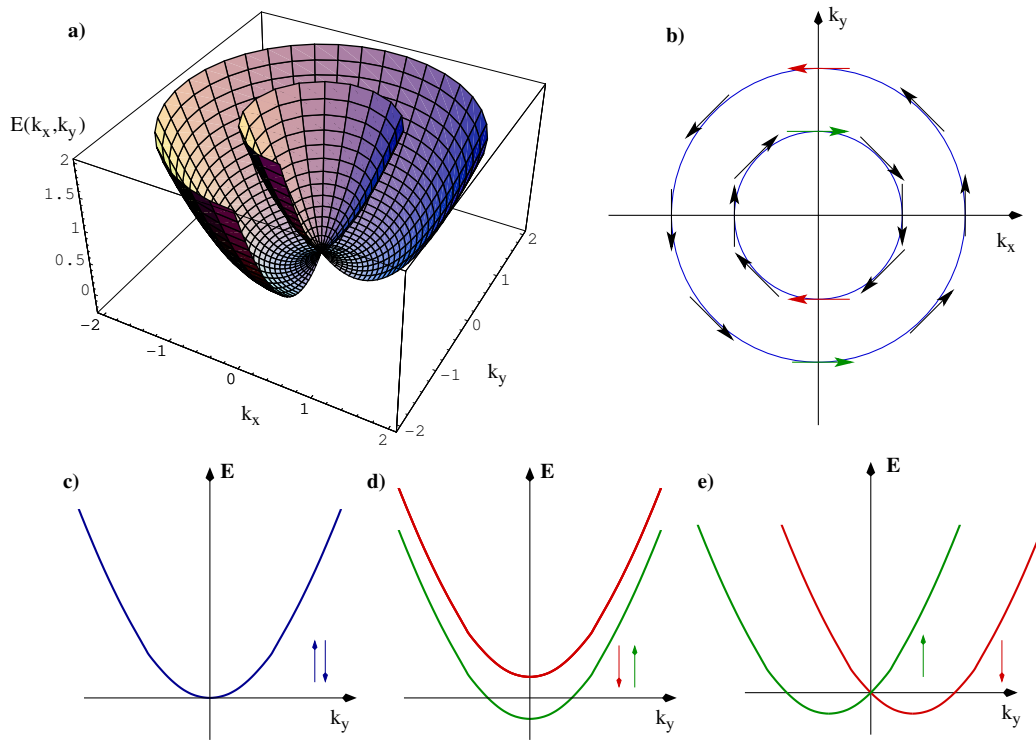
Figure 1.8: Properties of the Rashba energy spectrum. Panel a) Portion of the energy spectrum of the Hamiltonian (1.10). Panel b) The Fermi contours relative to the Hamiltonian (1.10), the spin states are indicated. Panel c) section of the energy spectrum for a free electron. Panel d) section of the energy spectrum for an electron in presence of a magnetic field (*Zeeman* slitting). Panel e) section of the energy spectrum for an electron in presence of Rashba spin-orbit interaction.

The semiclassical particle velocities are given by

$$\vec{v}_\pm(\vec{k}) = \frac{\partial \mathcal{E}_\pm(\vec{k})}{\hbar \partial \vec{k}} = \frac{\hbar \vec{k}}{m} \pm \alpha. \tag{1.14}$$

If I consider the quantum-mechanical velocity operator

$$\dot{\vec{r}} = \frac{i}{\hbar} \left[\mathcal{H}, \vec{r} \right] \tag{1.15}$$

and the expressions (1.12-1.13) for the eigenstates, it is straightforward to show that its matrix elements are given by

$$\langle \Psi_\pm(\vec{k}) | \, \dot{\vec{r}} \, | \Psi_\pm(\vec{k}') \rangle = \delta_{\vec{k}, \vec{k}'} \, \vec{v}_\pm(\vec{k}) \tag{1.16}$$

that is the semiclassical velocities $\vec{v}_\pm(\vec{k})$ are, as usual, the diagonal elements of the velocity operator. It is evident that in presence of the Rashba SO interaction the velocity operator and the momentum do not coincide.

Parameterizing wave vectors as $\vec{k} = k \, (\cos\varphi, \sin\varphi)$, one obtains for the positive Fermi energy $\mathcal{E}_F$ the following parameterization of the Fermi contours (see Fig. 1.8 Panel b)

$$k_\pm^F(\varphi, \mathcal{E}_F) = \mp \frac{\alpha \, m}{\hbar^2} + \sqrt{\left(\frac{\alpha \, m}{\hbar^2} \right)^2 + \frac{2m}{\hbar^2} \mathcal{E}_F}. \tag{1.17}$$

Here the double sign corresponds to the two dispersion branches (1.11). In the following the Fermi energy is always assumed to be positive. From the Eq. (1.17) one finds the electron density n as

$$n = \frac{1}{(2\pi)^2} \sum_{\mu=\pm} \int_0^{k_\mu^F} dk \int_0^{2\pi} d\varphi \, k = \frac{1}{2\pi} \left[\frac{2 \, m}{\hbar^2} \mathcal{E}_F + 2 \left(\frac{\alpha \, m}{\hbar^2} \right)^2 \right]. \tag{1.18}$$

If the Dresselhaus term (1.3) is taken into accunt the Fermi contour becomes

$$\begin{aligned} k_\pm^F(\varphi, \mathcal{E}_F) \;=\;& \mp \sqrt{\left(\frac{m}{\hbar^2} \right)^2 [\alpha^2 + \beta^2 + 2\alpha\beta \sin(2\varphi)]} \\ & + \sqrt{\frac{2m}{\hbar^2} \mathcal{E}_F + \left(\frac{m}{\hbar^2} \right)^2 [\alpha^2 + \beta^2 + 2\alpha\beta \sin(2\varphi)]} \end{aligned} \tag{1.19}$$

and the electron density

$$n = \frac{1}{2\pi} \left[\frac{2m}{\hbar^2} \mathcal{E}_F + 2 \left(\frac{m}{\hbar \, 2} \right)^2 (\alpha^2 + \beta^2) \right]. \tag{1.20}$$
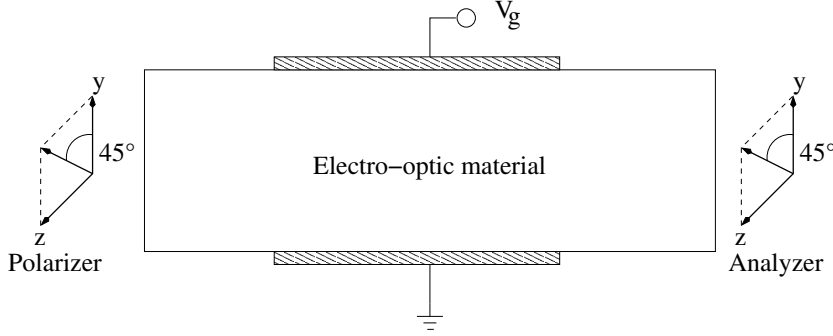
Figure 1.9: A schematic view of the electro-optic modulator.

If $\alpha = 0$ or $\beta = 0$ the disperions are isotropic and Fermi contours are centric circles. For $\alpha \neq \beta \neq 0$ the Fermi contours are anisotropic and this leads anisotropic transport properties. It is important to note that the dispersion relation and Fermi contours are symmetric around the points $\varphi \in \{\pi/4, 3\pi/4, 5\pi/4, 7\pi/4\}$, *i.e.*, these quantities are invariant under reflections along the $(1, 1)$ and $(1, -1)$ directions.

1.4 Spin-Field Effect Transistor

In the 1990 Datta and Das [17] proposed the first application using the Rashba SO interaction. It was an analog of the electro-optic modulator. Since the original proposal of this spin-Field Effect Transistor (spin-FET) has been obtained progress but so far there is any effective realization of this device.

The basic effect can be understood by analogy with the electro-optic light modulator shown in Fig. 1.9. A polarizer at the input polarizes the light at 45° to the y axis (in the $y - z$ plane) which can be represented as a linear combination of z- and y- polarized light:

$$\underset{(45^{\circ}\ \text{pol})}{\begin{pmatrix} 1 \\ 1 \end{pmatrix}} = \underset{(z\ \text{pol})}{\begin{pmatrix} 1 \\ 0 \end{pmatrix}} + \underset{(y\ \text{pol})}{\begin{pmatrix} 0 \\ 1 \end{pmatrix}} . \tag{1.21}$$

As the light passes through the electro-optic material, the two polarizations acquire different phase shifts $k_1 L$ and $k_2 L$ because the electro-optic effect makes the dielectric constant ϵ_{zz} different from ϵ_{yy}. The light emerging from the electro-optic material has a polarization given by $\begin{pmatrix} e^{ik_1 L} \\ e^{ik_2 L} \end{pmatrix}$. The analyzer at the output lets the component along $\begin{pmatrix} 1 \\ 1 \end{pmatrix}$ to pass through. The output power
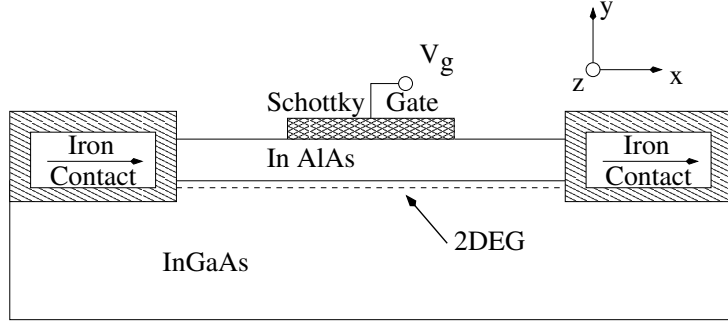
Figure 1.10: The spin-field effect transistor proposed by Datta and Das [17].

P_0 is given by

$$P_0 \propto \left| (1\ 1) \begin{pmatrix} e^{ik_1 L} \\ e^{ik_2 L} \end{pmatrix} \right|^2 = 4\cos^2 \frac{(k_1 - k_2)L}{2}. \qquad (1.22)$$

The light output is modulated with a gate voltage that controls the differential phase shift $\Delta\theta = (k_1 - k_2)L$.

The analog device based on the Rashba SO interaction is shown in Fig. 1.10. The polarizer and the analyzer are implemented using contacts made of ferromagnetic materials like iron [18]. At the the Fermi energy in such materials the density of states for electrons with one spin greatly exceeds that for the other, so that the contact preferentially injects and detects electrons with a particular spin. A contact magnetized in the x direction preferentially injectes and detects electrons spin polarized along positive x which is represented as a linear combination of the positive z-polarized and negative z-polarized electrons

$$\underset{(+x\ \mathrm{pol})}{\begin{pmatrix} 1 \\ 1 \end{pmatrix}} = (1+i) \left[\underset{(+y\ \mathrm{pol})}{\begin{pmatrix} 1 \\ -i \end{pmatrix}} + \underset{(-y\ \mathrm{pol})}{\begin{pmatrix} 1 \\ i \end{pmatrix}} \right]. \qquad (1.23)$$

Finally, the analogue of the electro-optic material is realized employing a 2DEG with Rashba SO interaction. In fact, this kind of interaction causes $+z$ polarized and $-z$ polarized electrons with the same energy to have different wave vectors k_1 and k_2 (see Fig. 1.8 Panel e). Consider an electron traveling in the x direction with $k_z = 0$ and $k_y \neq 0$. The eigenenergy corresponding to the two different spin carriers are

$$\mathcal{E}(z\ \mathrm{pol}) = \frac{\hbar^2 k_{x_1}^2}{2m} - \alpha k_{x_1}, \qquad (1.24)$$

$$\mathcal{E}(-z\ \mathrm{pol}) = \frac{\hbar^2 k_{x_2}^2}{2m} + \alpha k_{x_2}. \qquad (1.25)$$
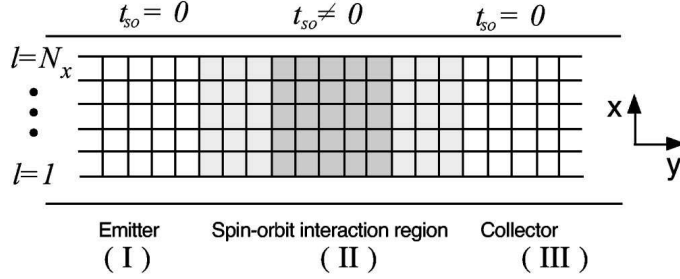
Figure 1.11: Schematic of the tight-binding model for the system. In the shaded areas the spin-orbit interaction if finite $t_{SO} \neq 0$ [19].

From the previous equations it is possible to recover the momentum difference because the two energies are fixed to the Fermi energy

$$k_{x_1} - k_{x_2} = \frac{2m\alpha}{\hbar^2}. \tag{1.26}$$

It is apparent that a differential phase shift

$$\Delta\theta = (k_{x_1} - k_{x_2}) = \frac{2m\alpha L}{\hbar^2} \tag{1.27}$$

is introduced between spin up and spin down electrons, which is proportional to the SO coupling α.

The above analysis is limited to a single-mode one-dimensional channel, that is an electron moving along a fixed energy. It is interesting to understand what happens when a multi-mode one-dimensional channel is taken in account. The Authors suggest a criterion to avoid the inter-subbands mixing due to the Rashba SO interaction based on choosing the with of the channel in such a way that $w \ll \hbar^2/\alpha \, m$.

A fully multi-mode analysis of the *Datta and Das* spin-FET has been proposed by Mireles and Kirczenow [19]. They investigate the effect of the strength of the Rashba SO coupling on the spin-transport properties of narrow quantum wires. The Rashba SO interaction is reformulated within the tight-binding approach in a lattice model. It is considered a quasi-one-dimensional wire, which is assumed to be infinitely long in the propagation direction. The wire is represented by a two-dimensional grid with a lattice constant a. It is chosen the coordinate system such that the x axis, with N_x lattice sites, is in the transverse direction, whereas the y axis, with N_y lattice sites in the longitudinal direction (see Fig. 1.11).

It is assumed only nearest-neighbor spin-dependent interactions for the Rashba interaction. Furthermore it is assumed that the localized site orbitals

have the symmetry of the s states. Then the tight-binding analog of the Eq. (1.1) takes the form

$$
\mathcal{H}_{\mathrm{SO}}^{\mathrm{tb}}(y) \;=\; -t_{\mathrm{SO}}(y) \sum_{\sigma,\sigma'} \sum_{l,m} \Big(c_{l+1,m,\sigma'}^{\dagger} \, (i\sigma_y)_{\sigma,\sigma'} \, c_{l,m,\sigma}
$$

$$
-c_{l,m+1,\sigma'}^{\dagger} \, (i\sigma_x)_{\sigma,\sigma'} \, c_{l,m,\sigma} \Big) + \mathrm{H.c.} \tag{1.28}
$$

with an isotropic nearest-neighbor transfer integral t_{SO} is the strength of the Rashba SO interaction corresponding to $t_{\mathrm{SO}} = \alpha/2a$, and with $c_{l,m,\sigma}^{\dagger}$, which represents the electron creation operator at site (l, m) with spin state σ ($\sigma = \uparrow, \downarrow$).

The wire is divided into three main regions. In two of these [I and III in Fig. 1.11], which are near the ferromagnetic source and drain, the SO hopping parameter t_{SO} is set to zero. In the middle region (II) the SO coupling is finite ($t_{\mathrm{SO}} \neq 0$).

The spin-dependent transport problem is solved numerically through the use of the spin-dependent Lippman-Schwinger equation,

$$
|\Psi\rangle = |\Phi\rangle + G_0(E)\hat{\mathcal{H}}_{\mathrm{SO}}^{\mathrm{tb}}|\Psi\rangle, \tag{1.29}
$$

where $|\Phi\rangle$ is the unperturbed wave function, *i.e.*, an eigenstate of the lattice Hamiltonian[1] $\mathcal{H}_0$, whereas $G_0(E) = (E + i\epsilon - \mathcal{H}_0)^{-1}$ is the Green's functions for the system in the absence of any kind of scattering.

The Authors introduce a criterion to distinguish the cases of *weak* and *strong* SO coupling. Since in the multi-channel scattering process the eigenstates of the full Hamiltonian are linear combination of the different spin subbands (due to the Rashba term), therefore, in the perturbative sense, the contribution of the mixing of the spin subbands should be negligible as long the subbands spacing $\Delta E_W = E_m - E_n$ is much greater than the subband intermixing energy

$$
\frac{\langle \phi_{n,\sigma} | \mathcal{H}_{\mathrm{SO}} | \phi_{m,\sigma'} \rangle}{E_m^0 - E_n^0} \tag{1.30}
$$

where $\phi_{n,\sigma}$ are the unperturbated electron wavefunctions. However, if the confinement energy and/or the SO coupling are of the same order as the energy shift introduced by the intersubband mixing contribution, then the above condition is about one or greater. In this case introducing

$$
\beta_{\mathrm{SO}} \approx \left(\frac{\pi a}{W}\right)^2 \frac{1}{\left(\frac{\pi a}{W}\right) + ak_F} = \beta_{\mathrm{SO}}^{\mathrm{c}}, \tag{1.31}
$$

where $\beta_{\mathrm{SO}} = t_{\mathrm{SO}}/|t|$, and k_F is the Fermi wave number. The critical value

---

[1] That is the kinetic Hamiltonian without SO interaction.
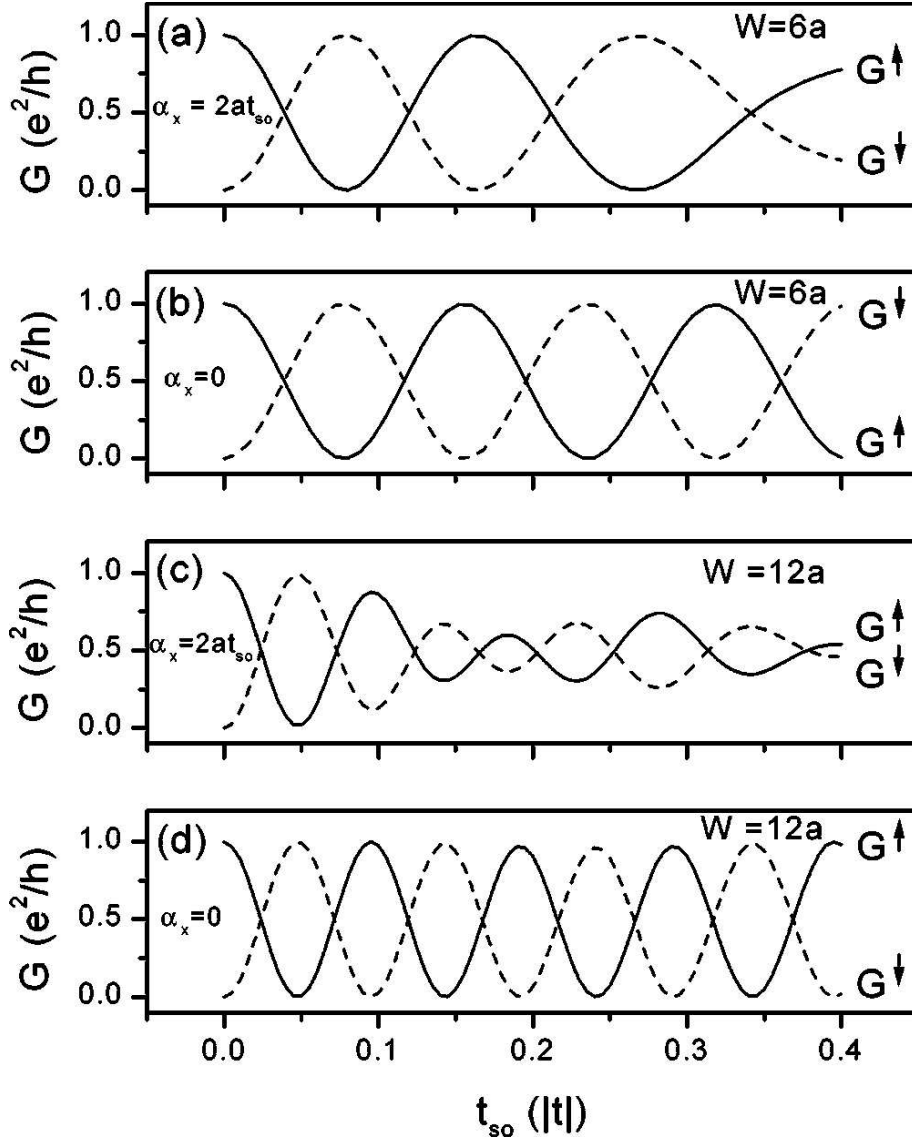
Figure 1.12: Spin-orbit coupling strength dependence of the ballistic spin conductance; solid line is $G^\uparrow$, dashed line $G^\downarrow$: (a) Narrow wire of $W = 6a$ and uniform spin-orbit coupling ($\alpha_x = \alpha_y = 2at_{SO}$). (b) Same as in (a) but with $\alpha_x = 0$ and $\alpha_y = 2at_{SO}$; perfect oscillations are seen for all t_{SO}. (c) Same as in (a) with $W = 12a$. (d) Modulation for $W = 12a$, with $\alpha_x = 0$ and $\alpha_y = 2at_{SO}$. The intersubband mixing clearly changes the otherwise perfectly sinusoidal spin-conductance modulation [19].

$\beta_{\mathrm{SO}}^{\mathrm{c}}$ define a *weak* SO coupling regime whenever $\beta_{\mathrm{SO}} < \beta_{\mathrm{SO}}^{\mathrm{c}}$ and a *strong* coupling regime if $\beta_{\mathrm{SO}} > \beta_{\mathrm{SO}}^{\mathrm{c}}$.

In Fig. 1.12 is reported the behaviors of the spin-conductance as function of the SO hopping parameter t_{SO}. In the Panel a) the incident Fermi energy is fixed to 0.5 ($k \approx 0.7a^{-1}$) and $W = 6a = 60$ nm, which gives a critical value $\beta_{\mathrm{SO}}^{\mathrm{c}} = 0.22$. This value of β_{SO} separates the sinusoidal behavior of $G^{\uparrow\downarrow}$ for $\beta_{\mathrm{SO}} \leq 0.22$ from its behavior for $\beta_{\mathrm{SO}} > 0.22$ where the confinement energy is of the order of the intersubband mixing energy. The effect is clearer for a wire with $W = 120$ nm (see Fig. 1.12 Panel c) for which the critical value of β_{SO} is 0.07. To show that the non-sinusoidal behavior is due mainly to the intersubband mixing, in the Panel b) and d) of Fig. 1.12 are reported the spin-conductance as function of t_{SO} with the same parameter of Panel a) and c) respectively but in the unphysical situation of $\alpha_x = 0$ and $\alpha_y \neq 0$. It is evident that the sinusoidal behavior is recovered.

So far several obstacles have been found on the way of the realization of the spin-FET proposed by Datta and Das [17]. The main one is related to the injection of spin polarized current. For example it has been shown that in diffusive transport regime, for typical ferromagnets only a current with a small polarization can be injected into a semiconductor 2DEG with long spin-flip length even if the conductivity of semiconductor and ferromagnet are equal [20]. This situation is dramatically exacerbated when ferromagnetic metals are used; in this case the spin polarization in the semiconductor is negligible.

A possible solution to circumvent this problem may be provided by the use of the dilute magnetic semiconductor [21] as source and drain. In these systems a few percent of the cations in the III-V or II-VI semiconductors compounds are randomly substituted by magnetic ions, usually Mn, which have local magnetic moments. The effective coupling between these local moments is mediated by free carriers in the host semiconductor compound (holes for p-doped materials and electrons for n-doped one) and can lead to ferromagnetic long-range order. Curie temperatures T_{c} in excess of 100 K have been found in bulk (Ga,Mn)As systems [21].

Using the properties of the dilute magnetic semiconductor have been proposed all-semiconductor spin-FET in which the conducting channel is provided by a two-dimensional hole gas [22].
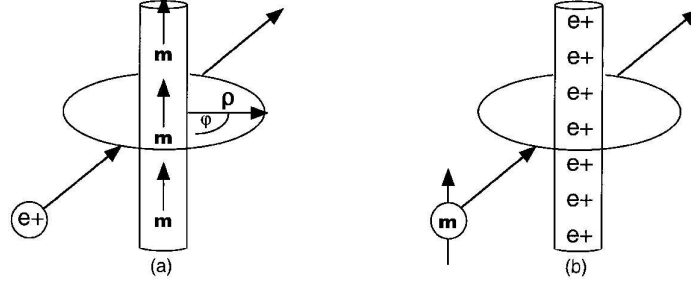
Figure 1.13: Schematic view of the Aharonov-Bohm (a) and Aharonov-Casher (b) effect. Here e is an electric charge, $\vec{m}$ is a magnetic dipole.

1.5 Rashba effect as signature of Aharonov-Casher effect

Aharonov and Bohm [23] showed long ago that a magnetic field enters quantum mechanics in two distinct ways, a distinction easily described in the semiclassical limit. In this limit, first the magnetic field determines the classical trajectory of the particle through the Lorentz force law, *dynamical effect*, and second it contributes to the phase accumulated along a trajectory through a line integral of the vector potential along it, *geometrical effect*. The latter effect has no classical analog. The term Aharonov-Bohm effect is now commonly used even in situations in which the dynamical effect is not rigorously zero, but is negligible compared to the geometrical effect. The Aharonov-Bohm phase is usually expressed as

$$\psi_{\mathrm{AB}} \equiv \frac{2\pi}{\phi_0} \oint \vec{A} \cdot d\vec{r} = 2\pi \frac{\phi_{\mathrm{B}}}{\phi_0}, \qquad (1.32)$$

where $\phi_0 = hc/e$ is the flux quantum and $\vec{A}$ is the vector potential associated to the magnetic field $\vec{B}$. There are now many well-known manifestations of the Aharonov-Bohm effect in the low-temperature transport properties of disordered normal conductors, *e.g.*, weak-localization magnetoresistance [24], and the closely related Altshuler-Aronov-Spivak effect [25], universal magnetoconductance fluctuations of mesoscopic samples [26], and persistent currents of array of rings.

Some years ago Aharonov and Casher [27] have found out an electromagnetic dual of the Aharonov-Bohm effect. The basic idea is the *interaction* of the electric field with neutral magnetic moments through the SO interaction.

The effect can be explained taking account of the Dirac equation for a magnetic moment μ in an external electric field. In the non relativistic limit

of this equation the Dirac Hamiltonian becomes

$$\mathcal{H}_{\mathrm{NR}} = \frac{1}{2m}\vec{\sigma}\cdot\left(\vec{p}-i\mu\vec{E}\right)\ \vec{\sigma}\cdot\left(\vec{p}+i\mu\vec{E}\right) \tag{1.33}$$

where m is the mass of the particle and $\vec{E}$ is the electric field. This is recast into the form

$$\mathcal{H}_{\mathrm{NR}} = \frac{1}{2m}\left(\vec{p}-\vec{E}\times\vec{\mu}\right)^2 - \frac{\mu^2 E^2}{2m} \tag{1.34}$$

where $\vec{\mu} = \mu\vec{\sigma}$. However the previous reduction is possible only if one drops a term proportional to $\vec{\nabla}\cdot\vec{E}$ which is, proportional to the charge density of the source of the electric field. Neglecting the terms in $\mathcal{O}(\mu^2)$ it is straightforward to show the phase contribution due to the interaction between magnetic moment and electric field is

$$\psi_{\mathrm{AC}} \equiv \frac{2\pi}{\phi_0\ e}\oint\left(\vec{\mu}\times\vec{E}\right)\cdot d\vec{r} = 2\pi\frac{\phi_{\mathrm{E}}}{\phi_0\ e}. \tag{1.35}$$

Tests of this idea using neutron interferometry have been limited by the fact that for realizable elctric fields and neutron fluxes, the phase shift is of the order of milliradians [28]. Using atoms instead than neutrons and a different interferometric setup, Sangaster *et. al.* [29] have shown a clear linear dependance of the acquired Aharonov-Casher phase as function of the applied electric field.

In the recent years much attention has been paid to have signature of the Aharonov-Casher in solid state devices. The main candidate the generate coupling between the spin of the carriers and some external electric field is the Rashba SO interaction. This features can be simply demonstrated. If the Hamiltonian (1.10) is taken into account, this can be easily recast

$$\mathcal{H} = \frac{1}{2m}\left(\vec{p}-\frac{\alpha}{\hbar}\vec{\sigma}\times\hat{z}\right)^2 \tag{1.36}$$

where terms of the order $\mathcal{O}(\alpha^2)$ are neglected. Remember that the coupling constant α is proportional to the external electric field [9, 11, 12, 14], it is natural to candidate the Rashba SO interaction to show signature of the Aharonov-Casher effect.

Many devices have been proposed to utilize additional topological phases acquired by the electrons traveling through quantum circuits [30–33]. Nitta *et. al.* proposed a *spin-interference* device [30] allowing considerable modulation on the electric current. This device (see Fig. 1.14) is a one-dimensional ring connected with two external leads, made of semiconductor structure in which the Rashba SO interaction is the dominant spin-splitting mechanism.
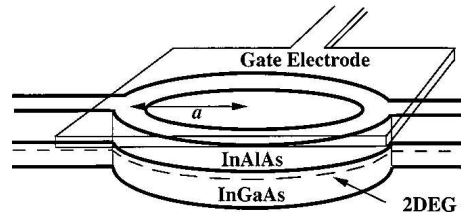
Figure 1.14: Schematic structure of a spin-interference device. The channel has a strong spin-orbit interaction. The Aharonov-Bohm ring area is covered with the gate electrode which controls the spin-orbit interaction.

The key idea was that, even in absence of an external magnetic field, the difference in the Aharonov-Casher phase acquired between carriers, traveling clockwise and counterclockwise, would produce interference effects in the spin-sensitive electron transport. By tuning the strength α of the SO interaction the phase difference could be changed, hence the conductance could be modulated.

Bibliography

[1] E.I. Rashba. Properties of semiconductors with an extremum loop I. cyclotron and combinational resonance in a magnetic field perpendicular to the plane of the loop. *Fiz. Tverd. Tela (Leningrad)*, 2:1224, 1960. [Sov. Phys. Solid State 2, 1109 (1960)].

[2] D. Stein, K. v. Klitzing, and G. Weimann. Electron spin resonance on GaAs-Al$_x$Ga$_{1-x}$As heterostructures. *Phys. Rev. Lett.*, 51:130, 1983.

[3] H. L. Stormer, Z. Schlesinger, A. Chang, D. C. Tsui, A. C. Gossard, and W. Wiegmann. Energy structure and quantized Hall effect of two-dimensional holes. *Phys. Rev. Lett.*, 51:126, 1983.

[4] Yu A. Bychkov and E.I. Rashba. Oscillatory effects and the magnetic susceptibility of carriers in inversion layers. *J. Phys. C: Solid State Phys.*, 17:6039, 1984.

[5] A. B. Fowler, F. F. Fang, W. E. Howard, , and P. J. Stiles. Magneto-oscillatory conductance in silicon surfaces. *Phys. Rev. Lett.*, 16:901, 1966.

[6] G. Dresselhaus. Spin-orbit coupling effects in zinc blende structures. *Phys. Rev.*, 100:580, 1955.

[7] M.I. D'yakonov and V. I. Perel. Spin relaxation of conduction electrons in noncentrosymetric semiconductors. *Fiz. Tverd. Tela*, 60:1954, 1971. [Sov. Phys. Solid State **33**, 1053 (1971)].

[8] E. A. de Andrada e Silva, G. C. La Rocca, and F. Bassani. Spin-split subbands and magneto-oscillations in III-V asymmetric heterostructures. *Phys. Rev. B*, 50:8523, 1994.

[9] J. Nitta, T. Akazaki, H. Takayanagi, and T. Enoki. Gate control of spin-orbit interaction in an inverted $In_{0.53}Ga_{0.47}As/In_{0.52}Al_{0.48}As$ heterostructure. *Phys. Rev. Lett.*, 78:1335, 1997.

[10] E. A. de Andrada e Silva, G. C. La Rocca, and F. Bassani. Spin-orbit splitting of electronic states in semiconductor asymmetric quantum wells. *Phys. Rev. B*, 55:16293, 1997.

[11] Th. Schäpers, G. Engels, J. Lange, Th. Klocke, M. Hollfelder, and H. Lüth. Effect of the heterointerface on the spin splitting in modulation doped $In_xGa_{1-x}As/InP$ quantum wells for $B \rightarrow 0$. *J. App. Phys.*, 83:4324, 1998.

[12] D. Grundler. Large Rashba splitting in InAs quantum wells due to electron wave function penetration into the barrier layers. *Phys. Rev. Lett.*, 84:6074, 2000.

[13] Patrick A. Lee and T. V. Ramakrishnan. Disordered electronic systems. *Rev. Mod. Phys.*, 57:287, 1985.

[14] J. B. Miller, D. M. Zumbühl, C. M. Marcus, Y. B. Lyanda-Geller, D. Goldhaber-Gordon, K. Campman, and A. C. Gossard. Gate-controlled spin-orbit quantum interference effects in lateral transport. *Phys. Rev. Lett.*, 90:076807, 2003.

[15] S.D. Ganichev, E.L. Ivchenko, V.V. Bel'kov, S.A. Tarasenko, M. Sollinger, D. Weiss, W. Wegscheider, and W. Prettl. Spin-galvanic effect. *Nature*, 417:153, 2002.

[16] S.D. Ganichev, V.V. Bel'kov, L.E. Golub, E.I. Ivchenko, Petra Schneider, S. Giglberger, J. Eroms, J. De Boeck, G. Borchs, W. Wegscheider andD. Weiss, and W. Prettl. Experimental separation of Rashba and Dresselhaus spin splittings in semiconductor quantum wells. *Phys. Rev. Lett.*, 92:256601, 2004.

[17] Supriyo Datta and Biswajit Das. Electronic analog of the electro-optic modulator. *Appl. Phys. Lett.*, 56:665, 1990.

[18] Mark Johnson and R. H. Silsbee. Spin-injection experiment. *Phys. Rev. B*, 37:5326, 1988.

[19] Francisco Mireles and George Kirczenow. Ballistic spin-polarized transport and Rashba spin precession in semiconductor nanowires. *Phys. Rev. B*, 64:024426, 2001.

[20] G. Schmidt, D. Ferrand, L. W. Molenkamp, A. T. Filip, and B. J. van Wees. Fundamental obstacle for electrical spin injection from a ferromagnetic metal into a diffusive semiconductor. *Phys. Rev. B*, 62:R4790, 2000.

[21] H. Ohno. Making nonmagnetic semiconductors ferromagnetic. *Science*, 281:951, 1998.

[22] Marco G. Pala, Michele Governale, Jurgen König, Ulrich Zülicke, and Giuseppe Iannaccone. Two-dimensional hole precession in an all-semiconductor spin field effect transistor. *Phys. Rev. B*, 69:045304, 2004.

[23] Y. Aharonov and D. Bohm. Significance of electromagnetic potentials in the quantum theory. *Phys. Rev.*, 115:485, 1959.

[24] G. Bergmann. Weak localization in thin films a time-of-flight experiment with conduction electrons. *Phys. Rep.*, 107:1, 1984.

[25] A. G. Aronov and Yu. V. Sharvin. Magnetic flux effects in disordered conductors. *Rev. Mod. Phys.*, 59:775, 1987.

[26] P. A. Lee, A. Douglas Stone, and H. Fukuyama. Universal conductance fluctuations in metals: Effects of finite temperature, interactions, and magnetic field. *Phys. Rev. B*, 35:1039, 1987.

[27] Y. Aharonov and A. Casher. Topological quantum effects for neutral particles. *Phys. Rev. Lett.*, 53:319, 1984.

[28] A. Cimmino, G. I. Opat, A. G. Klein, H. Kaiser, S. A. Werner, M. Arif, and R. Clothier. Observation of the topological Aharonov-Casher phase shift by neutron interferometry. *Phys. Rev. Lett.*, 63:380, 1989.

[29] Karin Sangster, E. A. Hinds, Stephen M. Barnett, and Erling Riis. Measurement of the Aharonov-Casher phase in an atomic system. *Phys. Rev. Lett.*, 71:3641, 1993.

[30] Junsaku Nitta, Frank E. Meijer, and Hideaki Takayanagi. Spin-interference device. *Appl. Phys. Lett.*, 75:695, 1999.

[31] D. Frustaglia, M. Hentschel, and K. Richter. Quantum transport in nonuniform magnetic fields: Aharonov-Bohm ring as a spin switch. *Phys. Rev. Lett.*, 87:256602, 2001.

[32] Radu Ionicioiu and Irene D'Amico. Mesoscopic Stern-Gerlach device to polarize spin currents. *Phys. Rev. B*, 67:041307, 2003.

[33] Jeng-Bang Yau, E. P. De Poortere, and M. Shayegan. Aharonov-Bohm oscillations with spin: Evidence for Berry's phase. *Phys. Rev. Lett.*, 88:146801, 2002.

Cauliflower is nothing but cabbage with a college education.

Mark Twain (1835-1910)

2

Spin-double refraction in two-dimensional electron gas

Introduction

The *spintronics* is a multidisciplinary field whose central subject is the active manipulation of the spin degrees of freedom in solid state system [1–3]. The control of spin takes account of either the population and the phase of spin of an ensemble of particle, or a coherent spin manipulation of a single or few-spin system. The goal of spintronics is to understand the interaction between the particle spin and its solid-state environments and to make useful devices using the acquired knowledge. Fundamental studies of spintronics include investigations of spin transport in electronic materials, as well as of spin dynamics and spin relaxation.

Generation of spin polarization usually means the creation of a nonequilibrium spin population. This can be achieved in several ways. One way is to orient spin by optical techniques in which circularly polarized photons transfer their angular momenta to electrons. In practical devices it is very important the electrical spin injection, in this case a magnetic electrode is connected to the sample. When the current drives spin-polarized electrons from the electrode to the sample, nonequilibrium spin accumulates there. The rate of spin accumulation depends on the spin relaxation. There are several mechanisms of spin relaxation, most involving spin-orbit coupling to provide spin-dependent potential, in combination with momentum scattering to provide a randomizing force. Typical time scale for spin relaxation in electronic system are measured in nanoseconds. Spin detection, also part of the generic spintronic scheme, typically relies on sensing the changes in the

signals caused by the presence of nonequilibrium spin in the system. The common goal in many spintronic devices is to maximize the spin detection sensitivity to the point of that it detects not the spin itself, but changes in the spin states.

The generic spintronic scheme is the Datta and Das spin-Field Effect Transistor (spin-FET) (see Sec. 1.4, pag. 13) based on the Rashba effect [4,5]. The Datta and Das ideas have inspired several investigations on spintronic devices that exhibit spin-valves effects [7–9]. In particular, the transport through a single interface ferromagnet-2DEG was considered claiming for an oscillatory spin-filtering due to a spin-dependent conductance [10–14]. However there are same intrinsic obstacles to use this technique due mainly to the conductivity mismatch between metals and semiconductors [15]. Some devices that achieve spin filtering without using ferromagnets have been proposed. I can mention among the others a mesoscopic Stern-Gerlach interferometric device based on non dispersive phases (Aharonov-Bohm and Rashba) [16] and a pair of quantum wires tunnel-coupled under Rashba SO interaction [17]. The attempt to avoid ferromagnets is the main aim of this chapter. It will be show that a spin-dependent conductance can be achieved by using large point contact and spin-unpolarized electrons. In order to support this claim, it is presented a detailed study of the scattering that an electron in a 2DEG undergoes when it passes from a region without the SO coupling to a region where the SO coupling is present. As starting point the electron is considered in a pure spin state fixed by the magnetization of a semimetallic ferromagnetic lead, then the results are applied to the case of unpolarized electrons injected by a metallic lead, that is in a statistical mixture of spin up and spin down. The attention is focused on the scattering with an incidence angle not orthogonal to the interface since it is expected to give spin dependent contributions to the conductance of a large point contact. Two different spin-polarized output channels appear. The behavior of electron spin in such scattering can be compared with the polarization of the light in a biaxial crystal: the incident ray splits, within the crystal, in two rays (ordinary and extraordinary) whose polarizations are orthogonal. The electron motion within the hybrid system is assumed to be ballistic and the conductance of a wide point contact separating the two zones can be calculated by summing up the transmission coefficients obtained varying the allowed incidence angles from 0 (normal incidence) to limit angles at which the two output spin channels are completely reflected. The conductance is made by different spin up and spin down contributions and depends on the spin state of the incoming electrons. The injection of electrons in the Rashba zone through the point contact is a way to spin-polarize the 2DEG electrons because the output spin up current is different from the spin down current.

The results presented in this chapter has been published in the reference [18].

The chapter is organized in the following way. In the first section I resume the properties of a 2DEG with Rashba SO coupling in the (x, z) plane. In the second one I analyze the electron scattering on the interface separating the (x, z) plane in two side: one without Rashba SO coupling and one where Rashba SO coupling is present. In the third section I present the calculation of the conductance of the point contact conductance separating the two previous sides of the (x, z) plane. In the last two sections I report the linear system of the wave amplitudes as stems out from the boundary conditions at the interface and a brief classification the Rashba Hamiltonian symmetry.

2.1 2DEG with Rashba SO coupling

In this section I recall the characteristics of a 2DEG with Rashba SO coupling occupying the (x, z) plane. I consider the Hamiltonian (1.10)

$$\mathcal{H} = \frac{\vec{p}}{2m_{\mathrm{S}}} + \frac{\alpha}{\hbar}(\vec{\sigma} \times \vec{p}) \cdot \hat{y}, \tag{2.1}$$

where m_{S} is the electron effective mass in the semiconductor. Contrary to the form (1.10), here the 2DEG is in the (x, z) plane and the electric field in the $\hat{y}$ direction. The electron eigenstates corresponding to the split energy levels $\mathcal{E}_{\pm}$ are the spinors

$$\begin{aligned} \psi_+(x, z) &= e^{i(k_x x + k_z z)} \begin{pmatrix} \cos\theta \\ \sin\theta \end{pmatrix} \\ \psi_-(x, z) &= e^{i(k_x x + k_z z)} \begin{pmatrix} -\sin\theta \\ \cos\theta \end{pmatrix} \end{aligned} \tag{2.2}$$

whose eigenvalues (1.11) are

$$\mathcal{E}_{\pm} = \frac{\hbar^2}{2m_{\mathrm{S}}} \left(k_x^2 + k_z^2 \right) \pm \alpha \sqrt{k_x^2 + k_z^2}. \tag{2.3}$$

Here

$$\theta = \arctan\left[\frac{k_x}{k_z} - \sqrt{\frac{k_x^2}{k_z^2} + 1} \right]. \tag{2.4}$$

If $k = \sqrt{k_z^2 + k_z^2}$ is the modulus of the momentum, and

$$\phi = \arctan\frac{k_z}{k_x}$$

its direction in the plane, then

$$\theta = -\frac{\phi}{2} \tag{2.5}$$

and

$$\mathcal{E}_\pm = \frac{\hbar^2}{2m_{\mathrm{S}}} \left(k^2 \pm 2k_{\mathrm{SO}}k\right) \quad \text{with} \ \ k_{\mathrm{SO}} = \frac{m_{\mathrm{S}}\alpha}{\hbar^2}. \tag{2.6}$$

One can see that the spin degeneracy on the Fermi surface is lifted but the Rashba term is not able to produce a spontaneous spin polarization of the electron states. For given energy there are two different values of k with any spin projection. The meaning of equation (2.5) is: when the direction of electron motion is chosen fixing its k_x and k_z, then it is automatically assigned the electron spin polarization state. If $\vec{k}$ is directed along x then $\phi = 0$ and ψ_+, ψ_- describe the pure "spin up" and "spin down" states in z direction, that is fixed as the spin quantization direction. It is important to note that the account for the SO interaction in the Hamiltonian (2.1) reduces the rank of the direct space group twice [19]: space rotation of 4π is needed to get the same spinor.

If I denote the complex conjugation operator as $\widehat{K}_0$:

$$\widehat{K}_0 f = f^*.$$

The time reversal operator [20] for the special case of a particle of spin $\frac{1}{2}$ takes the form

$$\widehat{K} = -i\sigma_y \widehat{K}_0$$

and

$$\widehat{K} \begin{pmatrix} f_1 \\ f_2 \end{pmatrix} = \begin{pmatrix} -f_2^* \\ f_1^* \end{pmatrix}. \tag{2.7}$$

It commutes with $\mathcal{H}$ [20]. Applying $\widehat{K}$ to the degenerate eigenstates ψ_+, ψ_- it is possible to see that one is the time reversed of the other

$$\widehat{K}\psi_+ = -\psi_-^*, \quad \widehat{K}\psi_- = \psi_+^* \tag{2.8}$$

whereas their spinor parts s_+ and s_-

$$s_+ = \begin{pmatrix} \cos\phi/2 \\ -\sin\phi/2 \end{pmatrix}, \ \ s_- = \begin{pmatrix} \sin\phi/2 \\ \cos\phi/2 \end{pmatrix}$$

are one orthogonal to the other.

Finally I stress that the SO interaction can be attributed to a magnetic field parallel to the plane and orthogonal to the wave vector $\vec{k}$. This magnetic

field couples with the spin magnetic moment and it aligns the spin along the direction orthogonal to $\vec{k}'$ [4,5]. The spin component in this direction is

$$\sigma_\perp = -\sin\phi \cdot \sigma_x + \cos\phi \cdot \sigma_z = \begin{pmatrix} \cos\phi & -\sin\phi \\ -\sin\phi & -\cos\phi \end{pmatrix}$$

and s_+ and s_- are eigenstates of $\sigma_\perp$

$$\sigma_\perp s_+ = s_+ \quad ; \quad \sigma_\perp s_- = -s_-$$

2.2 Scattering at an interface with a seminfinite Rashba 2DEG

Now I assume that in the (x, z) plane the Rashba SO coupling is restricted to $x > 0$ region and an electron with a momentum $\vec{k} \equiv (k\cos\gamma, k\sin\gamma)$ and an energy $\mathcal{E} = \hbar^2 k^2/2m_\mathrm{F}$ is incoming in the pure spin state $|\delta\rangle$ from the no Rashba (NR) zone ($x < 0$ and where m_F is the electron effective mass in the ferromagnetic material). The pure spin state can be described as

$$|\delta\rangle = \cos\delta|\uparrow\rangle + \sin\delta|\downarrow\rangle$$

where the ket $|\uparrow\rangle$ indicates the spin up state with $s_z = 1/2$ and $|\downarrow\rangle$ is the spin down state with $s_z = -1/2$. The incident wave function is

$$\psi_i = e^{ik(x\cos\gamma + z\sin\gamma)}|\delta\rangle$$

whereas the reflected wave function is

$$\psi_r = e^{ik(-x\cos\gamma + z\sin\gamma)} \left(r_\uparrow|\uparrow\rangle + r_\downarrow|\downarrow\rangle \right).$$

In the output, within the Rashba (R) zone ($x > 0$),there are a superposition of the two states of the spin split bands (2.6) $\mathcal{E}_\pm(k')$ degenerate with the same energy $\bar{\mathcal{E}}$. The energy conservation fixes two values for the modulus of the wave vector k', and from

$$\mathcal{E}_\pm(k') \equiv \bar{\mathcal{E}} = \frac{\hbar^2 k^2}{2m_\mathrm{F}},$$

it is possible to obtain

$$k' = \sqrt{\mu k^2 + k_\mathrm{SO}^2} \mp k_\mathrm{SO} = k_\pm \quad (\mu = \frac{m_\mathrm{S}}{m_\mathrm{F}}).$$
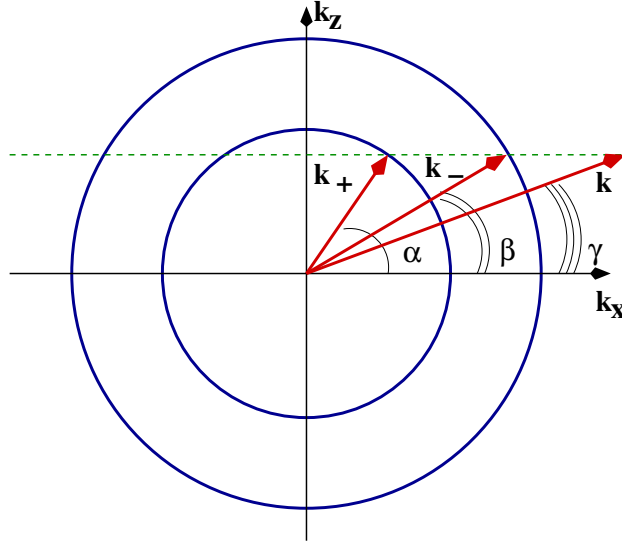
Figure 2.1: The vectors $\vec{k}_+$, $\vec{k}_-$ and $\vec{k}$ in k-space and the angles α, β and γ that they form with x direction normal to the interface. The two circles are the Fermi contour at the energy $\hbar^2 k^2 / 2m_\mathrm{F}$.

The directions of $\vec{k}_+$ and $\vec{k}_-$ are fixed by the conservation of the momentum parallel to the interface

$$k_{+,x} = k_{-,x} = k_x.$$

Now the angle ϕ for the mode $+$ takes a value α different from its value β for the mode $-$. The angle α of $\vec{k}_+$, the angle β of $\vec{k}_-$ and γ of $\vec{k}$ with the x axis are linked up by the relationship

$$k_+ \sin\alpha = k_- \sin\beta = k\sin\gamma.$$

The transmitted wave function at $x > 0$ is the superposition of the transmitted ones in both the modes $(+)$ and $(-)$

$$\psi_t = t_+ e^{ik_+(x\cos\alpha + z\sin\alpha)}\begin{pmatrix} \cos\alpha/2 \\ -\sin\alpha/2 \end{pmatrix} + t_- e^{ik_-(x\cos\beta + z\sin\beta)}\begin{pmatrix} \sin\beta/2 \\ \cos\beta/2 \end{pmatrix}. \quad (2.9)$$

The Fig. 2.1 shows the output angles α and β. The two modes have the same energy $\bar{\mathcal{E}}$ along the two circles. The conservation of k_z gives α and β as functions of the incidence angle γ. Only when the incidence is normal, with $\gamma = 0$, the outgoing wave functions $(+)$ and $(-)$ go in the same direction with $\alpha = \beta = 0$ and with the two different wave vectors k_+ and k_-. In the other cases they go along two different directions. This phenomenon is the analog of the double refraction that appears in biaxial crystals [21] with two

outgoing divergent rays. The birefringence arises when the characteristics of electromagnetic propagation depend on the directions of propagation and polarization of the light wave. In this case the spin of the electron wave functions behaves like the polarization of the light. It is possible to notice that the spin orientations of the outgoing waves $(+)$ and $(-)$ are fixed by the output angles α and β according to the equation (2.5). The crossing of the interface changes the spin state. The electron exits in the R zone in a superposition of the two spin states

$$\begin{pmatrix} \cos\alpha/2 \\ -\sin\alpha/2 \end{pmatrix} \quad \text{and} \quad \begin{pmatrix} \sin\beta/2 \\ \cos\beta/2 \end{pmatrix}.$$

The output angles α and β are functions of k, γ, k_0 and μ and they do not depend on the incident spin orientation angle δ.

The mode $(+)$ has the limit angle

$$\gamma_0 = \arcsin \frac{k_+}{k} \tag{2.10}$$

and, for $\gamma > \gamma_0$, this mode is totally reflected and it vanishes exponentially for $x > 0$. Here and in the following I take $0 < \mu < 1$: that is the effective mass in the R zone is less than the effective mass in the injection electrode in NR zone. When $k/k_{\mathrm{SO}} < 2/(1-\mu)$, the mode $(-)$ is always transmitted up to grazing incidence at $\gamma = \pi/2$. Increasing the kinetic energy with respect to SO coupling when $k/k_{\mathrm{SO}} > 2/(1-\mu)$, a second limit angle appears

$$\gamma_1 = \arcsin \frac{k_-}{k} > \gamma_0 \tag{2.11}$$

and for $\gamma > \gamma_1$, there is the total reflection (both the modes vanish for $x > 0$). When the strength of SO coupling goes to zero, γ_0 and γ_1 tend to the common limit $\arcsin\sqrt{\mu}$: lighter is the effective mass within the 2DEG nearer to the normal are the propagation directions $\alpha < \gamma_0$ and $\beta < \gamma_1$ allowed into R zone. The Fig. 2.2 shows the limit angles as a function of k/k_{SO}. We note that when $\gamma > \gamma_0$ then

$$\sin\alpha = \frac{k}{k_+}\sin\gamma > 1$$

and α becomes complex

$$\alpha = \frac{\pi}{2} - i\alpha'.$$

The correct determination for its imaginary part $-\alpha'$ is obtained when $\alpha' > 0$ because

$$\sin\alpha = \cosh\alpha' \quad \text{and} \quad \cos\alpha = i\sinh\alpha'.$$
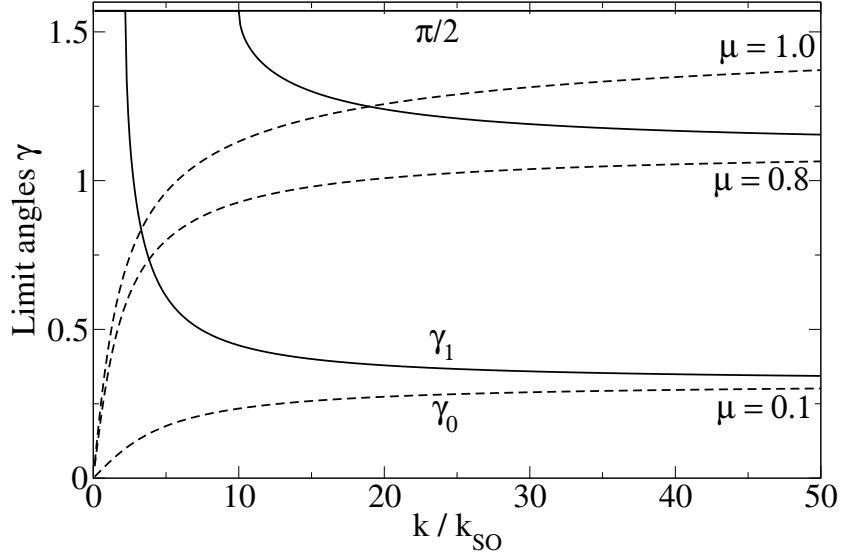
Figure 2.2: The limit angles γ_0 of $+$ mode (dashed line) and γ_1 of $-$ mode (full line), for three different values of mass ratio μ, as functions of k/k_0. For γ above γ_1 the total reflection occurs.

The mode $(+)$ becomes a vanishing wave decaying along x axis whereas it is a propagating wave along z direction

$$e^{-k_+ x \sinh \alpha'} e^{ik_+ z \cosh \alpha'} \begin{pmatrix} \cos\left(\frac{\pi}{4} - \frac{i\alpha'}{2}\right) \\ -\sin\left(\frac{\pi}{4} - \frac{i\alpha'}{2}\right) \end{pmatrix}.$$

When $\gamma > \gamma_1$, $\beta = \pi/2 - i\beta'$ and both the modes are damped within the 2DEG: the incident wave is totally reflected.

To calculate the transmitted amplitudes t_+ and t_- in the $(+)$ and $(-)$ modes the hybrid system Hamiltonian is introduced

$$\mathcal{H}_{\text{NR-R}} = \vec{p}\frac{1}{2m(x)}\vec{p} + \frac{k_{\text{SO}}(x)m(x)}{\hbar^2}(\vec{\sigma} \times \vec{p})_y - i\sigma_z\frac{1}{2}\frac{\partial k_{\text{SO}}(x)}{\partial x} + U\delta(x). \quad (2.12)$$

I am assuming that the mass and the strength of SO coupling are piecewise constant

$$\begin{aligned} \frac{1}{m}(x) &= \frac{\vartheta(-x)}{m_{\text{F}}} + \frac{\vartheta(x)}{m_{\text{S}}} \\ k_{\text{SO}}(x) &= k_{\text{SO}}\ \vartheta(x), \end{aligned} \quad (2.13)$$

where $\vartheta(x)$ is the step function. The third term in (2.12) is needed to get an hermitian operator $\mathcal{H}_{\text{NR-R}}$ and the fourth term regulates the transparency

of the interface. The spinor eigenstate ψ of $\mathcal{H}_{\text{NR-R}}$ is continuous whereas its derivative has a discontinuity fixed by the strength $u - i\sigma_z k_{\text{SO}}$ of the Dirac delta in $x = 0$

$$\psi(0^+) = \psi(0^-) \tag{2.14}$$
$$\frac{\partial \psi(0^+)}{\partial x} - \mu \frac{\partial \psi(0^-)}{\partial x} = (u - ik_{\text{SO}}\sigma_z)\psi(0).$$

This matching conditions give a four times four linear system for the amplitudes t_+, t_-, $r_\uparrow$ and $r_\downarrow$ that is reported in the Sec. 2.3.

The normal incidence case deserves a special care [12,22,23]. When $\gamma = 0$ then $\alpha = \beta = 0$, the mode $(+)$ is in the spin up state $|\uparrow\rangle$ whereas the mode $(-)$ is in spin down state $|\downarrow\rangle$. In this case σ_z is a motion constant and a spin up $|\uparrow\rangle$ state goes entirely in $(+)$ mode being zero the amplitude transmitted in $(-)$ mode. A spin down state $|\downarrow\rangle$ goes entirely in $(-)$ mode with zero amplitude in $(+)$ mode. When $\gamma = 0$ with an incoming spin state $|\delta\rangle$ the transmission amplitudes are

$$t_+ = \frac{2\mu k \cos \delta}{k_+ + k_{\text{SO}} + iu + \mu k}, \qquad t_- = \frac{2\mu k \sin \delta}{k_- - k_{\text{SO}} + iu + \mu k}$$

but $k_+ + k_{\text{SO}} = k_- - k_{\text{SO}} = \sqrt{\mu k^2 + k_{\text{SO}}^2}$ so that $t_+ = t_-$ and the transmitted spinor is

$$\psi_t(0^-) = \frac{2\mu k}{\sqrt{\mu k^2 + k_{\text{SO}}^2} + iu + \mu k}|\delta\rangle.$$

It is important to point out that the passage of the interface does not change the spin state. When $x > 0$ the spinor becomes $\exp(ik_+ x)\cos \delta |\uparrow\rangle + \exp(ik_- x)\sin \delta |\downarrow\rangle$ and the propagation along a distance L into the Rashba region gives the phase shift on which is based the Datta and Das spin-FET. The inefficiency of the scattering at normal incidence to modify the spin state stems out from the identity

$$k_+ + k_{\text{SO}} = k_- - k_{\text{SO}}$$

that comes from the following property of the Hamiltonian (2.12): changing the sign of k_{SO}, the two modes $(+)$ and $(-)$ are interchanged one with the other. The symmetry of the Hamiltonian $\mathcal{H}_{\text{NR-R}}$ is classified in the Sec. 2.3. When $\gamma \neq 0$ the amplitudes t_+, t_-, $r_\uparrow$ and $r_\downarrow$ depend on k, γ, k_{SO}, μ and on δ too, that is on the incoming spin state.

The square moduli of the transmitted amplitudes $|t_\pm(\delta)|^2$ are shown in Fig. 2.3 when γ is between 0 and $\pi/2$. In Fig. 2.3 Panel a) is shown that $|t_+(0)|^2$ and $|t_-(\pi/2)|^2$ start from the same value for $\gamma = 0$ but become
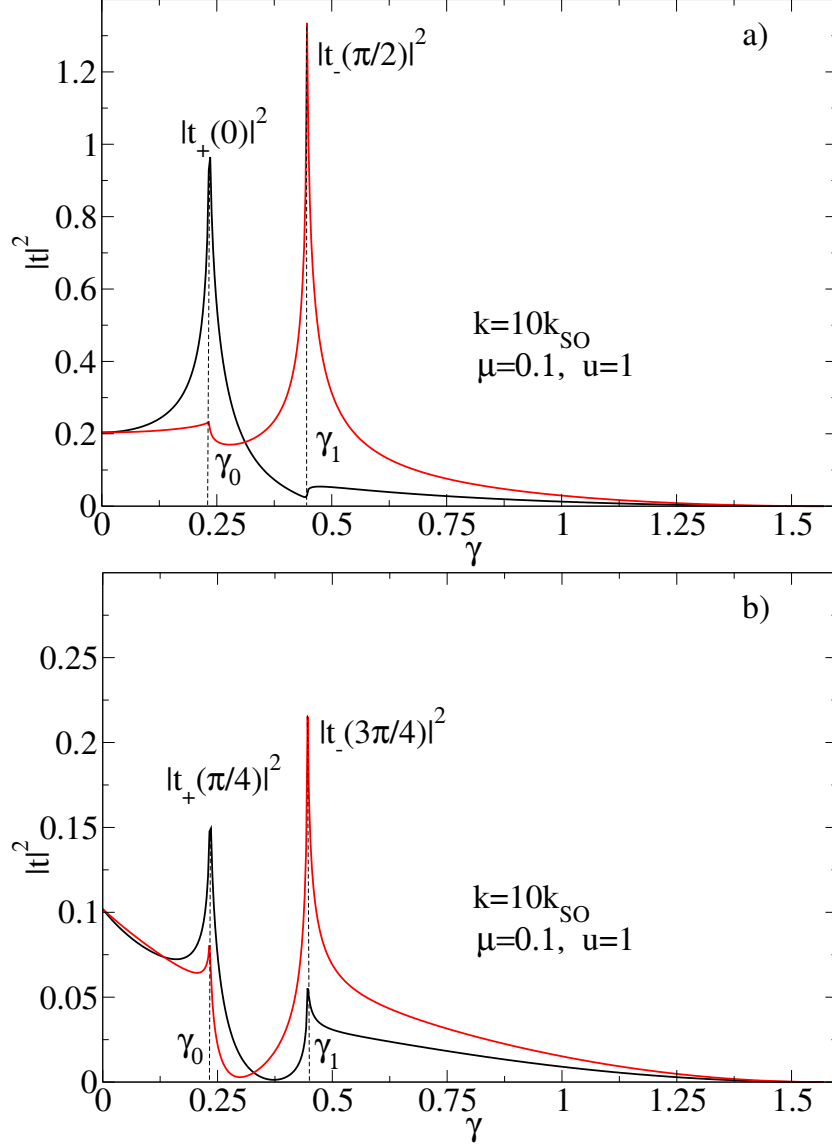
Figure 2.3: The squared moduli of the transmitted amplitudes for two couples of orthogonal spin polarizations. The cusps sign the passage through the limit angles. Panel a): The amplitudes $t_+ (0)$ and $t_- (\pi/2)$ refer to electrons injected in the R zone by a ferromagnet with a magnetization parallel or antiparallel to the z axis respectively. Panel b): The amplitudes $t_+ (\pi/4)$ and $t_- (3\pi/4)$ refer to electrons injected in the R zone by a ferromagnet with a magnetization orthogonal to the interface, that is antiparallel or parallel to the x axis respectively.

different when the incidence angle increases towards $\pi/2$. In Fig. 2.3 Panel b) is reported the same behavior for a different pair of orthogonal spins $\delta = \pi/4, 3\pi/4$. The derivatives of $|t_\pm(\delta)|^2$ jump in γ_0 and then in γ_1 when the character of the mode propagation changes. The cusps sign the limit angles.

In order to calculate the transmission coefficient T it is necessary to evaluate the probability current density

$$\vec{j}(x) = \begin{cases} \Re\left\{\psi^\dagger \vec{p} \psi\right\} & x < 0 \\ \Re\left\{\psi^\dagger \left[\vec{p} + \hbar k_{\mathrm{SO}}\left(\widehat{y} \times \vec{\sigma}\right)\right]\psi\right\} & x > 0 \end{cases} \tag{2.15}$$

whose x-components are

$$\begin{aligned} j_{xl} &= \hbar k \cos\gamma \left(1 - |r_\uparrow|^2 - |r_\downarrow|^2\right) m_{\mathrm{F}}^{-1} \quad \text{for} \quad x < 0 \\ j_{xr} &= j_{x+} + j_{x-} \quad\quad\quad\quad\quad\quad\quad\quad\ \text{for} \quad x > 0 \end{aligned} \tag{2.16}$$

with

$$\begin{aligned} j_{x+} &= \hbar\left(k_+ + k_{\mathrm{SO}}\right)\cos\alpha \, |t_+|^2 m_{\mathrm{S}}^{-1} \\ j_{x-} &= \hbar\left(k_- - k_{\mathrm{SO}}\right)\cos\beta \, |t_-|^2 m_{\mathrm{S}}^{-1} \end{aligned} \tag{2.17}$$

The boundary conditions (2.14) assure the continuity of the flux j_x as can be verified by a straightforward calculation from the Eqs. (2.16-2.17)

$$j_{xl} = j_{x+} + j_{x-} = j_{xr}.$$

When $\gamma < \gamma_0$ both the modes propagate in R zone. When $\gamma_0 < \gamma < \gamma_1$ only the $(-)$ mode remains. The transmission coefficient is the ratio of j_{xr} with the incident flux $j_i = \hbar k \cos\gamma m_{\mathrm{F}}^{-1}$,

$$T = \frac{j_{xr}}{j_i},$$

whereas the reflection coefficient is $R = (j_i - j_{xr})/j_i$:

$$\begin{aligned} T_+(\delta, \gamma) &= (k_+ + k_{\mathrm{SO}})\cos\alpha|t_+|^2\vartheta(\gamma_0 - \gamma)(\mu k \cos\gamma)^{-1} \\ T_-(\delta, \gamma) &= (k_- - k_{\mathrm{SO}})\cos\beta|t_-|^2\vartheta(\gamma_1 - \gamma)(\mu k \cos\gamma)^{-1} \\ T(\delta, \gamma) &= T_+(\delta, \gamma) + T_-(\delta, \gamma) \\ R(\delta, \gamma) &= |r_\uparrow|^2 + |r_\downarrow|^2. \end{aligned} \tag{2.18}$$

When γ overcomes γ_1, $T(\delta, \gamma) = 0$ and $R(\delta, \gamma) = 1$. The flux is conserved because in all the cases

$$T(\delta, \gamma) + R(\delta, \gamma) = 1.$$

The transmission coefficient as a function of γ has a first higher step up to γ_0 followed by a lower step that ends in γ_1. The Fig. 2.4 Panel a) shows how the shape and the height of the two steps vary with the spin polarization angle δ. At low values of μ, when the electrons in 2DEG are lighter, the propagation in the $x > 0$ region is allowed at angles nearer to the normal. At equal masses, $\mu = 1$, the passage is allowed up to grazing incidence and the steps appear more squared (see Fig. 2.4). The second step tends to disappear around $\delta = 3\pi/4$ and has the maximum height around $\delta = \pi/4$. The Fig. 2.4 refers to the case of an higher Fermi wave vector k. Obviously when $k/k_{\text{SO}} \to \infty$, $T = 1$ for γ from 0 to $\pi/2$ but the second step is again present for k greater then k_{SO} of two magnitude orders.

The transmission of the interface can be analyzed not only in terms of the $(+)$ and $(-)$ modes, but also separating the output probability current in spin up and a spin down parts. The spin up $T_\uparrow(\delta)$ and the spin down $T_\downarrow(\delta)$ transmission coefficients are

$$
\begin{aligned}
T_\uparrow(\delta, x) \;=\; & \frac{1}{\mu k \cos \gamma} \Big\{ |t_+|^2 \cos^2 \frac{\alpha}{2} \left(k_+ \cos \alpha + k_{\text{SO}} \right) \\
& + |t_-|^2 \sin^2 \frac{\beta}{2} \left(k_- \cos \beta + k_{\text{SO}} \right) + |t_+||t_-| \cos \frac{\alpha}{2} \sin \frac{\beta}{2} \\
& \left(k_+ \cos \alpha + k_- \cos \beta + 2 k_{\text{SO}} \right) \cos \left[\left(k_+ \cos \alpha - k_- \cos \beta \right) x + \tau_+ - \tau_- \right] \Big\}
\end{aligned}
\tag{2.19}
$$

$$
\begin{aligned}
T_\downarrow(\delta, x) \;=\; & \frac{1}{\mu k \cos \gamma} \Big\{ |t_+|^2 \sin^2 \frac{\alpha}{2} \left(k_+ \cos \alpha - k_{\text{SO}} \right) \\
& + |t_-|^2 \cos^2 \frac{\beta}{2} \left(k_- \cos \beta - k_{\text{SO}} \right) - |t_+||t_-| \sin \frac{\alpha}{2} \cos \frac{\beta}{2} \\
& \left(k_+ \cos \alpha + k_- \cos \beta - 2 k_{\text{SO}} \right) \cos \left[\left(k_+ \cos \alpha - k_- \cos \beta \right) x + \tau_+ - \tau_- \right] \Big\}.
\end{aligned}
\tag{2.20}
$$

Here $t_+ = |t_+| \exp(i\tau_+)$ and $t_- = |t_-| \exp(i\tau_-)$. Now the spin precession gives a spatial modulation of the transmission coefficients $T_\uparrow$ and $T_\downarrow$, whereas the transmission in $(+)$ and $(-)$ modes, T_+ and T_-, are independent on x. Obviously the oscillations in $T_\uparrow$ and $T_\downarrow$ are opposite in phase and

$$
T_\uparrow + T_\downarrow = T_+ + T_- = T.
$$

The Fig. 2.5 Panel a) shows the oscillations of $T_\uparrow$ and $T_\downarrow$ when the incidence angle is below the first limit angle γ_0 and the spin in entrance is down. The Fig. 2.5 Panel b) shows what happens when the incidence angle is above γ_0. Near to the interface the contribution of the evanescent waves of mode $+$ appears and far from $x = 0$ we have $T_\uparrow + T_\downarrow = T_-$ and all the transmission
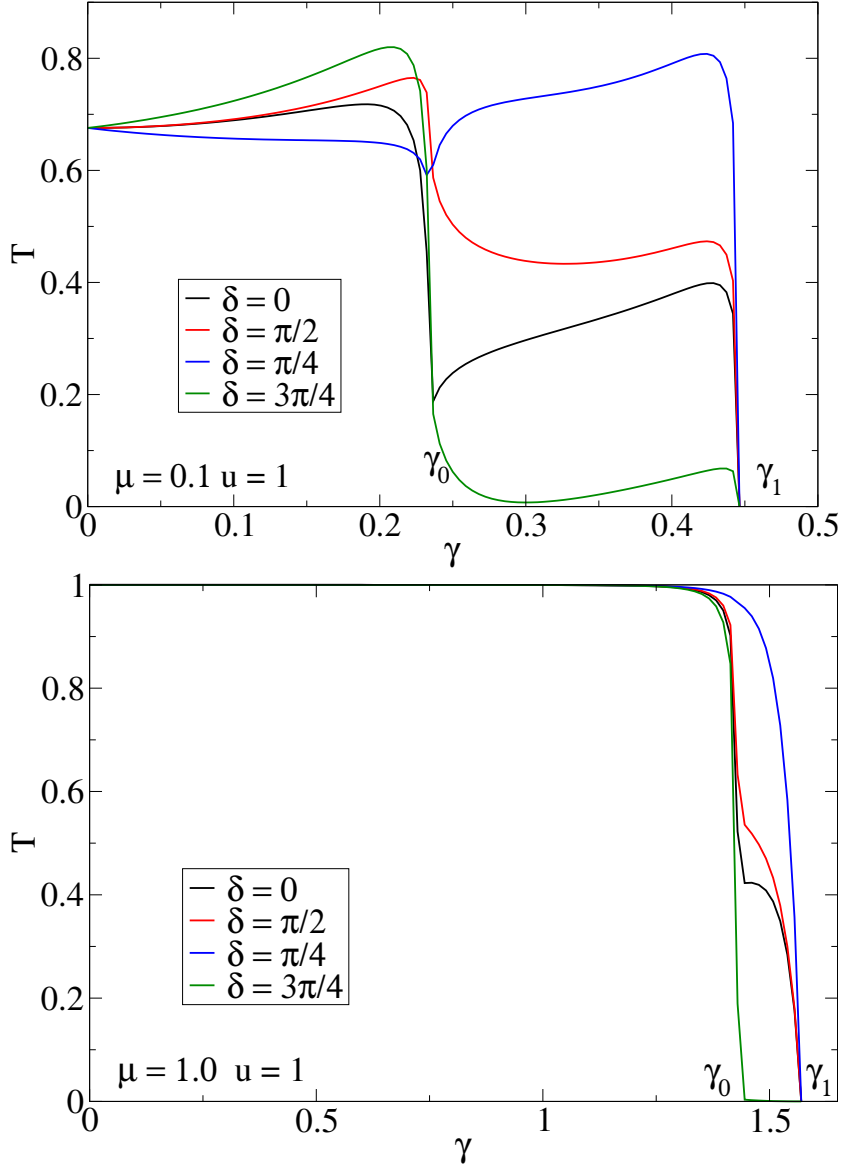
Figure 2.4: The two steps of the transmission coefficient T, for different values of the incoming electron's spin δ. Panel a) $k = 10k_{\mathrm{SO}}$, $\mu = 0.1$ and $u = 1$. The second step tends to disappear for $\delta = 3\pi/4$ and has the same height of the first one when $\delta = \pi/4$. Panel b) $k/k_{\mathrm{SO}} = 100$, $\mu = 1.0$ and $u = 1$. In the limit $k/k_{\mathrm{SO}} \to \infty$, $T = 1$ for $0 < \gamma < \pi/2$.

coefficients are independent on x. The incoming spin is up and far from the interface the transmitted spin is mostly down: at a distance large enough, the interface is able to turn down the spin.

An incidence out of the normal, with $\gamma \neq 0$, has been recently discussed for small incidence angles [22, 23]. Here I have presented a full analysis at any incidence angle focusing the attention on the birefringence.

The previous analysis applies when the incoming wave function is in the *pure* spin state $|\delta\rangle$. Now it is taken account of the scattering when the incoming electronic spin is in the unpolarized *statistical mixture*. When the electron is unpolarized, its state is not completely known. Therefore it can be represented with the density matrix operator [24]

$$\rho_U = \frac{1}{2}|\uparrow\rangle\langle\uparrow| + \frac{1}{2}|\downarrow\rangle\langle\downarrow| \tag{2.21}$$

whereas the density operator for the pure state is

$$\rho_P = |\delta\rangle\langle\delta|.$$

The mean value of an operator A for the statistical mixture ρ_U and for the pure spin state ρ_P is given by $\langle A\rangle_U = \mathrm{Tr}[\rho_U A]$ and $\langle A\rangle_P = \mathrm{Tr}[\rho_P A]$) respectively. Therefore for the spin components it is possible to obtain

$$\langle\sigma_x\rangle_P = \sin 2\delta, \quad \langle\sigma_y\rangle_P = 0, \quad \langle\sigma_z\rangle_P = \cos 2\delta \;\; ; \;\; 0 \leq \delta \leq \pi$$

in the pure state case and

$$\langle\sigma_x\rangle_U = \langle\sigma_y\rangle_U = \langle\sigma_z\rangle_U = 0$$

for the unpolarized statistical mixture: in this case the mean values of all the spin components of the incident wave function are null. This corresponds to have the injection in the Rashba 2DEG using a n-doped semiconductor contact without ferromagnets. The density current probabilities for the incoming spin states $|\uparrow\rangle$ and $|\downarrow\rangle$ sum up in a classical way without quantum interference with equal weights $1/2$ and $1/2$: all the necessary are the four transmission coefficients of the equations (2.19,2.20) $T_\uparrow(0)$, $T_\uparrow(\frac{\pi}{2})$, $T_\downarrow(0)$ and $T_\downarrow(\frac{\pi}{2})$. The previous notation indicate (0) as $(\uparrow)$ and $(\frac{\pi}{2})$ as $(\downarrow)$ in such a way that the indexes refer to outgoing spins whereas the incoming spins are shown between the parentheses. Now it is possible to compare the overall transmission coefficient in spin up state

$$\frac{T_\uparrow(\uparrow) + T_\uparrow(\downarrow)}{2}$$
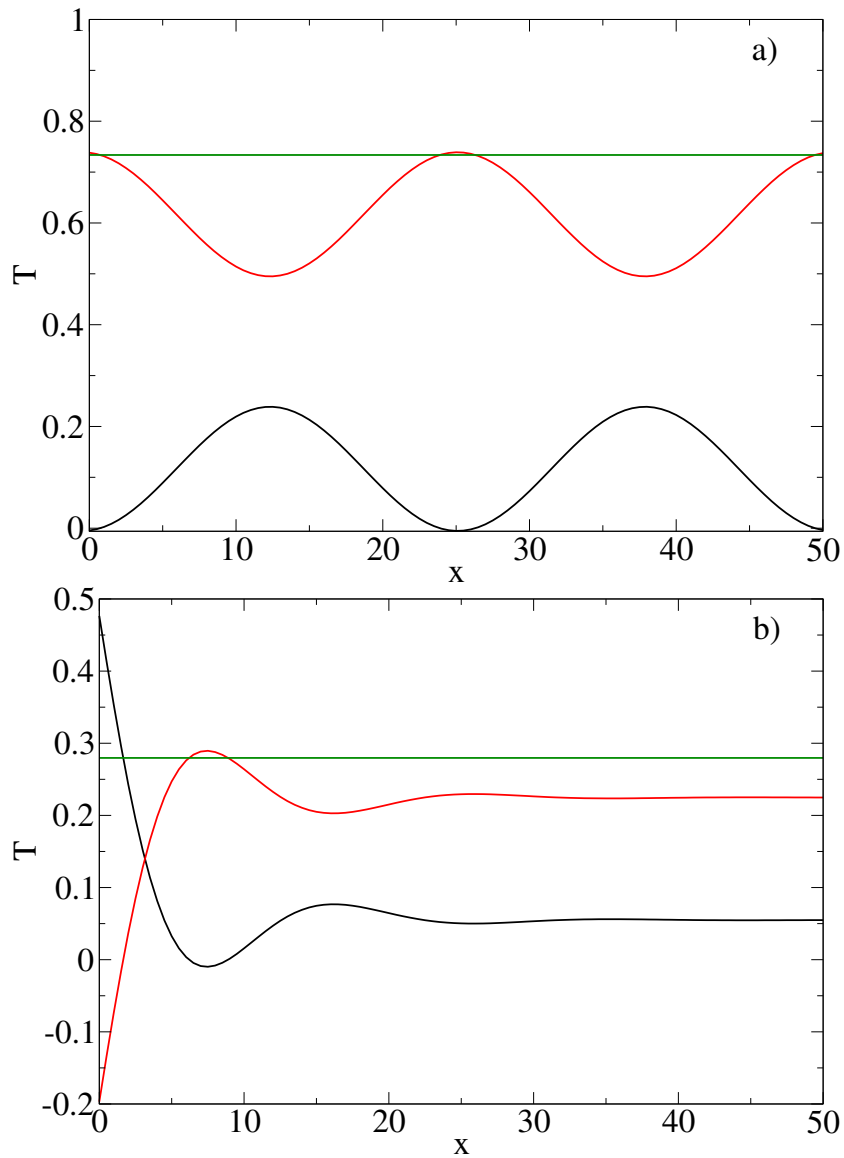
Figure 2.5: The transmission coefficients $T_\uparrow$ (black line), $T_\downarrow$ (red line) and $T_\uparrow + T_\downarrow$ (green curve) as function of the distance from the interface for $k/k_0 = 10$, $\mu = 0.1$ and $u = 1$. The Panel a) and b) refer, respectively, to incidence angles γ less than and greater than the first limit angle γ_0.
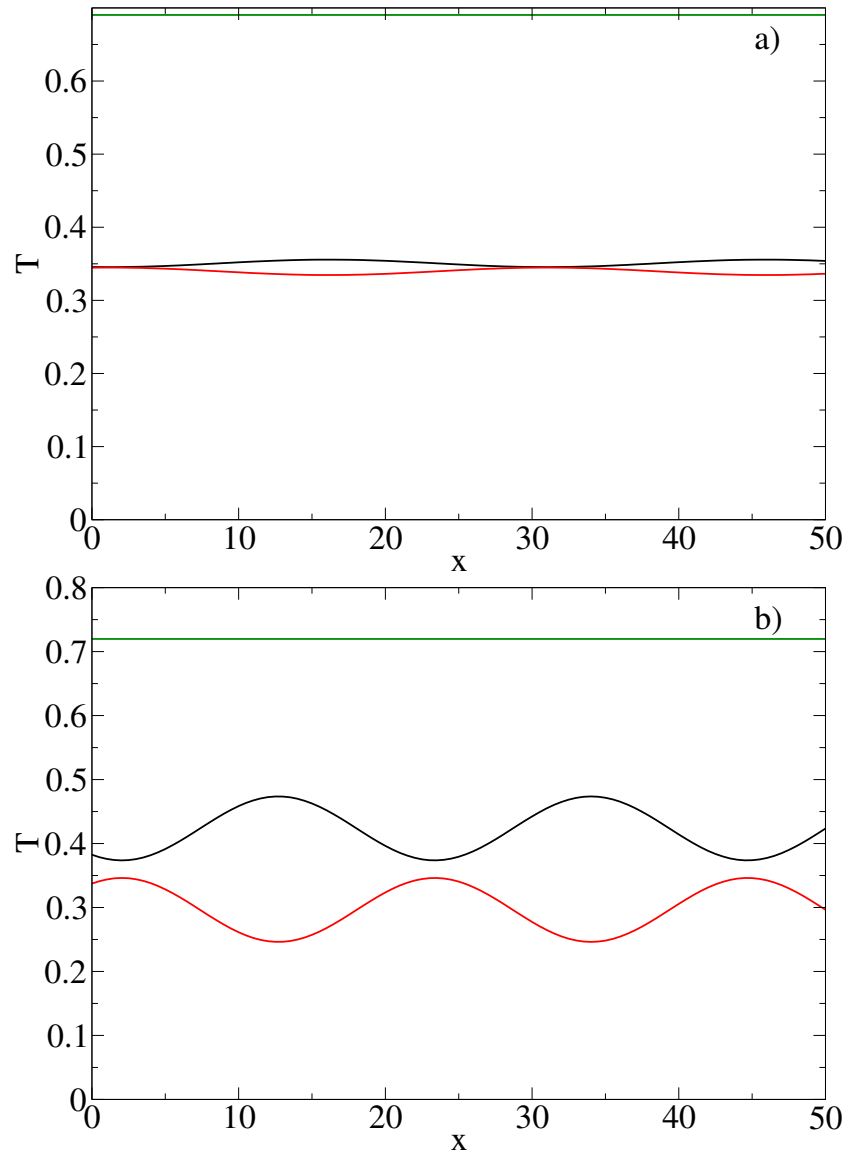
Figure 2.6: The transmission coefficients $(T_\uparrow(\uparrow)+T_\uparrow(\downarrow))/2$ (black line), $(T_\downarrow(\uparrow) + T_\downarrow(\downarrow))/2$ (red line) and $(T_\uparrow(\uparrow) + T_\uparrow(\downarrow) + T_\downarrow(\uparrow) + T_\downarrow(\downarrow))/2$ (green line) as function of the distance form the interface for an unpolarized incident wave with $k/k_{\mathrm{SO}} = 10$, $\mu = 0.1$ and $u = 1$. The Panel a) is relative to an almost normal incidence, Panel b) refers to γ a little below γ_0.

with the overall transmission coefficient in spin down state

$$\frac{T_\downarrow(\uparrow) + T_\downarrow(\downarrow)}{2}.$$

The Fig. 2.6 Panel a) shows the transmission of the unpolarized state in up and down spin channels when the incidence is near to the normal, whereas the Fig. 2.6 Panel b) shows the transmission coefficients at a larger incidence angle γ, a little below the first limit angle. In the first case the interface is not able to discriminate the spins, in the second one it introduces a polarization. The oblique scattering, due to the presence of the birefringence, gives in output a spin up probability current different from spin down probability current.

2.3 Conductance of a point contact

The previous analysis can be applied to describe a point contact device with a semimetallic ferromagnetic source (injecting polarized electrons) or a simply metallic source (injecting unpolarized electrons).

Let a constriction of width W separates the two regions that are connected with two perfect reservoirs at the Fermi energy

$$\mathcal{E}_\mathrm{F} = \frac{\hbar^2 k^2}{m_\mathrm{F}} = \mathcal{E}_\pm = \frac{\hbar^2}{2m_\mathrm{S}} \left(k'^2 \pm 2k_\mathrm{SO}k' \right).$$

The electron motion within the hybrid system is assumed as ballistic, that is, the electronic mean free path is much longer than the width W of the point contact. The Landauer-Büttiker formalism applies [25–27]. The conductance G at zero temperature is given by

$$G = \frac{e^2}{h} \sum_i T_i, \tag{2.22}$$

Figure 2.7: A schematic view of the interface with the point contact.

where T_i are the transmission coefficients for all the open channels i between the two reservoirs at the energy $\mathcal{E}_F$. In the present case the index i represents the incidence angle γ.
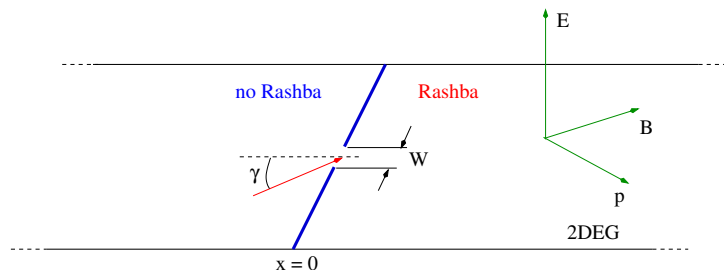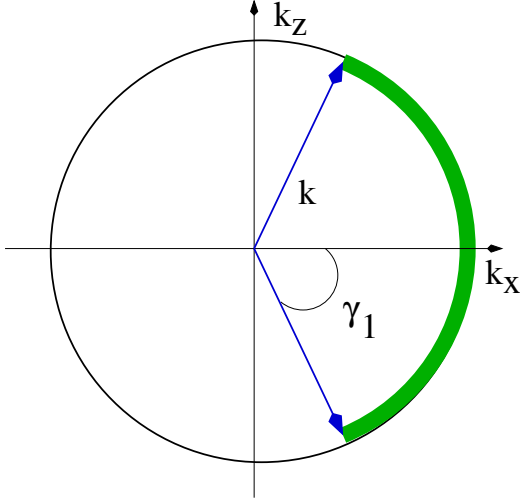

Figure 2.8: The Fermi contour in the k-space. The thick arch indicates the states that carry current into the point contact.

A sketch of the system is shown in Fig. 2.7. The two-dimensional Fermi contour in k-space is shown in Fig. 2.8 and only the states on its edge can carry current at zero temperature. The current is carried through the point contact by the states belonging to the arch from $-\gamma_1$ to γ_1 on the Fermi contour. Quantum mechanically, the current through the point contact is equipartitioned among the $1D$ subbands, or transverse modes, in the constriction. The gap along k_z axis between two consecutive subbands can be estimated of the order of π/W (this is exactly the result for a square well lateral confining potential of width W). The number of states contained in the element of arch $d\gamma$ is then $kd\gamma/(\pi/W)$. The equation (2.22) implies that hybrid system conductance G (with a ferromagnetic source in which the majority carriers are electrons in $|\delta\rangle$ spin state) is

$$G = \frac{e^2}{h} \int_{-\gamma_1}^{\gamma_1} T(\delta,\gamma) \frac{kW\mathrm{d}\gamma}{\pi} = \frac{e^2 kW}{h} \mathcal{G}(\delta) \qquad (2.23)$$

with

$$\mathcal{G}(\delta) = \frac{1}{\pi} \int_{-\gamma_1}^{\gamma_1} T(\delta,\gamma)\mathrm{d}\gamma. \qquad (2.24)$$

An exhaustive discussion about this approach can be found in Refs. [27, 28]. It is important to note that the restriction around the normal incidence $\gamma = 0$ gives

$$\mathcal{G}_0 = \frac{T(\delta,0)}{\pi}\mathrm{d}\gamma,$$

that is the Sharvin resistance formula [29] used by Grundler [11]. Therefore it has been shown that T at $\gamma = 0$ is independent on δ and $\mathcal{G}_0$ is independent on the spin polarization.

The Fig. 2.9 shows $\mathcal{G}(\delta)$ for δ between 0 and π. The symmetry relation $T(\pi - \delta, -\gamma) = T(\delta,\gamma)$ presented in Sec. 2.3 gives $\mathcal{G}(\pi - \delta) = \mathcal{G}(\delta)$. The conductance of a single interface when the incoming spin is up ($\delta = 0, \pi$) $\mathcal{G}(\uparrow)$
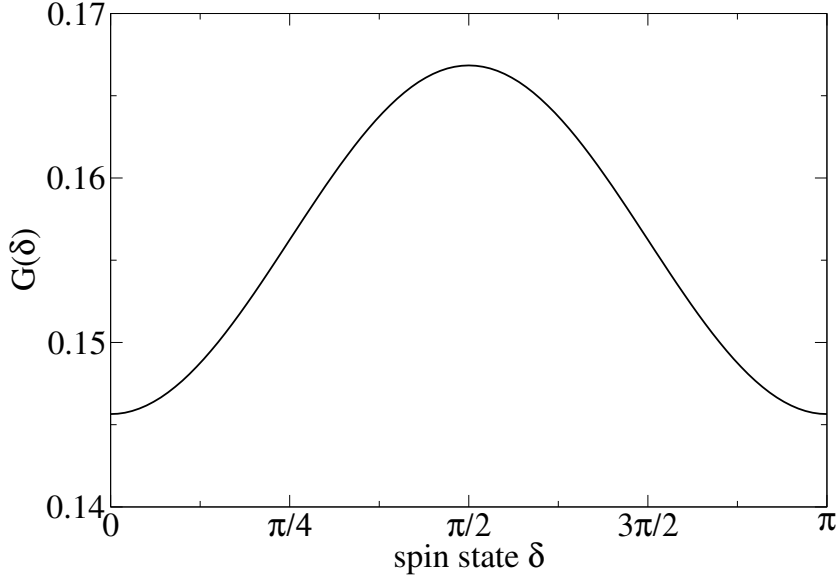
Figure 2.9: The conductance for polarized electrons $\mathcal{G}$ as a function of the spin polarization δ of the incoming electrons. The parameters are $k = 10k_{\text{SO}}$, $\mu = 0.1$ and $u = 1$. The value $\delta = 0$ corresponds to spin up and $\delta = \pi/2$ to spin down.

is different from the conductance when the incoming spin is down ($\delta = \pi/2$) $\mathcal{G}(\downarrow)$. This effect is a direct consequence of the spin-double refraction at the interface that changes the spin state when the electron comes into the R zone. Using the values of parameters of Fig. 2.9 it is obtained for the spin polarization of the conductance

$$\frac{\mathcal{G}(\downarrow) - \mathcal{G}(\uparrow)}{\mathcal{G}(\downarrow) + \mathcal{G}(\uparrow)} = 0.068.$$

The results for the transmission of an unpolarized beam can be used to discuss the case of a simply metallic source. It is interesting to notice that the integration over the angles of incidence does not cancel the effect of partial polarization that the scattering introduces on an unpolarized beam . The conductances for spin up and spin down in the unpolarized case

$$\frac{\mathcal{G}_{\uparrow}(\uparrow) + \mathcal{G}_{\uparrow}(\downarrow)}{2} \quad \text{and} \quad \frac{\mathcal{G}_{\uparrow}(\uparrow) + \mathcal{G}_{\uparrow}(\downarrow)}{2}$$

are shown in Fig. 2.10. For the unpolarized case, with the same parameters of Fig. 2.9, the spin conductance polarization at $x = 0$ is

$$\frac{(\mathcal{G}_{\uparrow}(\uparrow) + \mathcal{G}_{\uparrow}(\downarrow)) - (\mathcal{G}_{\uparrow}(\uparrow) + \mathcal{G}_{\uparrow}(\downarrow))}{(\mathcal{G}_{\uparrow}(\uparrow) + \mathcal{G}_{\uparrow}(\downarrow)) + (\mathcal{G}_{\uparrow}(\uparrow) + \mathcal{G}_{\uparrow}(\downarrow))} = 0.0362.$$
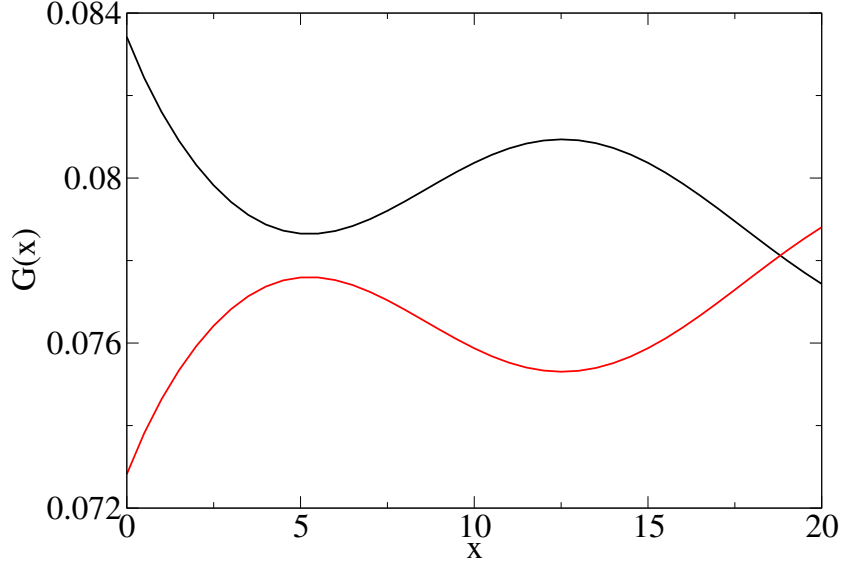
Figure 2.10: The conductances for unpolarized electrons $(\mathcal{G}_{\uparrow}(\uparrow) + \mathcal{G}_{\uparrow}(\downarrow))/2$ (black curve) and $(\mathcal{G}_{\uparrow}(\uparrow) + \mathcal{G}_{\uparrow}(\downarrow))/2$ (red curve) as functions of x. The oscillation period is equal to the precession length π/k_{SO}.

For unpolarized electrons the spin polarization of the conductance reduces at half of the value for polarized electrons. If the output in spin up channel or in spin down channel is considered, the scattering at the single interface gives rise to a partial polarization. A second interface, acting as an analyzer of the spin, is needed to let the effect be experimentally detectable. In this case Fabry-Perot oscillations have to be superimposed to those shown in Fig. 2.9 [22, 30]. This analysis is presented in the next chapter.

The key ingredient in order to achieve a different transmission of spin up and spin down is the oblique incidence of the electron combined with the strict relation between the propagation direction and spin state (see Eq. 2.5). This is in contrast with the case of normal incidence which has been usually considered, but it is in agreement with the results reported for confined structures [31].

Appendix A: Boundary conditions calculation

The boundary conditions at $x = 0$ give the following linear system for the amplitudes

$$t_+ \cos\frac{\alpha}{2} + t_- \sin\frac{\beta}{2} - r_+ = \cos\delta$$

$$-t_+ \sin\frac{\alpha}{2} + t_- \cos\frac{\beta}{2} - r_- = \sin\delta \qquad (2.25)$$

$$k_+ t_+ \cos\alpha\cos\frac{\alpha}{2} + k_- t_- \cos\beta\sin\frac{\beta}{2} +$$
$$r_+(\mu k\cos\gamma + k_{\mathrm{SO}} + iu) = \cos\delta(\mu k\cos\gamma - k_{\mathrm{SO}} - iu)$$

$$-k_+ t_+ \cos\alpha\sin\frac{\alpha}{2} + k_- t_- \cos\beta\cos\frac{\beta}{2} +$$
$$r_-(\mu k\cos\gamma - k_{\mathrm{SO}} + iu) = \sin\delta(\mu k\cos\gamma + k_{\mathrm{SO}} - iu)$$

whose solution is

$$r_+ = (C_+ A_{--}\cos\frac{\alpha}{2} + C_- A_{+-}\sin\frac{\beta}{2})D^{-1}$$

$$r_- = (C_- A_{++}\cos\frac{\beta}{2} + C_+ A_{-+}\sin\frac{\alpha}{2})D^{-1} \qquad (2.26)$$

$$t_+ = \left[(\cos\delta + r_+)\cos\frac{\beta}{2} - (\sin\delta + r_-)\sin\frac{\beta}{2}\right]\cos^{-1}\frac{\alpha - \beta}{2}$$

$$t_- = \left[(\sin\delta + r_-)\cos\frac{\alpha}{2} + (\cos\delta + r_+)\sin\frac{\alpha}{2}\right]\cos^{-1}\frac{\alpha - \beta}{2}$$

where

$$A_{++} = k_+ \cos\alpha + \mu k\cos\gamma + k_{\mathrm{SO}} + iu$$
$$A_{+-} = k_+ \cos\alpha + \mu k\cos\gamma - k_{\mathrm{SO}} + iu$$
$$A_{-+} = -k_- \cos\beta - \mu k\cos\gamma - k_{\mathrm{SO}} - iu$$
$$A_{--} = k_- \cos\beta + \mu k\cos\gamma - k_{\mathrm{SO}} + iu$$

$$C_+ = (-k_+ \cos\alpha + \mu k\cos\gamma - k_{\mathrm{SO}} - iu)\cos\delta\cos\frac{\beta}{2} -$$
$$(-k_+ \cos\alpha + \mu k\cos\gamma + k_{\mathrm{SO}} - iu)\sin\delta\sin\frac{\beta}{2}$$

$$C_- = -(k_- \cos\beta - \mu k\cos\gamma + k_{\mathrm{SO}} + iu)\cos\delta\sin\frac{\alpha}{2} +$$
$$(-k_- \cos\beta + \mu k\cos\gamma + k_{\mathrm{SO}} - iu)\sin\delta\cos\frac{\alpha}{2}$$

$$D = A_{++}A_{--}\cos\frac{\beta}{2}\cos\frac{\alpha}{2} - A_{+-}A_{-+}\sin\frac{\beta}{2}\sin\frac{\alpha}{2}.$$

The amplitudes depend on the spin of the incident wave, represented by the parameter δ, and on the incident wave vector $\vec{k}$. These parameters are not conserved but they characterize the asymptotic wave packet directed towards the surface $x = 0$ before the time at which the scattering starts.

Appendix B: On the symmetries of the system

I start considering the symmetry transformation $\widehat{K}_1$ that inverts both p_z and σ_x and leaves p_x and σ_z unchanged

$$\widehat{K}_1 p_z \widehat{K}_1^\dagger = -p_z \quad ; \quad \widehat{K}_1 \sigma_x \widehat{K}_1^\dagger = -\sigma_x$$

so that $[H, \widehat{K}_1] = 0$. As

$$\alpha(-\gamma) = -\alpha(\gamma) \quad ; \quad \beta(-\gamma) = -\beta(\gamma)$$

and changing the incident spin orientation δ in $\pi - \delta$, I get

$$
\begin{aligned}
t_+(\pi - \delta, -\gamma) &= -t_+^*(\delta, \gamma) \\
t_-(\pi - \delta, -\gamma) &= t_-(\delta, \gamma) \\
r_+(\pi - \delta, -\gamma) &= -r_+^*(\delta, \gamma) \\
r_-(\pi - \delta, -\gamma) &= r_-(\delta, \gamma).
\end{aligned}
$$

The total transmission obeys the equation

$$T(\pi - \delta, -\gamma) = T(\delta, \gamma) \tag{2.27}$$

and T is an even function of γ only for spin up ($\delta = 0$) and spin down ($\delta = \pi/2$) whereas T is asymmetrical around the normal incidence $\gamma = 0$ for a generic spin state. At $\gamma = 0$ the "partial" time-reversal $\widehat{K}_1$ again does not say anything about the relationship between $T(\delta = 0, \gamma = 0)$ and $T(\delta = \pi/2, \gamma = 0)$.

The Hamiltonian $\mathcal{H}$ depends on the electrical field as a parameter through the SO coupling constant k_{SO} [32–35]. The inversion of the electrical field is obtained by changing the sign of k_{SO}. The spectrum of $\mathcal{H}(k_{\text{SO}})$ can be mapped into the spectrum of $\mathcal{H}(-k_{\text{SO}})$ by means of an operator $\widehat{K}_2$ that inverts $\vec{\sigma}$ that is

$$\widehat{K}_2 \vec{\sigma} \widehat{K}_2^\dagger = -\vec{\sigma}.$$

The operator $\widehat{K}_2$ transforms all the spinors into orthogonal spin states and interchanges the $(+)$ mode with the $(-)$ mode. The result is

$$
\begin{aligned}
k_\pm(k_{\text{SO}}) &= k_\mp(-k_{\text{SO}}) \\
\alpha(-k_{\text{SO}}) &= \beta(k_{\text{SO}})
\end{aligned}
$$

and

$$
\begin{aligned}
t_+(k_{\mathrm{SO}}, \delta) &= t_- \left(-k_{\mathrm{SO}}, \delta + \frac{\pi}{2}\right) \\
t_-(k_{\mathrm{SO}}, \delta) &= -t_+ \left(-k_{\mathrm{SO}}, \delta + \frac{\pi}{2}\right) \\
r_+(k_{\mathrm{SO}}, \delta) &= r_- \left(-k_{\mathrm{SO}}, \delta + \frac{\pi}{2}\right) \\
r_-(k_{\mathrm{SO}}, \delta) &= -r_+ \left(-k_{\mathrm{SO}}, \delta + \frac{\pi}{2}\right).
\end{aligned}
$$

The total transmission has the form

$$
T = \frac{1}{\mu} \; \frac{k_{\mathrm{SO}}}{k} \; \frac{\sin\alpha + \sin\beta}{\sin\alpha - \sin\beta} \; \frac{|t_+|^2 \cos\alpha + |t_-|^2 \cos\beta}{\cos\gamma}
$$

equivalent to that of equation (2.18) from it follows that

$$
T\left(-k_{\mathrm{SO}}, \delta + \frac{\pi}{2}\right) = T\left(k_{\mathrm{SO}}, \delta\right). \tag{2.28}
$$

The equation (2.28) sets up a relation between the spin up and spin down state at any incidence angle when the electrical field is inverted but again it is not able to give the equality of $T_+(\uparrow)$ and $T_-(\downarrow)$ when $\gamma = 0$ at the same value of the parameter k_{SO}.

Bibliography

[1] M. Ziese and M.J. Thornton, editors. *Spin Electronics*. Springer, Berlin, 2001.

[2] D.D. Awschalom, D. Loss, and N. Samarth, editors. *Semiconductor Spintronics and Quantum Computation*. Spinger, Berlin, 2002.

[3] Igor ˇ Zutí c, Jaroslav Fabian, and S. Das Sarma. Spintronics: Fundamentals and applications. *Rev. Mod. Phys.*, 76:323, 2004.

[4] E.I. Rashba. Properties of semiconductors with an extremum loop I. cyclotron and combinational resonance in a magnetic field perpendicular to the plane of the loop. *Fiz. Tverd. Tela (Leningrad)*, 2:1224, 1960. [Sov. Phys. Solid State 2, 1109 (1960)].

[5] Yu A. Bychkov and E.I. Rashba. Oscillatory effects and the magnetic susceptibility of carriers in inversion layers. *J. Phys. C: Solid State Phys.*, 17:6039, 1984.

[6] Supriyo Datta and Biswajit Das. Electronic analog of the electro-optic modulator. *Appl. Phys. Lett.*, 56:665, 1990.

[7] S. Gardelis, C. G. Smith, C. H. W. Barnes, E. H. Linfield, and D. A. Ritchie. Spin-valve effects in a semiconductor field-effect transistor: A spintronic device. *Phys. Rev. B*, 60:7764, 1999.

[8] W. Y. Lee, S. Gardelis, B.-C. Choi, Y. B. Xu, C. G. Smith, C. H. W. Barnes, D. A. Ritchie, E. H. Linfield, and J. A. C. Bland. Magnetization reversal and magnetoresistance in a lateral spin-injection device. *J. Appl. Phys.*, 85:6682, 1999.

[9] Takaaki Koga, Junsaku Nitta, Tatsushi Akazaki, and Hideaki Takayanagi. Rashba spin-orbit coupling probed by the weak antilocalization analysis in InAlAs/InGaAs/InAlAs quantum wells as a function of quantum well asymmetry. *Phys. Rev. Lett.*, 89:046801, 2002.

[10] D. Grundler. Ballistic spin-filter transistor. *Phys. Rev. B*, 63:161307, 2001.

[11] D. Grundler. Oscillatory spin-filtering due to gate control of spin-dependent interface conductance. *Phys. Rev. Lett.*, 86:1058, 2001.

[12] Laurens W. Molenkamp, Georg Schmidt, and Gerrit E. W. Bauer. Rashba hamiltonian and electron transport. *Phys. Rev. B*, 64:121202, 2001.

[13] U. Zülicke and C. Schroll. Interface conductance of ballistic Ferromagnetic-Metal-2DEG hybrid systems with rashba spin-orbit coupling. *Phys. Rev. Lett.*, 88:029701, 2002.

[14] George Kirczenow. Ideal spin filters: A theoretical study of electron transmission through ordered and disordered interfaces between ferromagnetic metals and semiconductors. *Phys. Rev. B*, 63:054422, 2001.

[15] G. Schmidt, D. Ferrand, L. W. Molenkamp, A. T. Filip, and B. J. van Wees. Fundamental obstacle for electrical spin injection from a ferromagnetic metal into a diffusive semiconductor. *Phys. Rev. B*, 62(8):R4790, 2000.

[16] Radu Ionicioiu and Irene D'Amico. Mesoscopic Stern-Gerlach device to polarize spin currents. *Phys. Rev. B*, 67:041307, 2003.

[17] M. Governale, D. Boese, U. Zülicke, and C. Schroll. Filtering spin with tunnel-coupled electron wave guides. *Phys. Rev. B*, 65:140403, 2002.

[18] V. Marigliano Ramaglia, D. Bercioux, V. Cataudella, G. De Filippis, C.A. Perroni, and F. Ventriglia. Conductance of a large point contact with Rashba effect. *Eur. Phys. J.*, 36:365, 2003.

[19] O. Madelung. *Introduction to solid state theory.* Spinger, Berlin, 1978.

[20] F. Haake. *Quantum signatures of chaos.* Spinger Berlin, 1991.

[21] J.M. Stone. *Radiation and optics.* McGraw Hill Book Company Inc, New York, 1963.

[22] T. Matsuyama, C.-M. Hu, D. Grundler, G. Meier, and U. Merkt. Ballistic spin transport and spin interference in ferromagnet/InAs(2DES)/ferromagnet devices. *Phys. Rev. B*, 65:155322, 2002.

[23] Morten Hogsbro Larsen, A. Mathias Lunde, and Karsten Flensberg. Conductance of Rashba spin-split systems with ferromagnetic contacts. *Phys. Rev. B*, 66:033304, 2002.

[24] U. Fano. Description of states in quantum mechanics by density matrix and operator techniques. *Rev. Mod. Phys.*, 29:74, 1957.

[25] Yoseph Imry and Rolf Landauer. Conductance viewed as transmission. *Rev. Mod. Phys.*, 71:S306, 1999.

[26] M. Büttiker. Four-terminal phase-coherent conductance. *Phys. Rev. Lett.*, 57:1761, 1986.

[27] C.W. Beenakker and H. van Houten. Quantum transport in semiconductor nanostructures. *Solid State Phys.*, 44:1, 1991.

[28] D.K. Ferry and S.M. Goodnick. *Transport in nanostructures.* Cambridge University Press, Cambridge, 1997.

[29] Y.V. Sharvin. A possible method for studying Fermi surfaces. *Zh. Eksp. Teor. Fiz.*, 48:984, 1965. [Sov. Phys. JETP **21**, 655 (1965)].

[30] Marco G. Pala, Michele Governale, Jurgen König, Ulrich Zülicke, and Giuseppe Iannaccone. Two-dimensional hole precession in an all-semiconductor spin field effect transistor. *Phys. Rev. B*, 69:045304, 2004.

[31] M. Governale and U. Zülicke. Spin accumulation in quantum wires with strong Rashba spin-orbit coupling. *Phys. Rev. B*, 66:073311, 2002.

[32] J. Nitta, T. Akazaki, H. Takayanagi, and T. Enoki. Gate control of spin-orbit interaction in an inverted $In_{0.53}Ga_{0.47}As/In_{0.52}Al_{0.48}As$ heterostructure. *Phys. Rev. Lett.*, 78:1335, 1997.

[33] Th. Schäpers, G. Engels, J. Lange, Th. Klocke, M. Hollfelder, and H. Lüth. Effect of the heterointerface on the spin splitting in modulation doped $In_xGa_{1-x}As/InP$ quantum wells for $B \rightarrow 0$. *J. App. Phys.*, 83:4324, 1998.

[34] D. Grundler. Large rashba splitting in inas quantum wells due to electron wave function penetration into the barrier layers. *Phys. Rev. Lett.*, 84:6074, 2000.

[35] J. B. Miller, D. M. Zumbühl, C. M. Marcus, Y. B. Lyanda-Geller, D. Goldhaber-Gordon, K. Campman, and A. C. Gossard. Gate-controlled spin-orbit quantum interference effects in lateral transport. *Phys. Rev. Lett.*, 90:076807, 2003.

3

Spin double-refraction field effect transistor

Introduction

As I have introduced in the previous chapters, the most popular proposal for a coherent spintronic device is the Datta and Das spin field-effect transistor (spin-FET) [1]. The major obstacles to the realization of this device is due to the non-efficient injection of spin-polarized electrons from the ferromagnetic contact into the nonmagnetic part of the spin-FET [2]. A possible solution to overcome this problem may be provided by the use of dilute magnetic semiconductor [3] as source and drain. On this bases Pala *et.al.* [4] have proposed an all-semiconductor spin-FET. An important aspect on the their proposal deals with the fact that ferromagnetic (III,Mn)V compounds are intrinsically p doped, implying that currents are carried by holes rather than electrons.

They have considered a MnGaAs/GaAs/MnGaAs heterostructure overgrown in the z direction with AlGaAs such that a two-dimensional hole gas is formed at the interface (see Fig. 3.1). A bulk semiconductor systems is characterized by heavy- and light-hole bands with total angular momentum $j = 3/2$. These bands are degenerate at the band edge and are well separated, due to the spin-orbit (SO) coupling, from the split-off bands with the total angular momentum $j = 1/2$. In quantum wells, each of these bands is transformed in a sequence of quasi-two-dimensional subbands, and the degeneracy between heavy- and light-hole band is lifted. They consider the case of low carrier concentration that implies that only the first heavy- and light-hole subband is occupied. Furthermore the presence of the Rashba SO

51
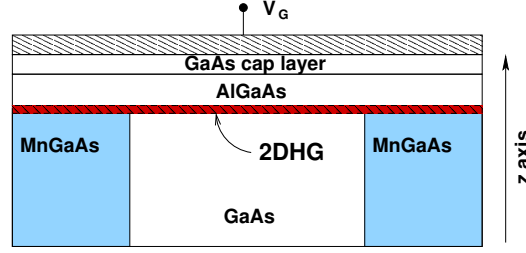
Figure 3.1: Schematic illustration of the proposed device. The two-dimensional hole gas (2DHG) in the GaAs part is attached to spin-polarized source and drain contacts, formed by 2DHGs in the MnGaAs parts. The gate electrode on the top controls both the carrier concentration and the Rashba spin-orbit coupling strength.
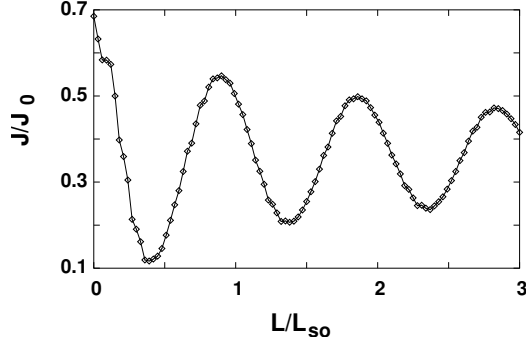
Figure 3.2: The total current density as a function of the quantity L/L_{so} in the 2D system treatment, where L is the channel length and L_{so} is the total modulation length. The magnetization in the contacts is perpendicular to the plane of the 2DHG.

coupling [11] lifts the spin degeneracy.

On the basis of this four bands model for the two-dimensional hole gas and using a phenomenological approach for the dilute magnetic semiconductor they evaluate the transmission properties of the system of Fig. 3.1.

Thay take account of the two-dimensional nature of device and therefore they consider the current contributions for all the injection angles. This fact does not washed out the effect of spin modulation that has been introduced in the previous chapter [5]. However, it turns out that oscillations are still visible, although damped. In Fig. 3.2 are shown this results for magnetization direction in the source being $\hat{n} = (0, 0, 1)$.

In this chapter it is presented the study of a hybrid system based on Rashba SO coupling without ferromagnetic contacts. It is shown that electrons injected unpolarized from a source are extracted with a partial spin po-
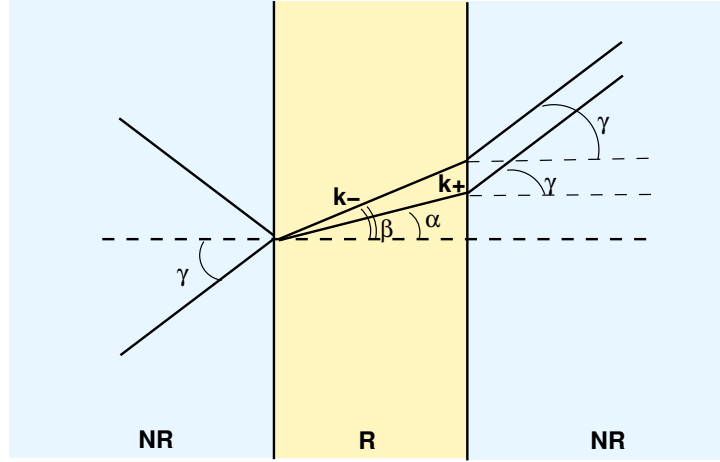
Figure 3.3: Schematic illustration of the proposed devices. The two-dimensional electron gas is divided in three region. In central region a Rashba spin-orbit coupling is present.

larization into a non-ferromagnetic drain. The electron of a two-dimensional electron gas are injected at an out of normal incidence angle and the spin-FET operates by means of the spin-double refraction that appears at the interface between a region without SO coupling and a region where the SO coupling is present [5, 6]. The use of spin-double refraction to produce and control spin-polarized current by means of the appearance of a limit angle for the refraction has been recently proposed by [6] in a system complementary to the one proposed here: spin-unpolarized electrons from a Rashba source traverse a region with a lower SO coupling and are collected by a drain with a stronger Rashba coupling. In this case the strength of the SO coupling in the source and in the drain is zero. The source and the drain could be realized by using n$^+$-semiconductors. This model uses an abrupt interface but a smooth Rashba field should not change the effects of the spin-double refraction as the WKB approximation of Ref. [6] shows. The novel feature of this setup is the transmission double step shown in Fig. (3.4), that is accompanied by the appearance of a spin polarization. It is important to stress that a modulation of the output current can be obtained with a spin-unpolarized input current, whereas in the original Datta and Das [1] proposal the current oscillation stems out from the difference of phase accumulated along a path in the Rashba region by the two spin propagating modes. In this system the current modulation and the spin polarization appear when *only one mode* propagates through the Rashba barrier.

The phase averaging due to the thermal broadening is taken into account,

it tends to wash out the effect of the multiple scattering against the two interfaces. It is shown how the resonances that appears when the electronic beam hits the interface with an angle greater than the first limit angle, when only one mode traverse the barrier, remain when the temperature is increased. On the other hand the more rapid Fabry-Perot oscillation, with rapid changes of the transmission, due to the propagation of both the modes at low incidence angles are canceled. The thermal average preserves the halving of the transmission strictly related to the appearance of the spin polarization, so that these features do not follow from the multiple scattering against the two interfaces.

3.1 Scattering against a region with SO coupling

Let us consider a two-dimensional electron gas (2DEG) filling the plane (x, z). A stripe, where is present the Rashba SO coupling, divides the plane in three regions as in the Fig. (3.3). In the inner region R ($0 < x < L$) the Rashba SO coupling term is

$$\mathcal{H}_{\text{SO}} = \frac{\hbar k_{\text{SO}}}{m} \left(\vec{\sigma} \times \vec{p} \right) \cdot \hat{y} \tag{3.1}$$

where k_{SO} is the SO coupling constant, $\vec{\sigma}$ is the vector of Pauli matrices, $\vec{p}$ the momentum and m the electron mass. The strength of the SO coupling can be tuned by external gate voltages, as it has been experimentally demonstrated [7–10]. In the outer regions NR ($x < 0$ and $x > L$) there is no SO coupling ($k_{\text{SO}} = 0$).

Within the R zone there are two spin-split bands $E_\pm (k')$

$$E_\pm (k') = \frac{\hbar^2}{2m} \left(k'^2 \pm 2k_{\text{SO}} k' \right) \tag{3.2}$$

where $k' = \sqrt{k_x'^2 + k_z'^2}$ is the wave vector. The SO interaction can be viewed as due to a magnetic field parallel to the plane and orthogonal to the wave vector $\vec{k'}$. This magnetic field couples with the spin-magnetic moment and aligns the spin along the direction orthogonal to $\vec{k'}$ [11]. If $\vec{k'}$ is directed along x then the signs $+$ and $-$ indicate the "spin up" and "spin down" states in z direction.

The spin split bands may be shifted applying an offset gate voltage V_{off} with respect to the source and drain bands $\hbar^2 k^2 / 2m$. The energy bands (3.2)
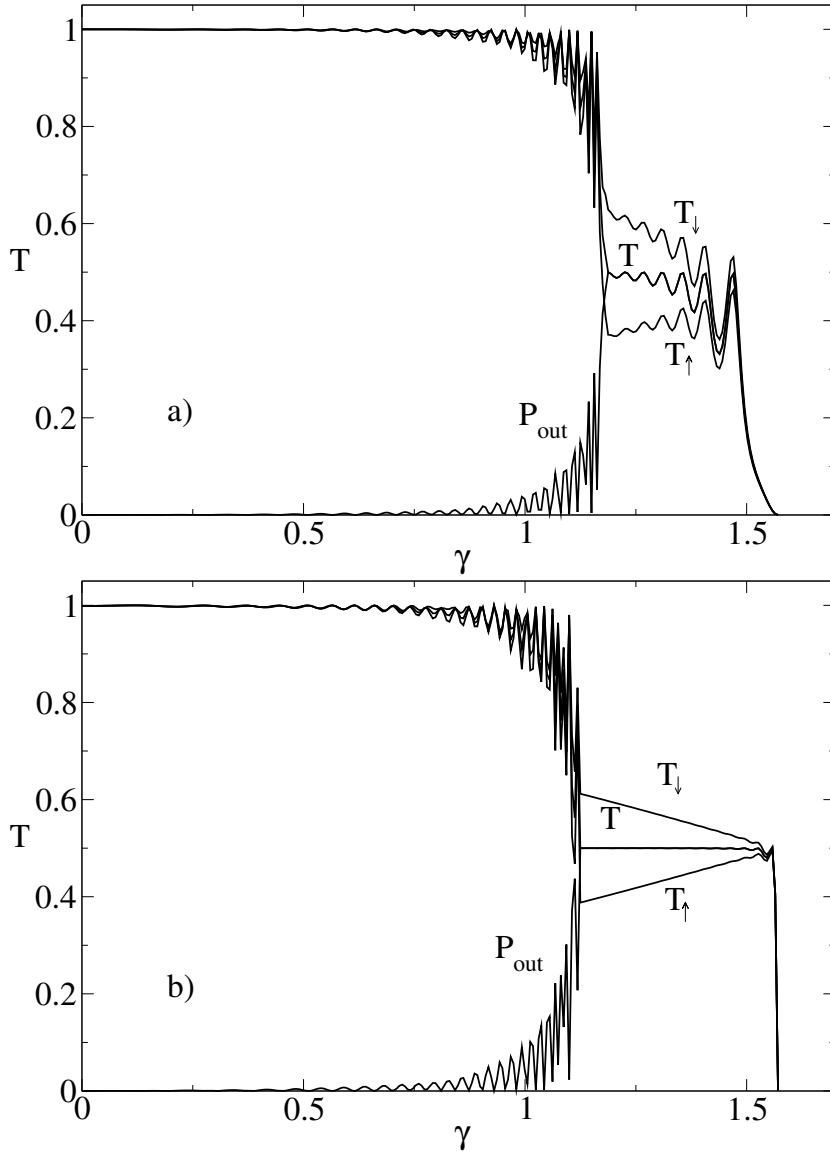
Figure 3.4: The transmission coefficients $T_\downarrow(\gamma), T(\gamma), T_\uparrow(\gamma)$ as functions of the incidence angle γ (in radiants) at two values of the offset. The length L is 283 nanometers. The panel a) shows the 1/2 height resonances, where $k_{SO}/k = 0.05$ and $u_1/k^2 = 0.05$. The offset in the panel b) is $2k_{SO}/k$ with the largest and the flattest low step as obtainable, here $k_{SO}/k = 0.05$ and $u_1/k^2 = 0.1..$

recast in

$$E_{\pm}\left(k'\right) = \frac{\hbar^2}{2m}\left(k'^2 \pm 2k_{\mathrm{SO}}k'\right) + eV_{\mathrm{off}} = \frac{\hbar^2}{2m}k^2$$
$$k' = \sqrt{k^2 - u_1 + k_0^2} \mp k_{\mathrm{SO}} = k_{\pm} \qquad (3.3)$$
$$u_1 = \frac{2meV_{\mathrm{off}}}{\hbar^2}.$$

The electron motion within the hybrid NR–R–NR system is supposed as ballistic and within the Landauer-Büttiker regime [12].

As it has been shown in the previuous chapter the single NR-R interface has a transmission coefficient dependent on the injection angle γ and on the incident spin state $|\delta\rangle = \cos\delta\,|\uparrow\rangle + \sin\delta\,|\downarrow\rangle$ because the Rashba effect gives rise to the double refraction at the interface with two orthogonal spin polarizations that simultaneously propagate within the R zone only when $\gamma \neq 0$ [5] (out of the normal incidence).

It is now studied the conductance of NR–R–NR system in term of the double interface transmission coefficient $T\left(\delta,\gamma\right)$.

In the $x < 0$ region an incident and a reflected wave are present

$$\begin{pmatrix} \cos\delta \\ \sin\delta \end{pmatrix} e^{ik(x\cos\gamma + z\sin\gamma)} + \begin{pmatrix} r_{\uparrow} \\ r_{\downarrow} \end{pmatrix} e^{ik(-x\cos\gamma + z\sin\gamma)},$$

in the R region $(0 < x < L)$ is characterized by two propagating and two counterpropagating waves

$$\begin{pmatrix} \cos\alpha/2 \\ -\sin\alpha/2 \end{pmatrix} t_+ e^{ik_+(x\cos\alpha + z\sin\alpha)} + \begin{pmatrix} \sin\beta/2 \\ \cos\beta/2 \end{pmatrix} t_- e^{ik_-(x\cos\beta + z\sin\beta)}$$

$$\begin{pmatrix} \sin\alpha/2 \\ -\cos\alpha/2 \end{pmatrix} r_+ e^{ik_+(-x\cos\alpha + z\sin\alpha)} + \begin{pmatrix} \cos\beta/2 \\ \sin\beta/2 \end{pmatrix} r_- e^{ik_-(-x\cos\beta + z\sin\beta)}$$

and, finally, the transmitted wave for $x > L$ is

$$\begin{pmatrix} t_{\uparrow} \\ t_{\downarrow} \end{pmatrix} e^{ik(x\cos\gamma + z\sin\gamma)}.$$

The k_z parallel momentum conservation fixes the angular α and β directions of $\vec{k}'$

$$\alpha = \arcsin\frac{k\sin\gamma}{k_+} \qquad \text{and} \qquad \beta = \arcsin\frac{k\sin\gamma}{k_-}.$$

The modes $(+)$ and $(-)$ have the limit angles γ_0 and γ_1 respectively

$$\gamma_0 = \arcsin\frac{k_+}{k} \qquad \text{and} \qquad \gamma_1 = \arcsin\frac{k_-}{k}, \qquad (3.4)$$

that is when γ exceeds γ_0 or γ_1 the corresponding mode becomes a decaying wave. The spinors of the wave function ψ for $0 < x < L$ are independent on δ. On the contrary the spinors of the reflected and the transmitted wave depend on δ. In the inner region R the four amplitudes t_+, t_-, r_+, r_- vary with δ. The single NR-R interface is described by the Hamiltonian

$$\mathcal{H}_{\text{NR-R}} = \vec{p}\frac{1}{2m(x)}\vec{p} + \frac{k_{\text{SO}}(x)m(x)}{\hbar^2}\left(\sigma_z p_x - \sigma_x p_z\right) - i\sigma_z\frac{1}{2}\frac{\partial k_{\text{SO}}(x)}{\partial x} + u\delta(x). \quad (3.5)$$

It is assumed that the mass and the strength of SO coupling are piecewise constant

$$\begin{aligned}
\frac{1}{m}(x) &= \frac{\vartheta(-x)}{m_{\text{NR}}} + \frac{\vartheta(x)}{m_{\text{R}}} \\
k_{\text{SO}}(x) &= k_{\text{SO}}\ \vartheta(x),
\end{aligned} \quad (3.6)$$

where $\vartheta(x)$ is the step function. To have a model as simple as possible, it is assumes that the electron effective mass in the NR region m_{NR} and the electron effective mass in the R m_{R} region are equal. The third term in (3.5) is needed to get an hermitian operator $\mathcal{H}_{\text{NR-R}}$. The fourth term regulates the transparency of the interface and describes insulating barriers separating the semiconductors. The matching conditions at $x = 0$ and L

$$\begin{cases}
\psi(0+) - \psi(0-) &= 0 \\
\psi(L+) - \psi(L-) &= 0 \\
\partial_x\psi(0+) - \partial_x\psi(0-) &= (u - ik_{\text{SO}})\psi(0) \\
\partial_x\psi(L+) - \partial_x\psi(L-) &= (u + ik_{\text{SO}})\psi(L)
\end{cases}$$

provide a linear system for the eight quantities $r_\uparrow, r_\downarrow, t_\uparrow, t_\downarrow, t_+, t_-, r_+, r_-$. The R region behaves as a resonant cavity whose action can be reinforced by the couple of additional Dirac-delta potentials. The strength u of those controls the interfaces transparency.

To avoid ferromagnetic leads unpolarized electrons injected into the NR–R–NR system are considered. The unpolarized statistical mixture at $x = 0$

$$\rho_{\text{in}} = \frac{1}{2}|\uparrow\rangle\langle\uparrow| + \frac{1}{2}|\downarrow\rangle\langle\downarrow|$$

becomes the density matrix ρ_{out} at $x = L$

$$\rho_{\text{out}} = \frac{1}{2}T_\uparrow|1\rangle\langle 1| + \frac{1}{2}T_\downarrow|2\rangle\langle 2| \quad (3.7)$$

where $T_\uparrow = |t_{\uparrow\uparrow}|^2 + |t_{\downarrow\uparrow}|^2$ is the coefficient for incoming spin up state and $T_\downarrow = |t_{\uparrow\downarrow}|^2 + |t_{\downarrow\downarrow}|^2$ is that for the incoming spin down state [1]. The spinors in

---

[1]The first arrow in the label of the transmitted amplitudes represents the output spin, whereas the second arrow indicates the input spin.

the operator (3.7) are

$$|1\rangle = \frac{1}{\sqrt{T_\uparrow}} \begin{pmatrix} t_{\uparrow\uparrow} \\ t_{\downarrow\uparrow} \end{pmatrix} \quad \text{and} \quad |2\rangle = \frac{1}{\sqrt{T_\downarrow}} \begin{pmatrix} t_{\uparrow\downarrow} \\ t_{\downarrow\downarrow} \end{pmatrix} \tag{3.8}$$

corresponding to input spin up and down respectively. The transmission coefficient of the unpolarized electrons is

$$T = \left(T_\uparrow + T_\downarrow\right)/2.$$

The density matrix ρ_{out} can be represented in terms of the output polarization $\vec{P}$ as

$$\rho_{\text{out}}\left(\gamma\right) = \frac{1}{2}\left(\mathbf{1} + \vec{P}\left(\gamma\right) \cdot \vec{\sigma}\right) \tag{3.9}$$

where $\vec{P}$ is the average of $\vec{\sigma}$:

$$\vec{P} = <\vec{\sigma}> = \text{Tr}\left[\rho_{\text{out}}\vec{\sigma}\right].$$

The modulus of $\vec{P}$ gives the degree of polarization in the output. A simple calculation shows that the modulus of the polarization $P_\uparrow$ of the spinor $\sqrt{T_\uparrow}|1\rangle$ is $P_\uparrow \equiv T_\uparrow$, whereas the modulus of the polarization $P_\downarrow$ of $\sqrt{T_\downarrow}|2\rangle$ is $P_\downarrow \equiv T_\downarrow$. Finally, when the input state is unpolarized the output state is partially polarized. In particular, for $\gamma > \gamma_0$

$$\left|\vec{P}_{\text{out}}\right| = \frac{1}{2}\left(T_\uparrow + T_\downarrow\right) = T \quad \text{for} \quad \gamma > \gamma_0 \tag{3.10}$$

since $|\langle 1|2\rangle|$ goes very quickly to 1. On the contrary when the incidence angle γ is lower than γ_0, $\left|\vec{P}_{\text{out}}\right| < T$ and the polarization vanishes when γ goes to zero (see Appendix A).

Finally for $\gamma > \gamma_0$ some resonances appear (see Fig. 3.4) for which

$$\begin{aligned} R_\uparrow &= T_\downarrow \\ R_\downarrow &= T_\uparrow, \end{aligned}$$

where $R_\uparrow$ and $R_\downarrow$ are the reflection coefficients with an incident spin up or down. For the unpolarized statistical mixture the flux conservation implies that at the resonances

$$T = \frac{1}{2}\left(T_\uparrow + T_\downarrow\right) = R = \frac{1}{2}\left(R_\uparrow + R_\downarrow\right) = \frac{1}{2}.$$

Figure 3.5: Panel a): The transmission coefficient for unpolarized electrons as function of the injection angle. The solid line is for $u_1/k^2 = 0.1$, $u/k = 0.4$ and $k_{\rm SO}/k = 0.05$, the dashed line is for $u_1/k^2 = 0.1$, $u/k = 0.4$ and $k_{\rm SO}/k = 0$ and finally the dotted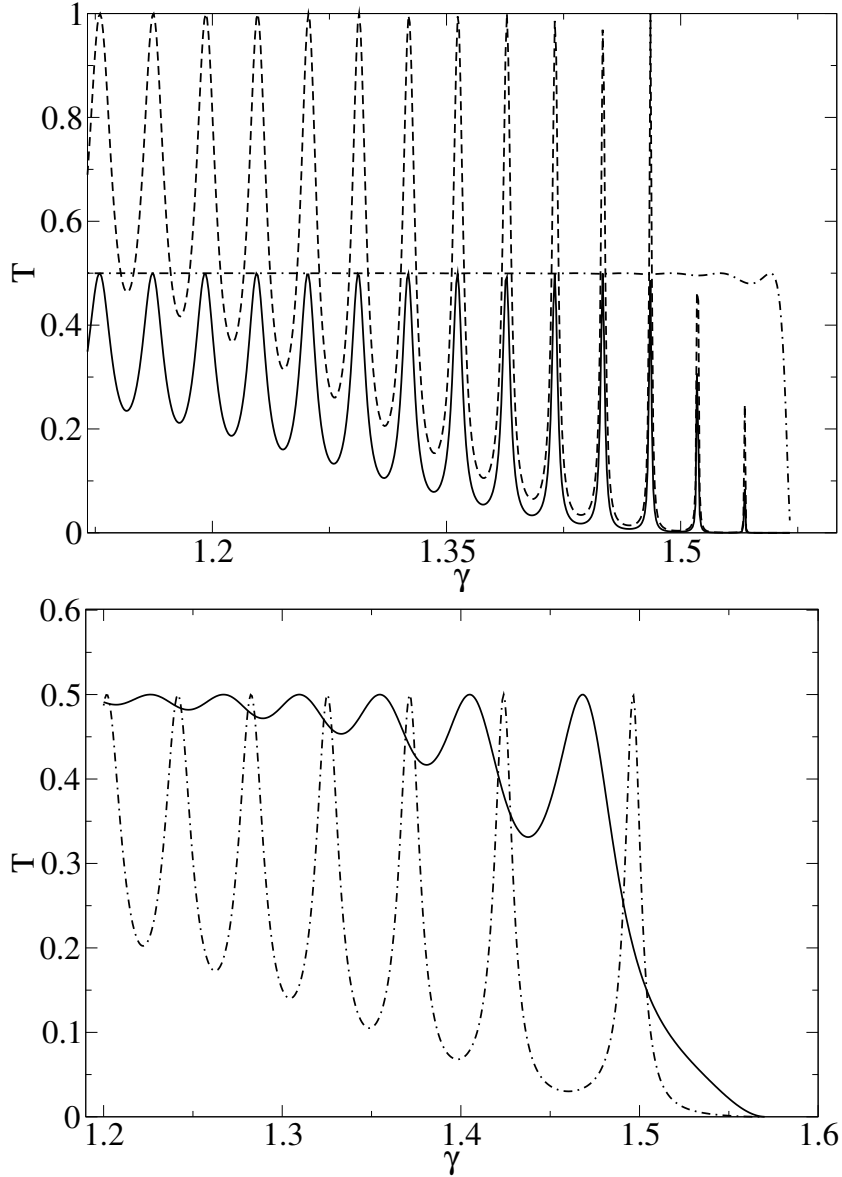-dashed line is for $u_1/k^2 = 0$, $u/k = 0.4$ and $k_{\rm SO}/k = 0.05$. Panel b): The transmission coefficient for unpolarized electrons as function of the injection angle. The solid line is for $u_1/k^2 = 0.05$, $u/k = 0.4$ and $k_{\rm SO}/k = 0.05$ and the dotted-dashed line is for $u_1/k^2 = 0.05$, $u/k = 0$ and $k_{\rm SO}/k = 0.05$.

The calculated transmission coefficients for unpolarized $(T(\gamma))$ and polarized $(T_\downarrow(\gamma), T_\uparrow(\gamma))$ injected electrons are shown in Fig. (3.4) with realistic parameters [7]. For the inverted $In_{0.53}Ga_{0.47}As/In_{0.52}Al_{0.48}As$ heterostructure the value of the Fermi wave vector is $k = 3.53 \times 10^6 cm^{-1}$, the effective mass is $m = 0.05\, m_e$, whereas the strength of the SO k_{SO} ranges from $0.01\,k$ to $0.05\,k$. The main feature of $T_\downarrow, T, T_\uparrow$ is the double step that originates from the spin-double refraction. When γ goes over γ_0 only the wave $(-)$ can reach the second interface and the transmission coefficients tend to halve themself. The panel a) of the Fig. (3.4) shows that, when $\gamma > \gamma_0$, the resonances of the unpolarized transmission T have height $1/2$. At the offset $u_1/k^2 = 2k_{SO}/k$ a limit angle γ_1 appears also for the the wave $(-)$. Increasing the offset at higher values both the limit angles γ_0 and γ_1 tend to zero. At the offset $2k_{SO}k$ the second step of the transmission becomes almost perfectly squared as the panel b) of the Fig. (3.4) shows. At this optimum value, $k_- \equiv k$ and $\beta \equiv \gamma$: the mode $(-)$ is no more refracted. With $u = 0$ and γ greater than γ_0 the resonances within the cavity disappear.

Since the output spin polarization of the electrons entering with spin up or down coincides at any angle γ with $T_\uparrow$ or $T_\downarrow$ then the crossing of R zone depolarizes the electrons. The polarization P_{out} of the electrons entering unpolarized is equal to T only for $\gamma > \gamma_0$, and for $\gamma < \gamma_0$ it tends to zero for $\gamma \rightarrow 0$: the crossing of R zone gives rise to a spin polarization that is absent at normal incidence. At the optimum value of the offset $u_1 = 2kk_{SO}$ and for $\gamma > \gamma_0$, P_{out} is independent of the incidence angle. This feature is robust with respect to few elastic scattering events that conserve k but change its direction. This behavior reminds the non-ballistic spin-FET proposed by Schliemann *et al.* [13, 14].

Is is interesting to do an analysis on the proper modes of the Rashba region. In Fig. (3.5) it is shown the transmission as function of the injection angle for $\gamma > \gamma_0$ and several values of the parameters. In the Panel a) of Fig. (3.5) the dashed curve corresponds to the proper mode of the cavity without SO coupling ($u_1/k^2 = 0$, $u/k = 0.4$ and $k_{SO}/k = 0$). If now the SO coupling is turned on and the offset is choosen to the optimum value $u_1 = 2k_{SO}k$ (solid curve – $u_1/k^2 = 0$, $u/k = 0.4$ and $k_{SO}/k = 0.05$) it is observed the halving of the transmission maxima but those preserve the proper modes of the cavity. The proper modes of the cavity are washed out for a perfectly transparent cavity at the optimum offset (dotted-dashed curve – $u_1/k^2 = 0.1$, $u/k = 0$ and $k_{SO}/k = 0.05$). In the last case the flatness of the transmission coefficient (and of polarization vector) is independent by effects related to multiple reflections inside the cavity. In the Panel b) of Fig. (3.5) are reported similar results with the offset to a value lower than the optimum one demonstrating how a perfectly transparent barrier ($u = 0$)
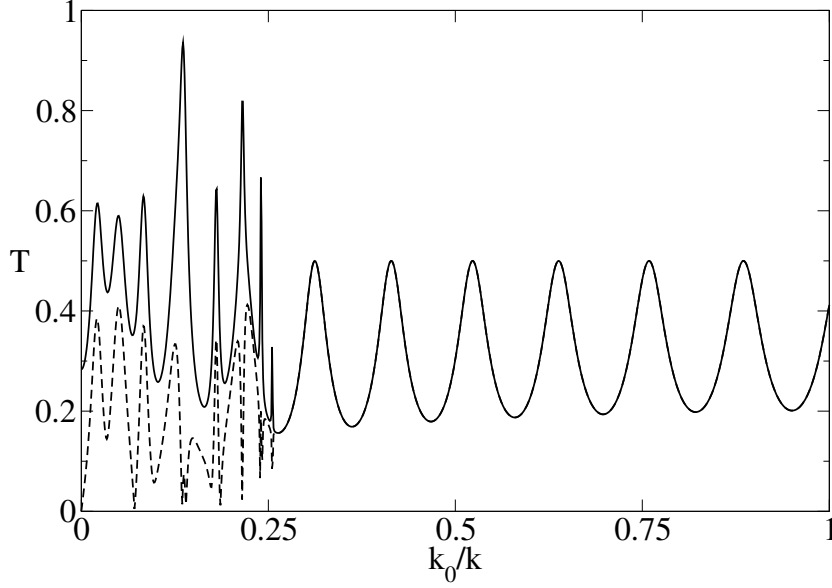
Figure 3.6: The transmission coefficient for unpolarized electrons when $\gamma = 1.25$. The threshold $\overline{k_{SO}}$ is $0.025k$. The dotted curve gives the output spin polarization, $L = 283$ nanometers and we have put $u/k = 0.4$ to enhance the resonances in the low step of the transmission.

has proper modes due only to SO coupling and how this modes modifies when u increases.

It is important to stress that the dependence of the limit angle γ_0 on the SO strength k_{SO} suggests the possibility to build up a spin-FET operating on spin unpolarized electrons injected in the R region. The electrons emerge in the NR drain region partially polarized with a polarization controlled by a gate electrode via the SO interaction. There is a SO strength $\overline{k_{SO}}$ at which $\gamma = \gamma_0$. The Fig. (3.6) shows that the transmission coefficient exhibits irregular Fabry-Perot oscillations below $\overline{k_{SO}}$, whereas for $k_{SO} > \overline{k_{SO}}$ the oscillations become regular with maxima equal to $1/2$. The threshold $\overline{k_{SO}}$ is determined by the offset

$$u_1/k^2 = 2\overline{k_{SO}}/k,$$

for which γ_0 goes over γ and the wave $(+)$ propagation ceases. When $k_{SO} > \overline{k_{SO}}$ the polarization of electrons in the NR drain P_{out} is equal to T (see Appendix A). The system behaves a source of a spin polarized current controlled by k_{SO} with a gate.

It is important to noti that Mireles and Kirczenow [15] have studied the scattering against a finite Rashba region within a quantum wire. They

show that the ballistic spin up or down conductances oscillate varying the SO coupling strength injecting the electrons in a spin up state and they claim that these results may be of relevance for the implementation of quasi-one dimensional spin transistor device. Here it is shown that a ballistic conductance oscillation with k_{SO} appear also without lateral confinement and without ferromagnetic source and drain, that is by handling spin unpolarized electrons.

3.2   Phase averaging due to the thermal broadening

tHere the smoothing effect of the Fermi surface due to finite temperatures are taken into account. Supposing that the system is in the linear response regime, the current I is given by

$$I = G\left(E_{\text{F}}\right) \frac{\mu_1 - \mu_2}{e}$$

$\mu_1 - \mu_2$ being the applied bias and $G\left(E_{\text{F}}\right)$ the conductance ($\mu_1 - \mu_2 << E_{\text{F}}$). For a ballistic conductor [16]

$$G\left(E_{\text{F}}\right) = \frac{2e^2}{h} \int T\left(E\right) F_{\text{T}}\left(E - E_{\text{F}}\right) dE$$

where $F_{\text{T}}\left(E - E_{\text{F}}\right)$ is the thermal broadening function

$$F_{\text{T}}\left(E - E_{\text{F}}\right) = -\frac{d}{dE} \frac{1}{\exp[\left(E - E_{\text{F}}\right)/k_{\text{B}}\overline{T}] + 1} = \frac{1}{4k_{\text{B}}\overline{T}} \text{sech}^2\left(\frac{E}{2k_{\text{B}}\overline{T}}\right)$$

$\overline{T}$ being the temperature. The thermal average of the transmission is

$$\langle T \rangle_{\text{th}} = \int T\left(E\right) F_{\text{T}}\left(E - E_{\text{F}}\right) dE.$$

If the Fermi-Dirac distribution is approximated with the ramp

$$\begin{cases} 1 & E < E_{\text{F}} - 2k_{\text{B}}\overline{T} \\ \frac{1}{2} - \left(E - E_{\text{F}}\right)/4k_{\text{B}}\overline{T} & E_{\text{F}} - 2k_{\text{B}}\overline{T} < E < E_{\text{F}} + 2k_{\text{B}}\overline{T} \\ 0 & E > E_{\text{F}} + 2k_{\text{B}}\overline{T} \end{cases}$$

then

$$\langle T \rangle_{\text{th}} = \frac{1}{2\Delta k} \int_{k_{\text{F}}-\Delta k}^{k_{\text{F}}+\Delta k} T\left(k\right) dk \tag{3.11}$$
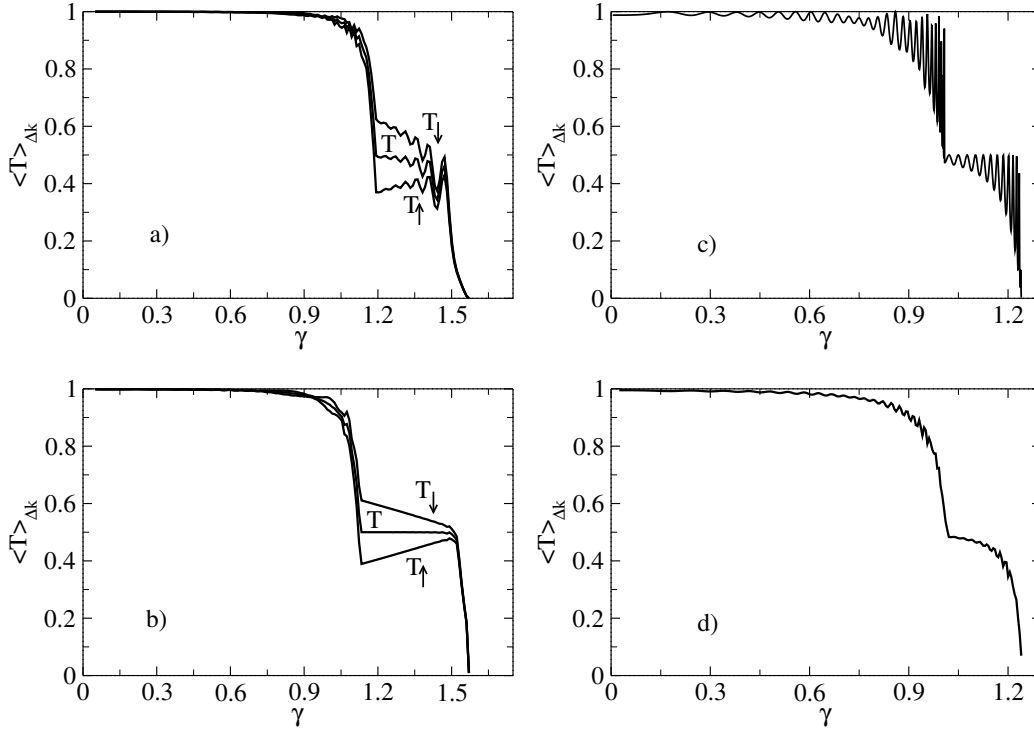
Figure 3.7: Panel a): Thermal-averaged transmission coefficient for unpolarized electrons as function of the injection angle. The curves are relatives to $u_1/k^2 = 0.05$, $u/k = 0$ and $k_{SO}/k = 0.03$. The thermal average corresponds to a temperature of 5 K.

Panel b): As in the Panel a) but with $u_1/k^2 = 0.1$, $u/k = 0$ and $k_{SO}/k = 0.03$. The thermal average corresponds to a temperature of 5 K.

Panel c): Transmission coefficient for unpolarized electrons as function of the injection angle with $u_1/k^2 = 0.2$, $u/k = 0$ and $k_{SO}/k = 0.03$.

Panel d): Thermal-averaged transmission coefficient for unpolarized electrons as function of the injection angle. The curves are relatives to $u_1/k^2 = 0.2$, $u/k = 0$ and $k_{SO}/k = 0.03$. The thermal average corresponds to a temperature of 5 K.

Figure 3.8: Thermal-averaged polarization as function of the injection angle. The solid curve is the module of the polarization vector, the dashed-dotted line corresponds to $< \sigma_x >$, the dashed line corresponds to $< \sigma_y >$ and the dotted line corresponds to $< \sigma_z >$. The curves are evaluated for $u_1/k^2 =$ 0.1, $u/k = 0$ and $k_{\mathrm{SO}}/k = 0.05$. The thermal average corresponds to a temperature of 5 K.

where it is assumed that

$$\Delta k = \frac{k_{\mathrm{B}}\overline{T}}{E_{\mathrm{F}}}k_{\mathrm{F}} \ll k_{\mathrm{F}}.$$
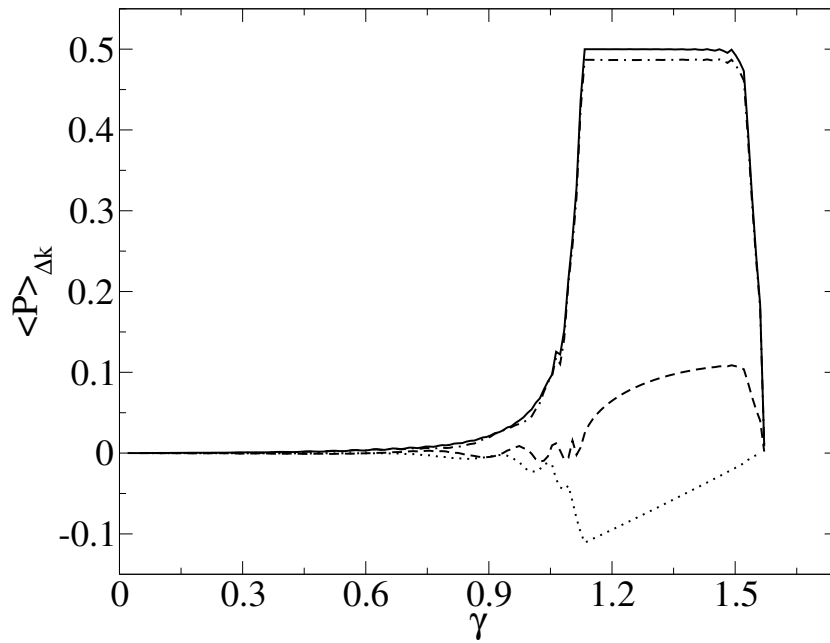
With a Fermi energy $E_{\mathrm{F}} = 14$ meV, and $\overline{T} = 3$ K it is obtained $\Delta k/k_{\mathrm{F}} = 0.018$ and in the following it is chosen $\Delta k/k_{\mathrm{F}} = 0.03$ corresponding to a temperature of 5 K. The effect of the thermal average of the transmissions are now considered. In the Fig. (3.7) it is shown the averaged transmission for various value of the offset. In the Panel a) of Fig. (3.7) the offset is $u_1/k^2 = 0.05$ and few resonances appear when γ is larger than γ_0; increasing the temperature up to 5 K the rapid oscillations of the transmission below γ_0 are almost completely canceled whereas the resonances of the $(-)$ mode are still well defined in the averaged transmission. In the Panel b) of Fig. (3.7) the offset is chosen at the optimum value $u_1/k^2 = 2k_{\mathrm{SO}}/k = 0.1$. It is observed again an almost perfectly squared transmission step among γ_0 and $\pi/2$, whereas below γ_0 the rapid Fabry-Perot oscillations are washed out. The transmission steps for a larger offset $u_1/k^2 = 0.2$ at 0 K and at 5 K are compared in the Panel c) and d) of Fig. (3.7). In this case the transmission oscillations are canceled at any incidence angle but the double step structure survives.

The thermal averaging has been performed also on the polarization vector and the Fig. (3.8) shows the average calculated with Eq. (3.11) of the modulus of the polarization vector and of its three components. The offset is at the optimum value and the output spin-polarization tends to be nearly orthogonal to the interfaces as one expect because $\vec{k}_-$ has a small component in x direction and the spin and the momentum are orthogonal each other.

The Fig. (3.9) shows the thermal average of the transmission of unpolarized electrons as a function of the SO strength with the same parameter of the Fig. (3.6) where the transmission has been calculated at 0 K. Therefore it is clear that an increase of few Kelvin degrees does not cancel the modulation effect.

Appendix A: Output spin polarization evaluation

In this appendix it is given the proof of the relation (3.10). In the general case, the density matrix operator is defined as

$$\rho = \sum_m |m\rangle p_m \langle m|,$$

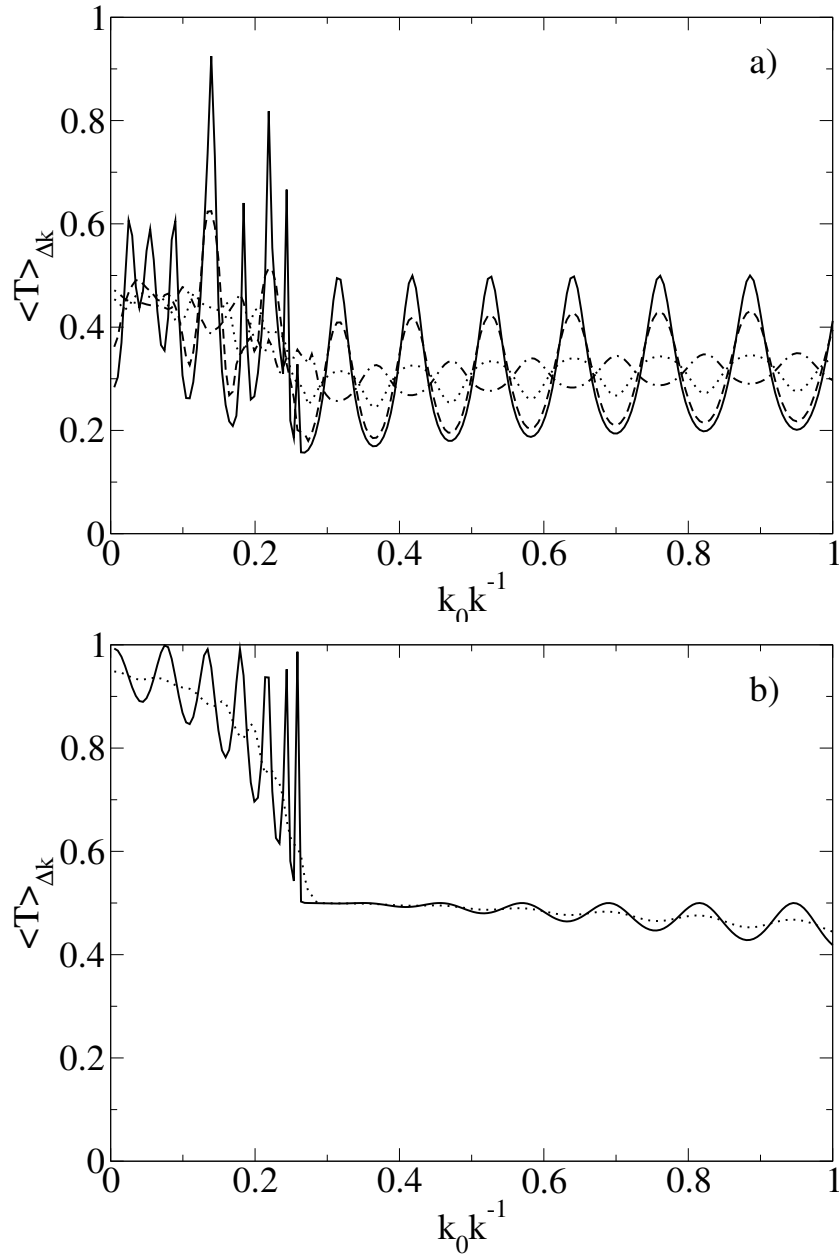**Figure 3.9:** The thermal-averaged transmission coefficient for unpolarized electrons when $\gamma = 1.25$. The threshold $\overline{k_{\mathrm{SO}}}$ is $0.025k$.

Panel a): The solid curve corresponds to zero temperature, the dashed line to a temperature of , the dotted line to a temperature of and the dashed-dotted to a temperature of .

Panel b):

the average value of the observable A is the trace of ρA:

$$\langle A \rangle = \mathrm{Tr}\left[\rho A\right],$$

that in terms of the density matrix elements is equal to

$$\mathrm{Tr}\left[\rho A\right] = \sum_m p_m(|m\rangle\langle m|A) = \sum_m p_m\langle m|A|m\rangle.$$

In present case the density matrix operator has been defined in the Eq. 3.7 with the components (3.8). The averaged value of the modulus of the polarization is defined by

$$\left|\vec{P}_{\mathrm{out}}\right| = \sqrt{\langle\sigma_x\rangle^2 + \langle\sigma_y\rangle^2 + \langle\sigma_z\rangle^2}. \tag{3.12}$$

Using the density matrix operator (3.7)

$$
\begin{aligned}
\langle\sigma_x\rangle &= \frac{1}{2}\left(t_{\uparrow\uparrow}^* t_{\downarrow\uparrow} + t_{\downarrow\uparrow}^* t_{\uparrow\uparrow} + t_{\uparrow\downarrow}^* t_{\downarrow\downarrow} + t_{\downarrow\downarrow}^* t_{\uparrow\downarrow}\right) \\
\langle\sigma_y\rangle &= -\frac{i}{2}\left(t_{\uparrow\uparrow}^* t_{\downarrow\uparrow} - t_{\downarrow\uparrow}^* t_{\uparrow\uparrow} + t_{\uparrow\downarrow}^* t_{\downarrow\downarrow} - t_{\downarrow\downarrow}^* t_{\uparrow\downarrow}\right) \\
\langle\sigma_z\rangle &= \frac{1}{2}\left(|t_{\uparrow\uparrow}|^2 - |t_{\downarrow\uparrow}|^2 + |t_{\uparrow\downarrow}|^2 - |t_{\downarrow\downarrow}|^2\right).
\end{aligned}
\tag{3.13}
$$

Substituting the relations (3.13) into (3.12) it has been obtained:

$$
\begin{aligned}
\left|\vec{P}_{\mathrm{out}}\right|^2 &= \tfrac{1}{4}\Big[|t_{\uparrow\uparrow}|^4 + |t_{\downarrow\uparrow}|^4 + |t_{\uparrow\downarrow}|^4 + |t_{\downarrow\downarrow}|^4 + 2\left(|t_{\uparrow\uparrow}|^2 |t_{\downarrow\uparrow}|^2 + |t_{\uparrow\uparrow}|^2 |t_{\uparrow\downarrow}|^2\right. \\
&\quad - |t_{\uparrow\downarrow}|^2 |t_{\downarrow\uparrow}|^2 + |t_{\downarrow\downarrow}|^2 |t_{\downarrow\uparrow}|^2 + |t_{\downarrow\downarrow}|^2 |t_{\uparrow\downarrow}|^2 - |t_{\downarrow\downarrow}|^2 |t_{\uparrow\uparrow}|^2 \\
&\quad \left. + 2t_{\downarrow\downarrow}t_{\uparrow\uparrow}t_{\downarrow\uparrow}^* t_{\uparrow\downarrow}^* + 2t_{\uparrow\uparrow}^* t_{\downarrow\downarrow}^* t_{\downarrow\uparrow}t_{\uparrow\downarrow}\right)\Big]
\end{aligned}
\tag{3.14}
$$

When the injection angle γ approaches to zero, the system does not flip the spin, that is $t_{\uparrow\downarrow} = t_{\downarrow\uparrow} = 0$ so that

$$\left|\vec{P}_{\mathrm{out}}\right| = \frac{1}{2}\left||t_{\uparrow\uparrow}|^2 - |t_{\downarrow\downarrow}|^2\right|, \tag{3.15}$$

that is in the case of injection of unpolarized electrons the output polarization is zero.

It is important to note that in the R zone the spin state of the $(+)$ and $(-)$ modes given by the spinors $|1\rangle$ and $|2\rangle$ are conserved [5]. The output spin state is strictly determined by the transmitted amplitudes of the interfaces. The interference between the mode $(+)$ and $(-)$ when both are present $(\gamma < \gamma_0)$, makes the polarization different from the transmission as the Eq. (3.15) shows. When $\gamma > \gamma_0$ only the $(-)$ mode survives in the R

zone. This is demonstrated by the fact that the inner product between the state $|1\rangle$ and $|2\rangle$ goes to one

$$|\langle 1|2\rangle| = 1 \quad \text{for } \gamma > \gamma_0,$$

this means that the two wave functions, for $\gamma > \gamma_0$, differ for a phase factor

$$|1\rangle = e^{-i\phi} |2\rangle \quad \rightarrow \quad \frac{1}{\sqrt{T_\uparrow}} \begin{pmatrix} t_{\uparrow\uparrow} \\ t_{\downarrow\uparrow} \end{pmatrix} = e^{-i\phi} \frac{1}{\sqrt{T_\downarrow}} \begin{pmatrix} t_{\uparrow\downarrow} \\ t_{\downarrow\downarrow} \end{pmatrix}. \tag{3.16}$$

Using the previous relation it is possible to express $t_{\uparrow\downarrow}$ and $t_{\downarrow\uparrow}$ as function of $t_{\uparrow\uparrow}$ and $t_{\downarrow\downarrow}$:

$$t_{\downarrow\uparrow} = e^{i\phi} \sqrt{\frac{T_\downarrow}{T_\uparrow}} t_{\uparrow\uparrow} \quad \text{and} \quad t_{\uparrow\downarrow} = e^{-i\phi} \sqrt{\frac{T_\uparrow}{T_\downarrow}} t_{\downarrow\downarrow}. \tag{3.17}$$

Substituting those expressions in the (3.14)

$$\left| \vec{P}_{\text{out}} \right| = \frac{1}{2} \left[|t_{\uparrow\uparrow}|^2 + |t_{\downarrow\downarrow}|^2 + \frac{T_\uparrow^2}{T_\downarrow^2} |t_{\downarrow\downarrow}|^2 + \frac{T_\downarrow^2}{T_\uparrow^2} |t_{\uparrow\uparrow}|^2 \right] \tag{3.18}$$

and using the relations (3.17) this is equivalent to

$$\left| \vec{P}_{\text{out}} \right| = \frac{1}{2} \left[|t_{\uparrow\uparrow}|^2 + |t_{\downarrow\downarrow}|^2 + |t_{\uparrow\downarrow}|^2 + |t_{\downarrow\uparrow}|^2 \right] = \frac{T_\uparrow + T_\downarrow}{2} = T. \tag{3.19}$$

Bibliography

[1] Supriyo Datta and Biswajit Das. Electronic analog of the electro-optic modulator. *Appl. Phys. Lett.*, 56:665, 1990.

[2] G. Schmidt, D. Ferrand, L. W. Molenkamp, A. T. Filip, and B. J. van Wees. Fundamental obstacle for electrical spin injection from a ferromagnetic metal into a diffusive semiconductor. *Phys. Rev. B*, 62(8):R4790, 2000.

[3] H. Ohno. Making nonmagnetic semiconductors ferromagnetic. *Science*, 281:951, 1998.

[4] Marco G. Pala, Michele Governale, Jurgen König, Ulrich Zülicke, and Giuseppe Iannaccone. Two-dimensional hole precession in an all-semiconductor spin field effect transistor. *Phys. Rev. B*, 69:045304, 2004.

[5] V. Marigliano Ramaglia, D. Bercioux, V. Cataudella, G. De Filippis, C.A. Perroni, and F. Ventriglia. Conductance of a large point contact with Rashba effect. *Eur. Phys. J.*, 36:365, 2003.

[6] M. Khodas, A. Shekhter, and A. M. Finkel'stein. Spin polarization of electrons by nonmagnetic heterostructures: The basics of spin optics. *Phys. Rev. Lett.*, 92:086602, 2004.

[7] J. Nitta, T. Akazaki, H. Takayanagi, and T. Enoki. Gate control of spin-orbit interaction in an inverted $In_{0.53}Ga_{0.47}As/In_{0.52}Al_{0.48}As$ heterostructure. *Phys. Rev. Lett.*, 78:1335, 1997.

[8] Th. Schäpers, G. Engels, J. Lange, Th. Klocke, M. Hollfelder, and H. Lüth. Effect of the heterointerface on the spin splitting in modulation doped $In_xGa_{1-x}As/InP$ quantum wells for $B \rightarrow 0$. *J. App. Phys.*, 83:4324, 1998.

[9] D. Grundler. Large rashba splitting in inas quantum wells due to electron wave function penetration into the barrier layers. *Phys. Rev. Lett.*, 84:6074, 2000.

[10] J. B. Miller, D. M. Zumbühl, C. M. Marcus, Y. B. Lyanda-Geller, D. Goldhaber-Gordon, K. Campman, and A. C. Gossard. Gate-controlled spin-orbit quantum interference effects in lateral transport. *Phys. Rev. Lett.*, 90:076807, 2003.

[11] Yu A. Bychkov and E.I. Rashba. Oscillatory effects and the magnetic susceptibility of carriers in inversion layers. *J. Phys. C: Solid State Phys.*, 17:6039, 1984.

[12] D.K. Ferry and S.M. Goodnick. *Transport in nanostructures.* Cambridge University Press, Cambridge, 1997.

[13] John Schliemann, J. Carlos Egues, and Daniel Loss. Nonballistic spin-field-effect transistor. *Phys. Rev. Lett.*, 90:146801, 2003.

[14] John Schliemann and Daniel Loss. Anisotropic transport in a two-dimensional electron gas in the presence of spin-orbit coupling. *Phys. Rev. B*, 68:165311, 2003.

[15] Francisco Mireles and George Kirczenow. Ballistic spin-polarized transport and rashba spin precession in semiconductor nanowires. *Phys. Rev. B*, 64:024426, 2001.

[16] S. Datta. *Electronic Transport in Mesoscopic Systems.* Cambridge University Press, Cambridge, 1995.

4

Rashba effect in quantum networks

Introduction

The dynamics of a quantum particle in a periodic potential in the presence of a uniform static magnetic field has revealed many beautiful effects and has been the subject of ongoing researches for several decades. The competition between the two characteristic length scales involved, *i.e.* the lattice period and the magnetic length, produces a very complex pattern of energy levels. In two dimensions, this leads to fractal structures in the spectrum [1]. Some striking experimental manifestation of these effects have been found in macroscopic properties of two-dimensional superconducting wire networks, such as variation of the critical temperature with respect to the external magnetic field, the magnetization, or the critical temperature.

In the recent years a new effect has been presented [2] in a two dimensional lattice with hexagonal symmetry, the so-called $\mathcal{T}_3$ lattice (see Fig. 4.1 (left)). This is a periodic hexagonal structure with three sites per unit cell, one sixfold coordinated and two threefold coordinated. This is an example of two-dimensional regular bipartite lattice containing nodes with different coordination numbers. For some value of the magnetic field corresponding to half of the flux quantum per elementary tile, the energy spectrum of a tight-binding model with nearest-neighbor hopping collapses into three highly degenerate levels (see Fig. 4.1 (right)). It has been also demonstrated that it is possible to build energy eigenstates where the probability of finding an electron is nonvanishing only in a finite size cluster that has been called Aharonov-Bohm (AB) cage. This corresponds to a localization mechanism
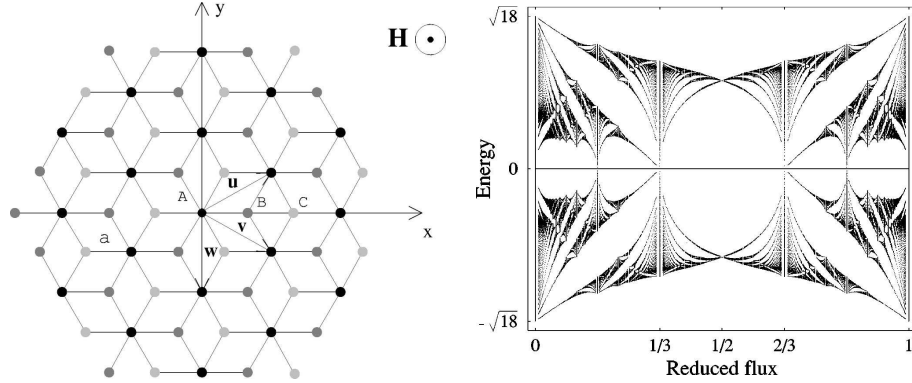
71

Figure 4.1: (Left) A piece of the $\mathcal{T}_3$ lattice embedded in the perpendicular magnetic field **H**; a denotes the lattice spacing. (Right) Spectrum of the $\mathcal{T}_3$ lattice as a function of the reduced flux.

due to quantum interference of Aharonov-Bohm type between paths enclosing a half-integer number of flux quanta. This kind of localization does not rely on disorder [3] but only on quantum-interference and on the geometry of the lattice. There have been several theoretical works addressing different aspects of AB cages as. The effect of several kind of disorder has been studied [4] showing that a weak Anderson-like disorder and finite size effects, do not drastically modify the main features of the ideal mode. In particular, if disorder is not too important, the single-particle energy eigenstates remain strongly localized for half-integer fluxes per elemetary tile, and this independently of the disorder strength. In the case of the electron-electron interaction [5], it has been demonstrated that partially destroy the localization. The AB cage effect has been studied also in the transport properties of a finite piece of $\mathcal{T}_3$ lattice and it has been shown that this effect is robust to a moderate amount of elastic disorder [6].

Two series of experiments have confirmed the existence of these AB cages. Abilio *et al.* [7] have shown that a superconducting wire network with the adapted structure exhibit a striking reduction of the critical current for the predicted values of the magnetic field. Naud *et al.* [8] have measured the megnetoresistance oscillations of a normal network tailored in a high mobility two-dimensional electron gas (2DEG) in the so called $\mathcal{T}_3$ lattice (see Fig. 4.2).

As I have introduced in the Chap. I, an electron wavefunction moving in the presence of Rashba Spin-Orbit (SO) coupling acquires quantum phases due to the Aharonov-Casher effect [9–14]. In a recent Letter [15], I have shown that in quantum networks with a particular bipartite geometry
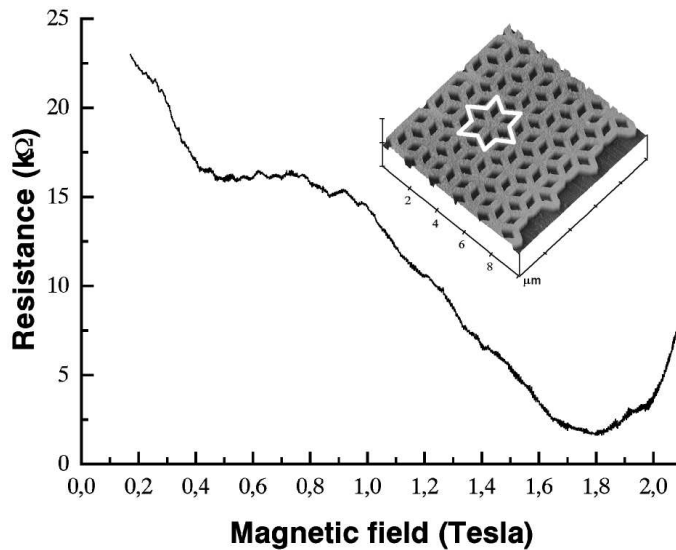
Figure 4.2: Magnetoresistance at $T = 30$ mK of the $\mathcal{T}_3$ lattice between 0 and 2 T. The inset shows an AFM view of the sample. The width of each wire is about 0.5 μm and the area of a unit rhombus is equal to 0.8 μm^2, leading to a quantum flux ϕ_0 for $B = 50$G. An AB cage in underlined in white [8].

containing nodes with different coordination numbers is possible to obtain localization of the electron wavefunction by means of the Rashba effect. This phenomenon has been shown in a linear chain of square loops connected at one vertex (see Fig. 4.3), which has been termed *diamond chain*.

In this chapter I improve the formalism introduced in my previous work [15], taking the effect of the magnetic field into account. Then I analyze the mechanism of the localization due to the Rashba SO coupling into detail in comparison with the AB effect.

The chapter is organized in the following way. In the Sec. 4.1 I introduce a very general formalism to study a quantum network realized with single-channel quantum wires in presence of Rashba SO coupling and an external magnetic field. Section 4.2 is devoted to the study of the spectral and the transport properties of the diamond chain in presence only of Rashba SO coupling. A physical interpretation of the localization phenomena due to the Rashba SO coupling and to the magnetic field respectively is presented in Sec. 4.3. The Sec. 4.4 is devoted to the study of two different kind of two-dimensional quantum network in presence of Rashba SO coupling and magnetic field. Here it is shown how the combination of both effect can

induce effect of anti-localization. The paper ends with short conclusions of
the results presented.

4.1   Model and formalism

I consider a single-channel quantum wire in a generic direction $\hat{\gamma}$ in the plane
(x, y). The system is in the presence of a magnetic field B perpendicular to
the plane (x, y) and Rashba SO coupling. The Hamiltonian for the single-
channel quantum wire is:

$$\mathcal{H} = \frac{\left(\vec{p} + q\vec{A}\right)^2}{2m} + \frac{\hbar k_{\mathrm{SO}}}{m} \left[\vec{\sigma} \times \left(\vec{p} + q\vec{A}\right)\right] \cdot \hat{z} + V(\hat{\gamma}), \qquad (4.1)$$

where m is the electron mass, $\vec{A}$ the vector potential relative to the magnetic
field $(\vec{B} = \vec{\nabla} \times \vec{A})$, k_{SO} is the SO coupling strength and $V(\hat{\gamma})$ is the wire
confining potential. The SO coupling strength k_{SO} is related to the spin
precession length L_{SO} by $L_{\mathrm{SO}} = \pi/k_{\mathrm{SO}}$. For InAs quantum wells the spin-
precession length ranges from 0.2 to 1 μm [16–19]. Then I perform a *Peierls*
transformation on the Hamiltonian (4.1) that recasts as

$$\mathcal{H} = \frac{p_\gamma^2}{2m} - \frac{\hbar k_{\mathrm{SO}}}{m} p_\gamma \left(\vec{\sigma} \times \hat{z}\right) \cdot \hat{\gamma}. \qquad (4.2)$$

where now p_γ is the momentum along the $\hat{\gamma}$ direction. The contribution of
the magnetic field comes out as a phase factor of the wavefunction of the
form

$$\exp\left\{-if_{\alpha,r}\right\} = \exp\left\{-i\frac{2\pi}{\phi_0} \int_\alpha^r \vec{A} \cdot \mathrm{d}\vec{l}\right\} \qquad (4.3)$$

where $\phi_0 = h/e$ is the flux quantum.

The wavefunction on a bond (quantum wire) connecting the nodes α and
β, along the direction $\hat{\gamma}_{\alpha\beta}$ that takes into account the phase factor (4.3) is

$$\mathbf{\Psi}_{\alpha\beta}(r) = \frac{e^{-if_{\alpha r}} e^{i(\vec{\sigma} \times \hat{z}) \cdot \hat{\gamma}_{\alpha\beta} \ k_{\mathrm{SO}} r}}{\sin(k l_{\alpha\beta})} \left\{\sin\left[k(l_{\alpha\beta} - r)\right] \mathbf{\Psi}_\alpha \right.$$
$$\left. + \sin(kr) e^{if_{\alpha\beta}} e^{-i(\vec{\sigma} \times \hat{z}) \cdot \hat{\gamma}_{\alpha\beta} \ k_{\mathrm{SO}} l_{\alpha\beta}} \mathbf{\Psi}_\beta \right\}. \qquad (4.4)$$

where k is related to the eigen energy by $\epsilon = \frac{\hbar^2}{2m}(k^2 - k_{\mathrm{SO}}^2)^1$, r is the coordinate
along the bond, and $l_{\alpha\beta}$ the length of the bond. The spinors $\mathbf{\Psi}_\alpha$ and $\mathbf{\Psi}_\beta$
are the values of the wavefunction at the nodes α and β respectively. The

---

[1]The term in k_{SO}^2 can be neglected in realistic situations.
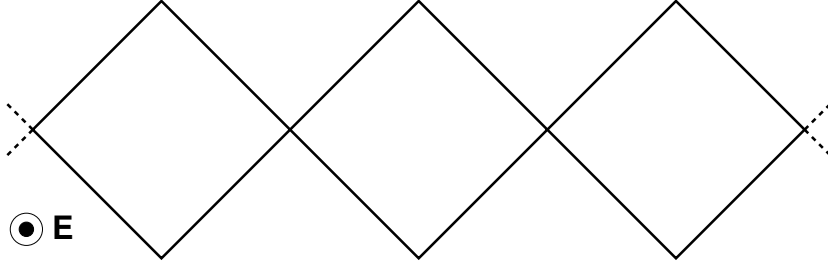
Figure 4.3: Schematic view of the diamond chain. The bonds are single-channel quantum wires with SO coupling. In the ideal case all bonds have the same length L. The unitary cell contain three nodes (4 wires): one with coordination number 4 and two with coordination number 2.

spin precession due to the Rashba effect is described by the exponentials containing Pauli matrices in Eq. (4.4).

The eq. (4.4) is the key step to generalize the existing methods to study quantum networks [6,15,20] in the presence of Rashba SO coupling and magnetic field. The wavefunction of the whole network is obtained by imposing the continuity of probability current at the nodes. For a generic node α it reads:

$$\mathbf{M}_{\alpha\alpha}\mathbf{\Psi}_\alpha + \sum_{\langle\alpha,\beta\rangle} \mathbf{M}_{\alpha\beta}\mathbf{\Psi}_\beta = 0, \tag{4.5}$$

where

$$\mathbf{M}_{\alpha\alpha} = \sum_{\langle\alpha,\beta\rangle} \cot kl_{\alpha\beta} \tag{4.6a}$$

$$\mathbf{M}_{\alpha\beta} = -\frac{e^{-if_{\alpha\beta}} e^{-i(\vec{\sigma}\times\hat{z})\cdot\hat{\gamma}_{\alpha\beta}\ k_{\mathrm{SO}}l_{\alpha\beta}}}{\sin kl_{\alpha\beta}}. \tag{4.6b}$$

In Eqs. (4.5,4.6) the sum $\sum_{\langle\alpha,\beta\rangle}$ runs over all nodes β which are connected by a bond to the node α. This set of boundary conditions ensures the self-adjointness of the Schrödinger operator (4.2).

4.2 One-dimensional case

The one-dimensional analysis takes account of the case where only the SO coupling is present, that is the magnetic field is zero ($B = 0$) [15].

4.2.1 Spectral properties

Here the method presented in the Sec. 4.1 is used to calculate the spectral properties of the minimal model of a bipartite structure containing nodes
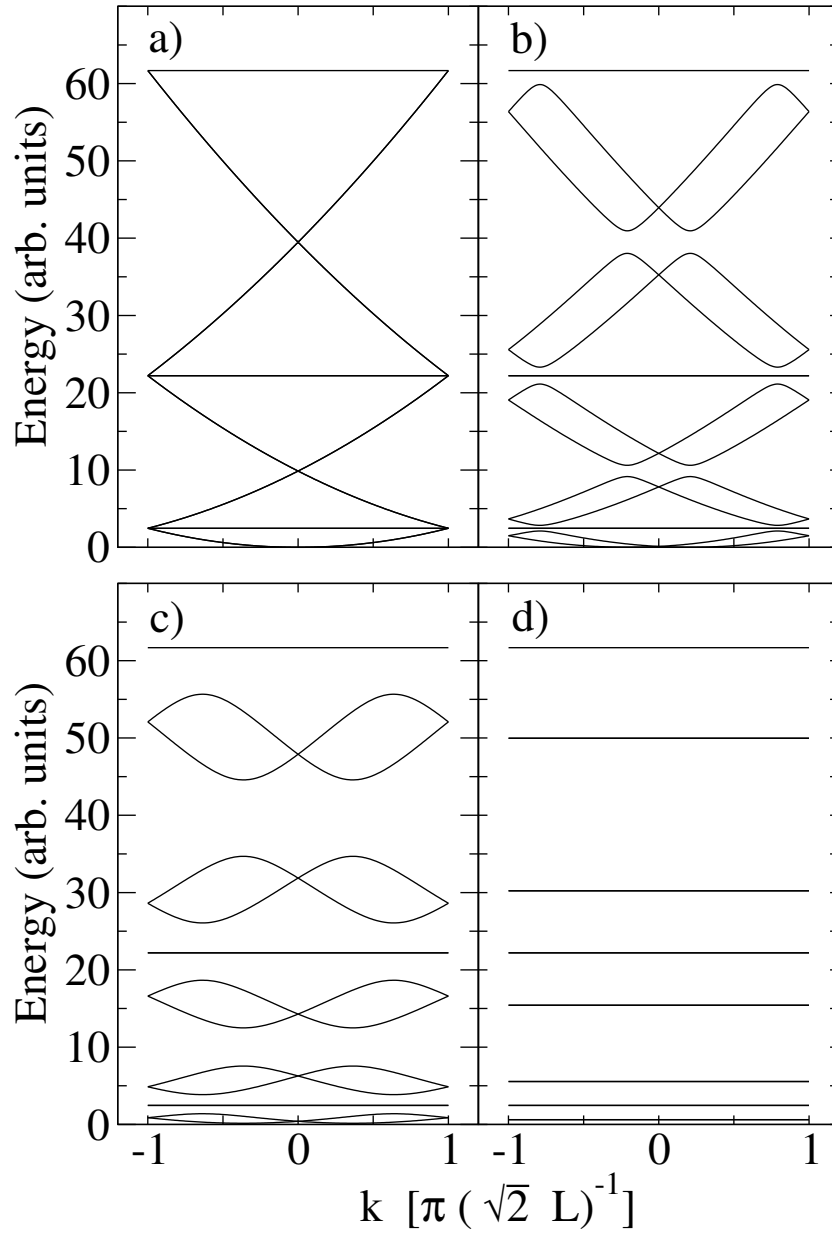
Figure 4.4: Spectrum of the diamond chain for different values of the strength of the spin-orbit coupling: a) $k_{\mathrm{SO}}L = 0$; b) $k_{\mathrm{SO}}L = 0.5$; c) $k_{\mathrm{SO}}L = 1.0$; and d) $k_{\mathrm{SO}}L = \pi/2$.

with different coordination numbers. This model structure is a linear chain of square loops connected at one vertex (see Fig. 4.3), called *diamond chain*. An infinite lattice is recovered imposing the Bloch condition on the wavefuction in the unit cell. This straightforward procedure yields for the spectrum the following analytical expressions

$$\varepsilon_n^{(0)}(k) = \left(\frac{\pi}{2} + n\pi\right)^2 \tag{4.7}$$

$$\varepsilon_n^{(\pm)}(k) = \left\{ n\pi + \arccos\left[\frac{1}{2}\left(2 + 2\cos(\sqrt{2}kL)\cos(k_{\mathrm{SO}}L)^2\right.\right.\right.$$
$$\left.\left.\left. \pm\sqrt{2}\sin(\sqrt{2}kL)\sin(2k_{\mathrm{SO}}L)\right)^{\frac{1}{2}}\right]\right\}^2 . \tag{4.8}$$

The momentum k is defined in the first Brillouin zone $\left[-\frac{\pi}{\sqrt{2}L}, \frac{\pi}{\sqrt{2}L}\right]$ where $\sqrt{2}L$ is the lattice constant. The spectrum is composed by three kinds of bands. The first one is non-dispersive: this is a characteristic of every bipartite structures containing nodes with different coordination numbers, its degeneracy is equal to the difference between the number of nodes with different coordination numbers [5]. The bands $\pm$ are degenerate for zero SO coupling and are split by it. The eq. (4.8) shows clearly that the spectrum become non-dispersive for $k_{\mathrm{SO}}L = (n + \frac{1}{2})\pi$, being n an integer. Using the spin-precession length, this condition can be recast as $L = (n + \frac{1}{2})L_{\mathrm{SO}}$. For these value of the SO coupling strength the system becomes localized. In the effective mass approximation it is evident that this is diverging. A portion of the spectrum Eqs. (4.7, 4.8) is shown in Fig. (4.4) for increasing values of the SO coupling strength. For zero SO coupling there are no gaps in the spectrum. For finite values of the Rashba coupling the spin degeneracy of the $\pm$ bands is lifted and gaps open in the spectrum. When the SO coupling strength approaches the value $k_{\mathrm{SO}}L = \pi/2$ the spectrum collapses to a series of non dispersive bands.

4.2.2 Transport properties: clean case

In the case of the AB cage, the first experimental verification came from transport measurements [7, 8]. To propose a possible experimental verifications of the Rashba-cage effect it is necessary to evaluate the linear conductance for a diamond chain of finite length. To show that this localization effect is due to the peculiar bipartite geometry of the lattice containing nodes with different coordination numbers, it is possible to contrast the diamond chain with square ladder, i.e a chain of square loopsconnected at two vertices, (see inset of Fig. 4.5). In the following, the latter topology is referred as

ladder. The conductance is evaluated making use of the Landauer–Büttiker formalism [21,22]. I consider a finite piece of lattice connected to semi-infinite leads (with no SO coupling) modeling reservoirs (see inset of Fig. 4.5). The transmission coefficients are computed proceeding along the lines proposed by Vidal *et al.* [6]. An electron with spin $\sigma = \pm$ along a generic direction, whose corresponding spinors are χ_σ, is inject from the left wire. The wavefunctions on the external leads are simply

$$\Psi_{\text{left}}(r) = e^{ik_{\text{in}}r}\chi_\sigma + \sum_{\sigma'} r_{\sigma'\sigma}e^{-ik_{\text{in}}r}\chi_{\sigma'} \tag{4.9}$$

$$\Psi_{\text{right}}(r) = \sum_{\sigma'} t_{\sigma'\sigma}e^{ik_{\text{in}}r}\chi_{\sigma'}, \tag{4.10}$$

where r is the coordinate on the semi-infinite input/output lead, with the origin fixed at the position of the input/output node.

The transmission and reflection coefficients ($t_{\sigma'\sigma}$ and $r_{\sigma'\sigma}$, respectively) can be obtained by solving the linear system of equations arising from the continuity of the probability current at all nodes in the network and of the wavefunction at the input and output nodes. The conditions for the continuity of the probability current at internal nodes are given in Eq. (4.5). For the external nodes they read

$$\mathbf{M}_{00}\mathbf{\Psi}_0 + \sum_{\langle 0,\beta\rangle} \mathbf{M}_{0\beta}\mathbf{\Psi}_\beta = -i(\chi_\sigma - \sum_{\sigma'} r_{\sigma'\sigma}\chi_{\sigma'}) \tag{4.11}$$

$$\mathbf{M}_{NN}\mathbf{\Psi}_N + \sum_{\langle N,\beta\rangle} \mathbf{M}_{N\beta}\mathbf{\Psi}_\beta = i\sum_{\sigma'} t_{\sigma'\sigma}\chi_{\sigma'}, \tag{4.12}$$

where the injection node is labeled as "0" and the output node as "N". The total transmission coefficient is then simply $|t|^2 = \sum_{\sigma,\sigma'} |t_{\sigma'\sigma}|^2$. As it can be seen by inspection of the terms Eq. (4.6) appearing in the continuity equations (setting $l_{\alpha\beta} = L$), all the properties are periodic in k with a periodicity $2\pi/L$. Furthermore, for the total conductance the period in k is halved, i.e. it is π/L. Finite temperature or finite voltage will introduce in a natural way an average over k_{in}. For $\text{Max}[K_BT, eV] \geq K_BT^* = \frac{\hbar^2}{m}k_F\frac{\pi}{L}$, the result of a transport measurement will be the conductance integrated over $k_{\text{in}} \in [0, \pi/L]$, indicated as $\langle G(k_{\text{SO}} L)\rangle_{k_{\text{in}}}$. Taking for the Fermi energy of the single-channel wires 10 meV, $m/m_e = 0.042$ for the effective mass (InAs), and $L = 1\mu$m, yields $T^* \approx 7$ K.

For a given k_{in}, the conductance has a rich structure that takes into account the complexity of the associate energy spectrum. In particular increasing k_{SO} gaps open and the energy of the incoming electrons ($\epsilon_{\text{in}} = \frac{\hbar^2 k_{\text{in}}^2}{2m}$)
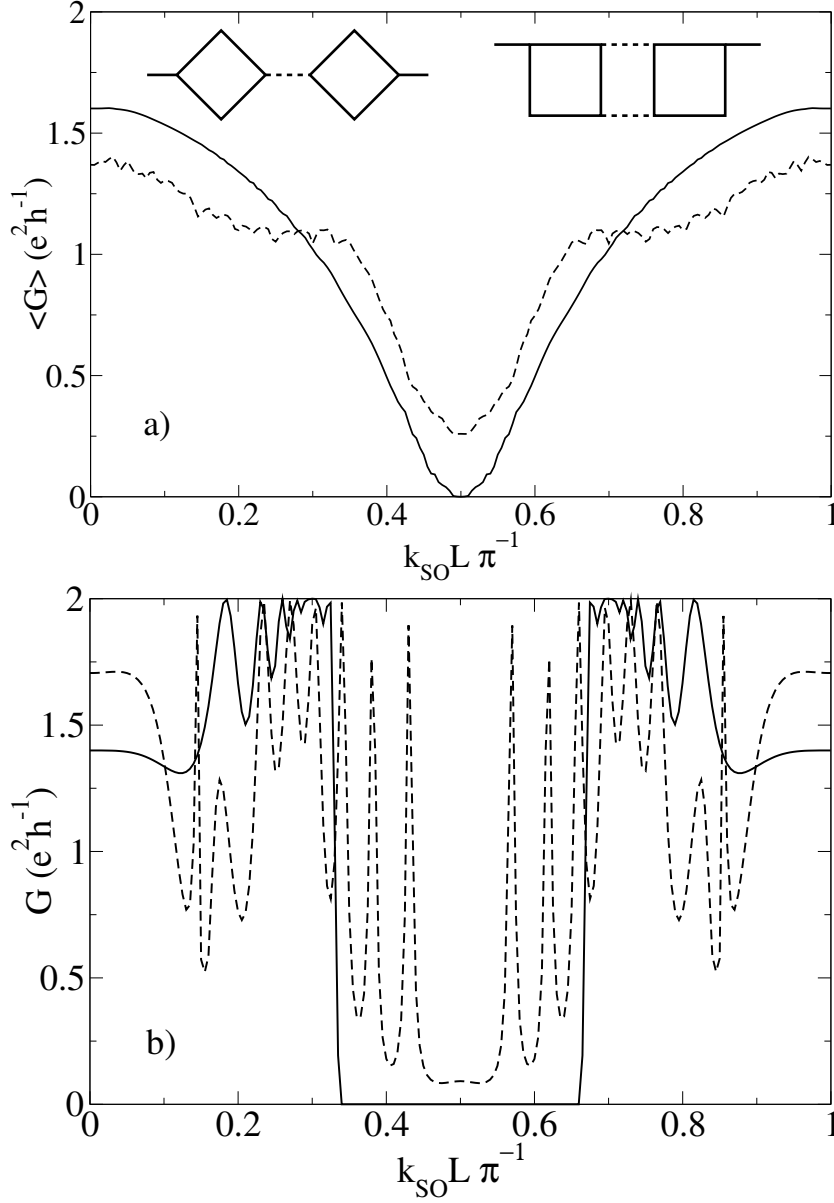
Figure 4.5: Panel a): Conductance (averaged over k_{in} as a function of the spin-orbit coupling strength for the diamond chain (continuous line) and for the ladder (dashed line). The two finite-size systems connected to input/output leads are shown in the inset. The parameters used for the calculation are: 50 elementary loops, k_{in} uniformly distributed in $[0, \pi/L]$.
Panel b): Conductance as a function of the spin-orbit coupling strength for the diamond chain (continuous line) and for the ladder (dashed line) for a fixed value of $k_{in} = k_F$. The parameters used for the calculation are: 50 elementary loops, $k_F L = n\pi + 2$, being n an integer.

can enter one of these gaps leading to a vanishing conductance but not to localization [see panel b) of Fig. 4.5]. In fact, in this case the insulating behavior is due to the absence of available states at the injection energy and not to the localization in space of the electron wavefunction. This effects is not present in $\langle G(k_{\mathrm{SO}} L)\rangle_{k_{\mathrm{in}}}$, as the integration over k_{in} is equivalent to an average over energy. The dependence of the average conductance $\langle G(k_{\mathrm{SO}} L)\rangle_{k_{\mathrm{in}}}$ on k_{SO} is shown in panel a) of Fig. (4.5) for both the diamond chain and the square ladder. The conductance for both kind of chains has a minimum for $k_{\mathrm{SO}} L = \pi/2$ due to interference caused by the phase differences induced by the Rashba effect. But due to the existence of the Rashba cages, this minimum reaches zero only for the diamond chain.

4.2.3   Transport properties: disordered case.

From the studies on the AB cages, it is expected that the localization induced by the Rashba effect to be robust against disorder only in the bipartite structure containing nodes with different coordination numbers (diamond chain). There are several kind of disorder that can be considered. Potential disorder along the wires (for example randomly located point-like scatterers) does not lead, in this purely one-dimensional model, to a modification of the phases acquired on a bond by spin-precession but only to a renormalization of the bond transmission. The disorder that is more dangerous for the Rashba-cage effect is a random fluctuation of the length of the bonds (see Vidal *et al.* [6]), as such length fluctuations induce fluctuations of the phase shifts due to spin-precession. Hence, it is taken into account a model where the length of each bond is randomly distributed in the interval $[L - \Delta L, L + \Delta L]$. The half width of the distribution ΔL gives the strength of the disorder.

In order to clarify if disorder affects the conductance, an average over disorder configurations is performed. This is relevant to experiments, as in a real sample averaging is introduced by the finite phase-coherence length. For intermediate values of disorder ($k_{\mathrm{F}}\Delta L \approx 1$) it is shown that the Rashba-cage effect is still present for the diamond chain, whereas the periodicity in k_{SO} is halved for the ladder, as shown in Fig. (4.6). This latter result can be interpreted as the analog of the Altshuler-Aharonov-Spivak (AAS) effect [23] induced by the SO coupling. The halving of the oscillation period is due to the enhancement of back-reflection due to interference of pair of paths traveling clockwise and counter-clockwise along a square of the chain (according to weak localization picture). At higher values of disorder the AAS effect prevails also in the diamond chain.
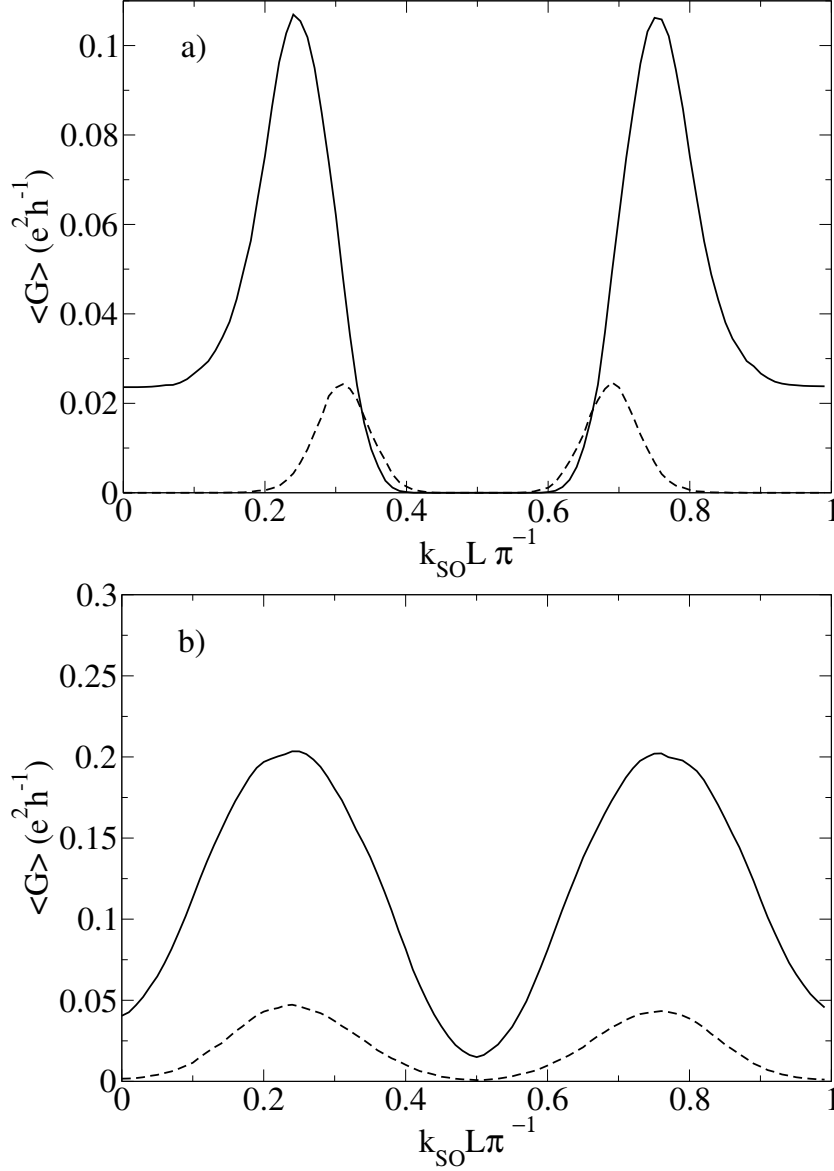
Figure 4.6: Conductance (averaged over disorder configurations and over k_{in}) plotted as a function of the spin-orbit coupling strength for the diamond chain [panel a)] and the ladder [panel b)]. The two values of the disorder strength used in the calculation are: $\Delta L = 0.01L$ (solid line) and $\Delta L = 0.02L$ (dashed line). Disorder averaging is done over 50 configurations, and k_{in} is uniformly distributed in $[k_F - \pi/2, k_F + \pi/2]$, with $k_F L = 100$. Both chains systems are composed by 50 elementary loops.

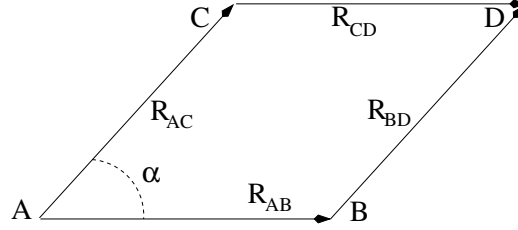**Figure 4.7:** Closed path between the point A and D. This is parametrized as function of the angle α.

4.3   Physical interpretation

In this Section I give a physical interpretation of the localization phenomenon that we have introduced in the latter section. In addition I show the crucial difference with AB effect.

I consider the closed path in Fig. 4.7, where the four arms have the same length. An electron injected in the point A can reach the point D moving through the upper path or though the lower path. The electron wavefunction gains a phase that depends on the Hamiltonian describing the system and on the traveling path. This corresponds to introduce a phase operator $\mathcal{R}_{pq}$ that relates the wavefunction in the starting point p with the its value in the ending point q:

$$\psi(q) = \mathcal{R}_{pq}\psi(p).$$

In this simple picture, condition to have localization in this closed path is that an electron injected in the point A undergoes destructive interference in D. This condition in mathematical form corresponds to

$$(\mathcal{R}_{BD} \cdot \mathcal{R}_{AB} + \mathcal{R}_{CD} \cdot \mathcal{R}_{AC})\psi = 0 \quad \forall \psi. \tag{4.13}$$

When is present the Rashba SO coupling and the magnetic field is zero, the phase operator takes spin precession into account and has the form

$$\mathcal{R}_{pq} = \exp\left\{ -i \int_p^q \vec{\sigma} \cdot \left(\hat{z} \times \mathrm{d}\vec{l} \right) k_{\mathrm{SO}} \right\}, \tag{4.14}$$

this is a spin dependent operator. When (4.14) is replaced it in the Eq. 4.13, the latter recast in the form $\{\mathcal{R}_{AB}, \mathcal{R}_{AC}\} = 0$, being $\{\ldots\}$ the anticommutator, that is because in the closed path of Fig. 4.7 the phase operator (4.14) acts in the same way along the paths AB/CD and AC/BD. From the Eq. 4.13 it is possible to have information about the transmission probability through the relation

$$|t|^2 = \mathrm{Tr}\left[\Gamma\Gamma^\dagger \right] \tag{4.15}$$

where $\Gamma = \mathcal{R}_{BD} \cdot \mathcal{R}_{AB} + \mathcal{R}_{CD} \cdot \mathcal{R}_{AC}$. In the Fig. 4.8 is shown the behavior of the transmission probability (4.15) as function of the angle α and of the SO coupling $k_{\text{SO}}L$. It is clear that the transmission probability goes to zero if and only if the angle between the path is equal to $\pi/2$ and the SO coupling is equal to $\pi/2$. This imply that complete localization is achieved only in
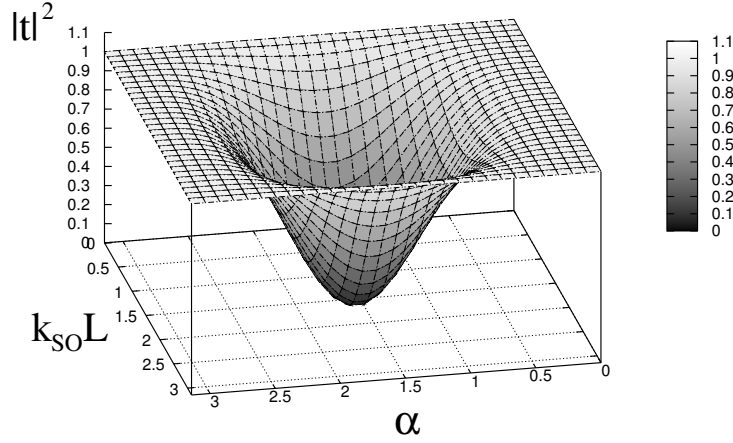

Figure 4.8: Three-dimensional plot of the transmission probability (4.15) as function on the angle α between the paths AB and AC, and of the spin-orbit coupling $k_{\text{SO}}L$. The graph shows that we get zero transmission probability if and only if $\alpha = \pi/2$ and $k_{\text{SO}}L = \pi/2$.

a linear chain of square loops connected at one vertex and not in chain of rhombi. This not imply that the localization due to the Rashba SO coupling cannot be achieved in any other structures. The previous analysis is applied to a set of closed paths composed of for arms.

The same analysis can be performed on the set of the regular polygons. In order to evaluate the transmission probability the length of each bond is fixed equal to P/N where N is the number of vertices and P the perimeter of the polygon that is kept on constant. The transmission amplitude is

$$\begin{aligned}
\Gamma &= \mathcal{R}_1 \cdot \mathcal{R}_2 \cdot \ldots \cdot \mathcal{R}_{N/2} + \mathcal{R}_{N/2} \cdot \mathcal{R}_{N/2-1} \cdot \ldots \cdot \mathcal{R}_1 \\
&= \prod_{i=1}^{N/2} \mathcal{R}_i + \prod_{j=0}^{N/2-1} \mathcal{R}_{N/2-j}.
\end{aligned} \tag{4.16}$$

Than the transmission probability is given by the relation (4.15).In Fig.4.9 are shown the transmission probability (4.15) for $N = 4$, $N = 6$ and $N = 8$
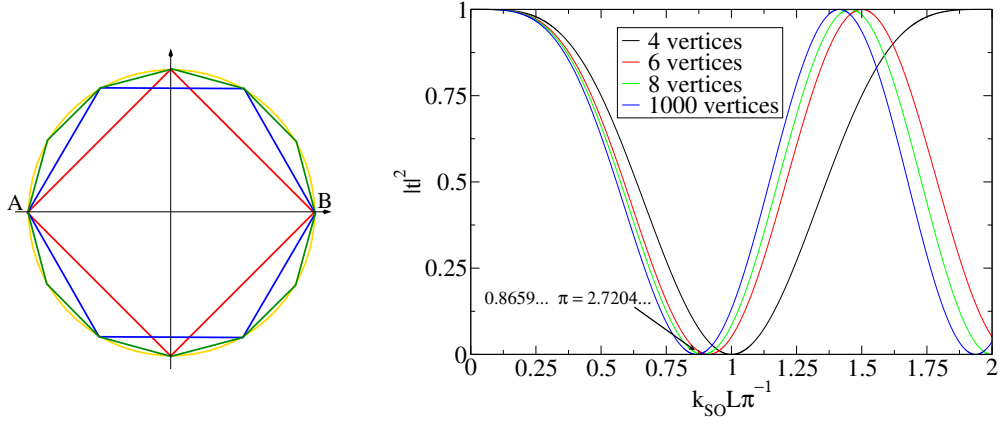
Figure 4.9: (Left) A set of regular polygons that in the limit of $N \to \infty$ is equivalent to a ring. Each vertex of the polygons is a single-channel quantum wire. (Right) Transmission probability as function of the Rashba spin-orbit coupling for several polygons. It is important to note that the length of each vertex is P/N where N is the number of vertices and P the perimeter of the polygon that is kept constant.

and $N = 1000$. All the curves have a periodicity equal to the number of vertices N. It is interesting to note that there are value of the SO coupling $k_{\mathrm{SO}}P$ such that the conductance is zero. This is due to the quantum interference stemming from the fact that an electron traveling along different paths acquire different SO phases. In the periodicity range the number of zero-conductance points is equal to $N/2 - 1$. A set of this point of zero conductance can be classified by the following relation:

$$k_{\mathrm{SO}}P^{(n)} = \frac{N}{2}\pi\left(2n + 1\right), \tag{4.17}$$

where N is the number of vertices and n is the order of the zero.

It is interesting to study the limit of large N. It is natural to aspect that in this limit the result for the transport through a quantum ring [14] are recovered. In the formalism presented in this chapter the spin-eigenstates are vectors of the x–y plane. In the paper of Frustaglia *et al.* is shown that this result is recovered adiabatic limit, *i.e.* when the eigenstates of the ring Hamiltonian are in the (x, y) plane. In this situation the values of SO coupling to have the suppression of the conductance are:

$$k_{\mathrm{SO}}P = \pi\sqrt{(2n)^2 - 1} \quad \forall n \in \mathbb{N}^*. \tag{4.18}$$

The analysis of the zeros presented in this Fig. 4.9 for $N = 1000$ are in accordance with the Eq. (4.18).
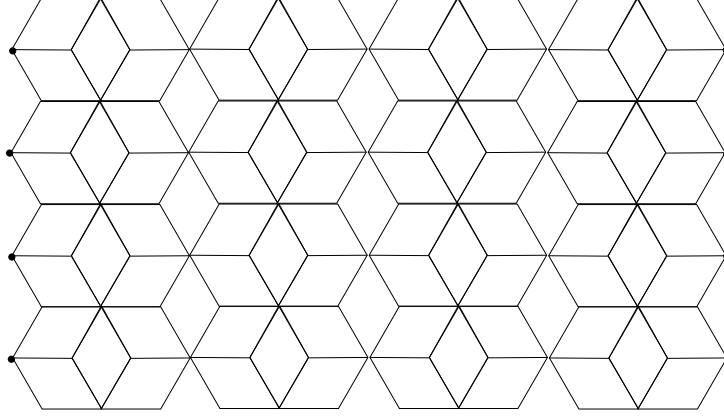
Figure 4.10: A piece of the $\mathcal{T}_3$ network. Black (respectively, grey) dots represent the connections to the input (respectively, output) channels.

When is present a magnetic field B and the Rashba SO coupling is zero the phase operator has the form

$$\mathcal{R}_{pq} = \exp\left\{-i\frac{2\pi}{\phi_0}\int_p^q \vec{A}\cdot\mathrm{d}\vec{l}\right\}.\qquad(4.19)$$

This operator is strongly dependent on the path on which the electron travels and it does not depend on spin. If this phase operator is replaced in the Eq. (4.13) then the solution of the localization problem is given by

$$B = \left(n+\frac{1}{2}\right)\frac{\phi_0}{\sin(\alpha)L^2}.\qquad(4.20)$$

This equation relates inversely the magnetic field to the area of the closed path and tells us that for every value of the area it is possible to apply a magnetic field that induces complete localization [24].

4.4 Two-dimensional case

I now pay attention to a periodic tilling with hexagonal symmetry called $\mathcal{T}_3$ (see Fig 4.10). On the basis of the results of Sec. 4.3 I show that, in this kind of structure, transport properties have a signature of the localization effects due to the Rashba SO coupling and of the magnetic field. In fact I aspect to recover complete localization with the magnetic field [6] but for the Rashba SO coupling. This is due to the fact that the characteristic angles of the $\mathcal{T}_3$ do not permit to the Rashba SO coupling to induce complete localization.
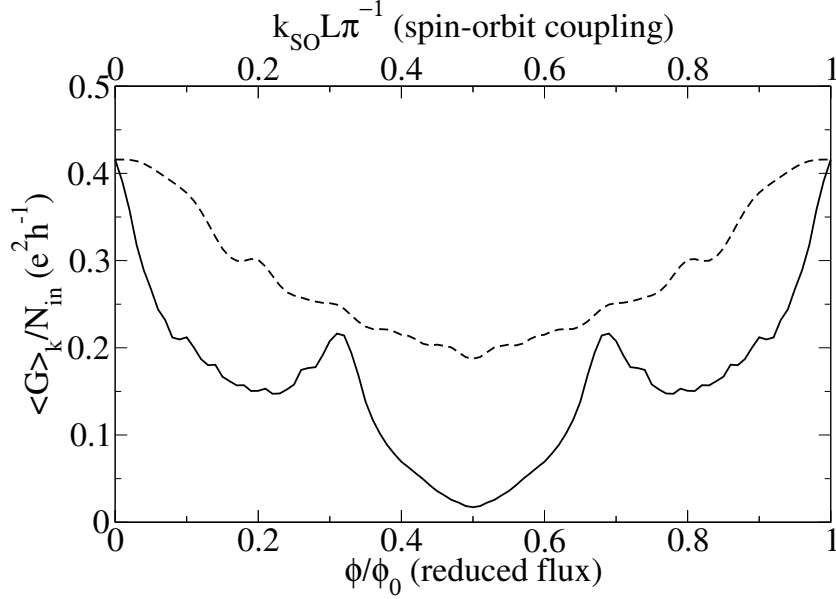
Figure 4.11: Averaged conductance $\langle G \rangle_k / N_{in}$ as function of the reduced flux (solid curve) and of spin-orbit coupling (dashed curve) for the $\mathcal{T}_3$ lattice with 200 quantum wires.

In Fig. 4.11 are shown the behaviors of the averaged conductance for a finite piece of the $\mathcal{T}_3$ lattice as function of the reduced flux with zero SO coupling (solid line) and of the SO coupling with zero magnetic field (dashed line). In the case of the magnetic field it is possible to observe a suppression of the conductance due to the existence of the AB cage. The value of the averaged conductance minimum is not exactly zero. This is due to the existence of dispersive edge states [6] that are able to carry current even for $\phi/\phi_0 = 1/2$. This value is independent on the number of the injection channels. In the case of the SO coupling it is not observed a strong suppression of the averaged conductance as in the case of the magnetic field. A minimum is present but this is due to interference phenomena that do not induce complete localization. Furthermore, this minimum cannot be due to existence of edge states because depends on the number of injection channels.

In Fig. 4.12 are shown the behaviors of the averaged conductance as function of the SO coupling with $\phi/\phi_0 = 0.5$ and as function of the magnetic field with $k_{SO} L \pi^{-1} = 0.5$. In the first case the averaged conductance starts from the point of maximum localization due to the AB effect, in the second case the averaged conductance starts from the point of maximum localization due to the Rashba SO coupling. The main features of those two curves are that in the case of fixed SO coupling the general behavior is similar to the
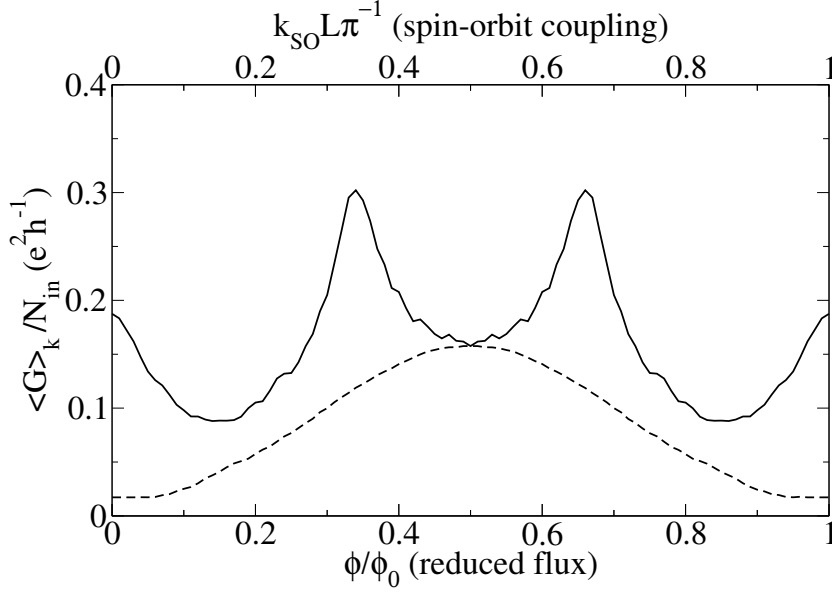
Figure 4.12: Averaged conductance $\langle G \rangle_k / N_{in}$ as function of the reduced flux evaluated at $k_{SO} L \pi^{-1} = 0.5$ (solid curve) and of spin-orbit coupling evaluated at $\phi/\phi_0 = 0.5$ (dashed curve) for the $\mathcal{T}_3$ lattice with 200 quantum wires.

case without it. The main features of those to curves are that in the case of fixed SO coupling the general behavior is similar to the case without it. A well defined minimum for $\phi/\phi_0 = 0.5$ is still observed. On the contrary in the case of fixed magnetic field we observe as the SO coupling suppress the destructive interference due to the AB effect and an anti-localization peak takes place.

Since in the $\mathcal{T}_3$ under SO coupling complete localization is not observed, AAS oscillations in the case of a disordered system have to observed. In Fig. 4.13 are shown the behaviors of the averaged conductance with respect to the disorder as function of the reduced flux (solid line) and as function of the SO coupling (dashed line) for fixed disorder strength. It is clearly seen that for the the averaged conductance as function of the SO coupling the periodicity is no longer $k_{SO} L$ but $k_{SO} L/2$. The $k_{SO} L$-periodic oscillation have been washed out since they do not have a given phase. By the contrast, the $k_{SO} L/2$-periodic oscillation are still present since they are related to phase-coherent pairs of time reversed trajectories according to the weak-localization pictures. The averaged conductance as function of the reduced flux remains ϕ_0 periodic with a large amplitude. This strongly suggests that the AB cage effect survives for this strength of disorder.

I now consider the transport through a finite square lattice (see Fig. 4.14).
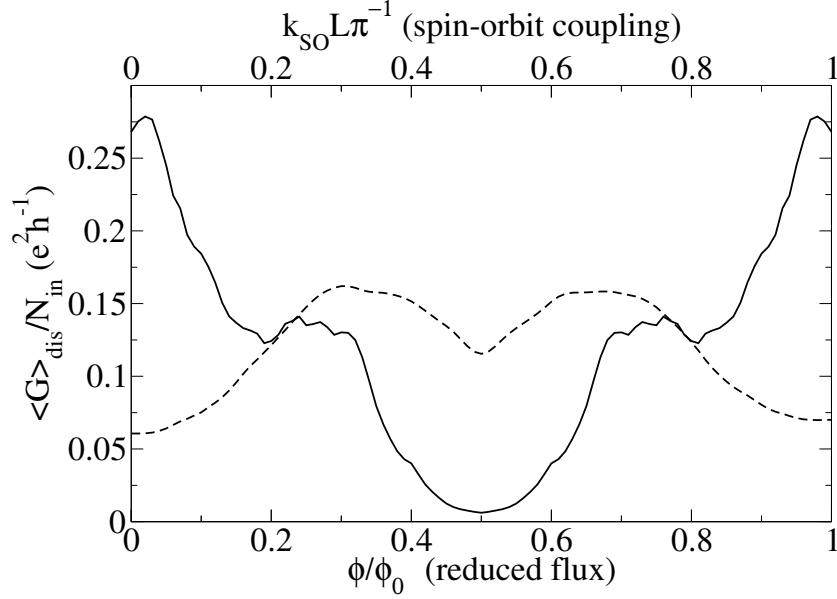
Figure 4.13: Averaged conductance $\langle G \rangle_{dis}/N_{in}$ for a disordered network as function of the reduced flux evaluated (solid curve) and of spin-orbit coupling (dashed curve) for the $\mathcal{T}_3$ lattice with 200 quantum wires.

This network, unlike the $\mathcal{T}_3$ lattice, does not present a bipartite structures containing nodes with different coordination numbers. So any localization phenomenon due either to the AB effect or to the SO coupling is observed. On the other hand, as shown in the Sec. 4.3, the square network is composed by elementary cells (the square) that , as single elements, permit to observe complete localization due both to magnetic field and to the SO coupling.

In the Fig.4.15 are shown the behaviors of the averaged conductance for a finite piece of the square lattice as function of the reduced flux with zero SO coupling (solid line) and of the SO coupling with zero magnetic field (dashed line). The behavior of the averaged conductance in the case of SO coupling is completely different from the one of the magnetic field. However the former in the point $k_{SO}L\pi^{-1} = 1/2$ and the latter in the point $\phi/\phi_0 = 1/2$ reach the same value. This can be interpreted using the results of the Sec. 4.3. In fact, for those values, both the AB effect and the SO coupling induce complete localization in the elementary cell of the square network, that is for those two critical values the system behaves in the same way. Now, exporting this simple idea to the case of the square network, it is possible to infer that the conductance evaluate in $k_{SO}L\pi^{-1} = 1/2$ or in $\phi/\phi_0 = 1/2$ has to show the same value.

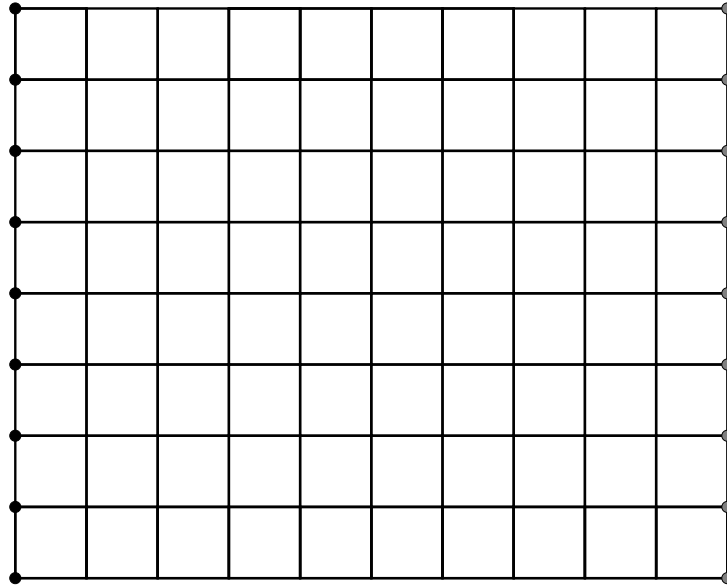It is interesting to analyze what happens when both the magnetic field

Figure 4.14: A piece of the square lattice. Black (respectively, grey) dots represent the connections to the input (respectively, output) channels.
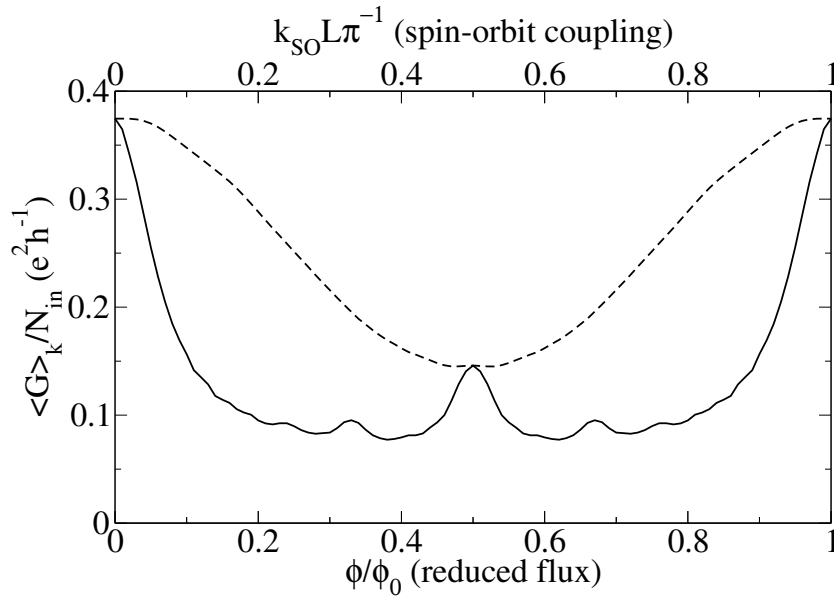

Figure 4.15: Averaged conductance $\langle G \rangle_k / N_{in}$ as function of the reduced flux (solid curve) and of spin-orbit coupling (dashed curve) for the square lattice with 178 quantum wires.
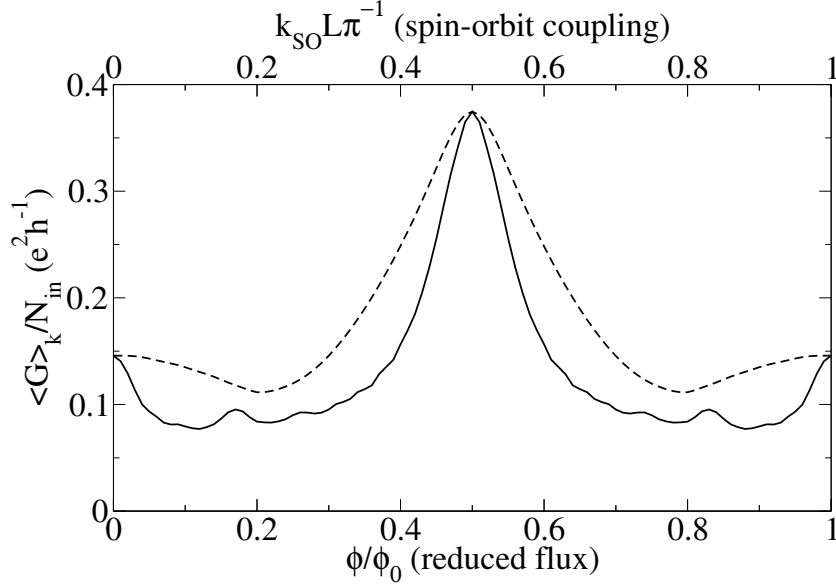
Figure 4.16: Averaged conductance $\langle G \rangle_k / N_{in}$ as function of the reduced flux evaluated at $k_{\text{SO}} L \pi^{-1} = 0.5$ (solid curve) and of spin-orbit coupling evaluated at $\phi/\phi_0 = 0.5$ (dashed curve) for the square lattice with 178 quantum wires.

and the SO coupling are present at the same time. In Fig. 4.16 are shown the behaviors of the averaged conductance as function of the SO coupling with $\phi/\phi_0 = 0.5$ and the averaged conductance as function of the magnetic field with $k_{\text{SO}} L \pi^{-1} = 0.5$. The behavior of both curves is very similar. Using the results of the Sec. 4.3 it is evident that those two localization phenomena conduct to the same effect as consequence of different physical aspects. In the case of the SO coupling it is observed destructive interference between electrons undergoing a spin-precession instead in the case of the AB effect the destructive interference process is spin independent. This issue gives to possibility of understanding what happens when both localization phenomena are present at the maximum intensity. The destructive interference is completely lost. Anti-localization is observed rather than localization. The averaged conductance goes to the same value that we observe for zero magnetic field and zero SO coupling (see Fig. 4.15).

In Fig. 4.17 are shown the behaviors of the averaged conductance as function of the reduced flux and of the SO coupling in the case of a disordered system. Also in this case, it is manifest that the periodicity with respect to the magnetic flux and to the SO coupling is no longer ϕ_0 and $k_{\text{SO}} L$ but $\phi_0/2$ and $k_{\text{SO}} L/2$ respectively.
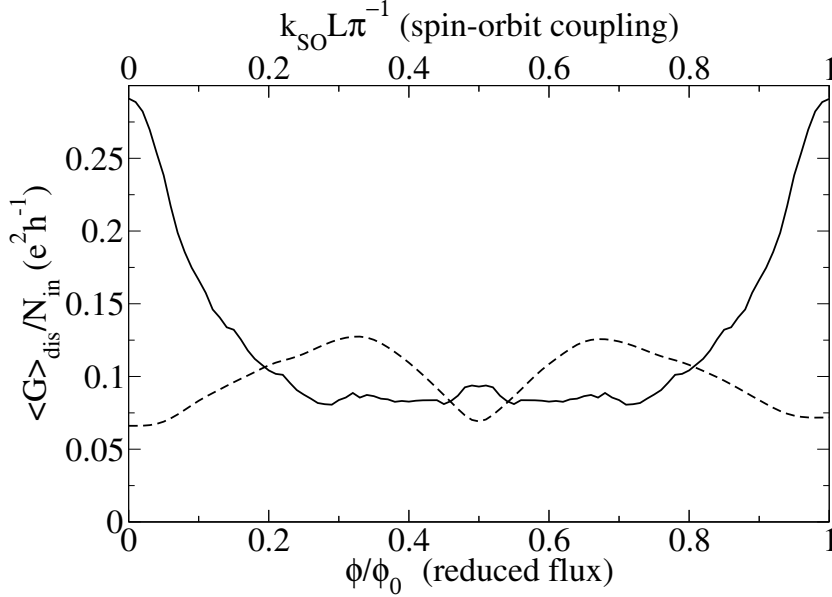
Figure 4.17: Averaged conductance $\langle G \rangle_{dis}/N_{in}$ for a disordered network as function of the reduced flux (solid curve) and of spin-orbit coupling (dashed curve) for the square lattice with 178 quantum wires.

Appendix A: Quantum graphs

Usually the term *quantum graph* or *quantum network* is used for a graph considered as a one-dimensional singular variety and equipped with a self-adjoint differential operator, the *Hamiltonian*. There are several reason to study the quantum graphs. They arise as simplified model in mathematics, physics, chemistry, and engineering, when one considers propagation of waves of different nature through a *mesoscopic* quasi-one-dimensional system that looks like a thin neighborhood of a graph [25]. One can mention in particular the free-electron theory of conjugated molecules in chemistry [26], quantum chaos [20,27–29], quantum wire dynamical system [30], photonic crystals [31], scattering theory [32], and a variety of other applications [33,34]. The problems addressed in quantum graph theory include justifications of quantum graphs as approximations for more realistic and complex models of waves in complex structures, analysis of various direct and inverse spectral problems and many other.

A *graph* Γ consists of a finite or countably infinite set of vertices $V = \{v_i\}$ and a set $E = \{e_j\}$ of edges connecting the vertices. Each edge e can be identified with a pair (v_j, v_k) of vertices. Loops and multiple edges between vertices are allowed. It is indicated with E_v the set of all edges incident to

the vertex v. It is assumed that the degree $d_v = |E_v|$ of any vertex v is finite and positive. Therefore the vertices with no edges coming in or going out are excluded. This is natural, since for the quantum graph purposes such vertices are irrelevant.

In the following the definition to introduce a topological and metric object are introduced.

Definition 1 *A graph Γ is said to be a metric graph if each edge e is assigned a positive length $l_e \in (0, \infty]$.*

In this case, having the length assigned, an edge e will be identified with a finite or infinite segment $[0, l_e]$ of the real line with the natural coordinate x_e along it. This enables one to interpret the graph Γ as a topological space that is the union of all edges where the ends corresponding to the same vertex are identified.

Graph Γ can be equipped with a natural metric. If a sequence of edges $\{e_j\}_{j=1}^M$ forms a path, its length is defined as $\sum l_j$. For two vertices v and w, the distance $\rho(v, w)$ is defined as the minimal path length between them.

It is important to underline that a graph is not only the set of all vertices, but all intermediate points x in the edges as well. Therefore, it is natural define the Lebesgue measure $\mathrm{d}x$ on the graph. Functions $f(x)$ on Γ are defined along the edges. Having this, and the measure, one can define in a natural way some function space on the graph.
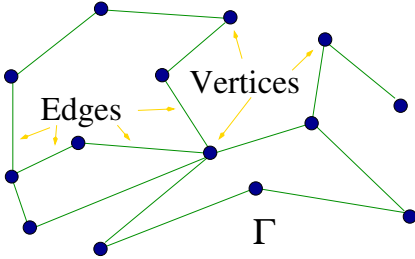
Figure 4.18: A generic quantum graph Γ.

Definition 2 *(1) The space $L_2(\Gamma)$ on Γ consists of functions that are measurable and square integrable on each edge e and such that*

$$\|f\|_{L_2(\Gamma)}^2 = \sum_{e \in E} \|f\|_{L_2(e)}^2 < \infty.$$

In other words, $L_2(\Gamma)$ is the orthogonal direct sum of the space $L_2(e)$.
(2) The Sobolev space $H^1(\Gamma)$ consists of all continuous functions on Γ that belong to $H^1(e)$ for each edge e and such that

$$\sum_{e \in E} \|f\|_{H^1(e)}^2 < \infty.$$

There seems to be no natural definition of the Sobolev spaces f $H^k(\Gamma)$ of the order k higher than unity, since boundary conditions at vertices depend on the Hamiltonian.

In the fields of applications of the quantum graph theory usually it is interesting to study self-adjoint operator of Γ. The operator of interest in the simplest case are the negative second derivate

$$f(x) \rightarrow -\frac{\mathrm{d}^2 f}{\mathrm{d}x^2}, \tag{4.21}$$

a more general Schrödinger operator

$$f(x) \rightarrow -\frac{\mathrm{d}^2 f}{\mathrm{d}x^2} + V(x)f(x), \tag{4.22}$$

or a Schrödinger operator that takes account of the of a magnetic field

$$f(x) \rightarrow \left(\frac{1}{\mathrm{i}}\frac{\mathrm{d}}{\mathrm{d}x} - A(x)\right)^2 + V(x)f(x). \tag{4.23}$$

Here x denotes the coordinate x_e along the edge e.

In order to complete the definition of operators, one needs to describe their domains. The natural conditions requires that f belong to the Sobolev space $H^2(e)$ on each edge e. One also needs to impose boundary value conditions at the vertices.

Appendix B: Boundary conditions and self-adjointness

There is the problem to add boundary conditions to the operators (4.21-4.23) in order to assure the self-adjointness property. The analysis can be done both for finite and infinite quantum graph but in the following it will be restricted to the finite case.

The problem is addressed to the local (or vertex) boundary conditions, that is in those that involve the values at a single vertex only at a time. Because along each edge the operators (4.21-4.23) acts as the second derivative, it is necessary to establish two conditions per edge, and hence at each vertex the number of conditions must coincide with the degree d of the vertex. For function in H^2 on each vertex, the conditions may involve only the boundary values of the function and its derivative. The most general form of such condition is

$$A_v F + B_v F' = 0, \tag{4.24}$$

where A_v and B_v are $d \times d$ matrices, F is the vector $(f_1(v), \ldots, f_d(v))^t$ of the vertex values of the function along each edge, and $F' = (f_1(v), \ldots, f_d(v))^t$ is the vector of the vertex values of the derivative taken along the edges in the outgoing direction at the vertex v.

Now the problem is focused of which are the necessary and sufficient conditions on matrices A and B in (4.24) that would guarantee self-adjointness of the resulting operator. All this conditions are completely described in [30]. The main result is collected in the following

Theorem 1 *Let Γ be a metric graph with finitely many edges. Consider the operator $\mathcal{H}$ acting as $-d^2/dx^2$ on the edge e, with the domain consisting of functions that belong to $H^2(e)$ on each edge e and satisfy the boundary conditions (4.24) at each vertex. Here $\{A_v, B_v \mid v \in V\}$ is a collection of matrices of size $d_v \times d_v$ such that each matrix $(A_v B_v)$ has the maximal rank d. In order for $\mathcal{H}$ to be self-adjoint, the following condition at each vertex is necessary and sufficient:*

$$\text{the matrix} \quad A_v B_v^* \quad \text{is self-adjoint.} \tag{4.25}$$

The proof of this theorem can be found in [30].

Examples of boundary conditions

In this section I illustrate briefly various form of vertex conditions.

δ-type conditions.

These are defined as follows:

$$\boxed{\begin{aligned} &f(x) \text{ is continuous on } \Gamma \quad \text{and} \\ &\text{at each vertex } v, \ \sum_{e \in E_v} \frac{\mathrm{d}f}{\mathrm{d}x_e}(v) = \alpha_v f(v). \end{aligned}} \tag{4.26}$$

Here α_v are some fixed numbers. One can recognize these conditions as an analogue of the conditions one obtains from a Schrödinger operator on the line with a δ potential. In this case the conditions can be written in the form (4.24) with

$$A_v = \begin{pmatrix} 1 & -1 & 0 & \ldots & 0 \\ 0 & 1 & -1 & \ldots & 0 \\ \ldots & \ldots & 0 & 1 & -1 \\ -\alpha_v & 0 & \ldots & 0 & 0 \end{pmatrix}$$

and

$$B_v = \begin{pmatrix} 0 & 0 & \dots & 0 \\ \dots & \dots & \dots & \dots \\ 0 & 0 & 0 & 0 \\ 1 & 1 & \dots & 1 \end{pmatrix}$$

Since

$$A_v B_v^* = \begin{pmatrix} 0 & 0 & \dots & 0 & 0 \\ \dots & \dots & \dots & \dots & \dots \\ 0 & 0 & \dots & 0 & -\alpha_v \end{pmatrix}$$

the self-adjointness condition (4.25) is satisfied if and only if α is real.

Neumann (Kirchhoff) conditions.

These conditions represent the most common case of the δ-type conditions (4.26) when $a_v = 0$, that is

$$\boxed{\begin{aligned} &f(x) \text{ is continuous on } \Gamma \quad \text{and} \\ &\text{at each vertex } v, \ \sum_{e \in E_v} \frac{\mathrm{d}f}{\mathrm{d}x_e}(v) = 0. \quad\quad (4.27) \end{aligned}}$$

Conditions of δ'-type.

These conditions recall the δ-type ones, but with the roles of functions and derivatives reversed at each vertex. In order to describe them, I introduce the notation f_v for the restriction of a function onto the edge e. Then the conditions at each vertex v can be described as follow.

$$\boxed{\begin{aligned} &\text{The value of} \quad \frac{\mathrm{d}f_e}{\mathrm{d}x_e}(v) \quad \text{is the same for all edges } e \in E_v \\ &\text{and} \quad \sum_{e \in E_v} f_e(v) \quad = \quad \alpha_v \frac{\mathrm{d}f}{\mathrm{d}x}(v). \quad\quad (4.28) \end{aligned}}$$

Here, as before, $\frac{\mathrm{d}f_e}{\mathrm{d}x_e}(v)$ is the derivative in the outgoing direction at the vertex v. It is clear that compared with the δ-type case the matrices A_v and B_v are switched:

$$B_v = \begin{pmatrix} 1 & -1 & 0 & \dots & 0 \\ 0 & 1 & -1 & \dots & 0 \\ \dots & \dots & 0 & 1 & -1 \\ -\alpha_v & 0 & \dots & 0 & 0 \end{pmatrix}$$

and

$$A_v = \begin{pmatrix} 0 & 0 & \dots & 0 \\ \dots & \dots & \dots & \dots \\ 0 & 0 & 0 & 0 \\ 1 & 1 & \dots & 1 \end{pmatrix}$$

Since

$$A_v B_v^* = \begin{pmatrix} 0 & 0 & \dots & 0 & 0 \\ \dots & \dots & \dots & \dots & \dots \\ 0 & 0 & \dots & 0 & -\alpha_v \end{pmatrix}$$

the self-adjointness condition (4.25) is satisfied if and only if α is real.

Vertex Dirichlet conditions.

The *Vertex Dirichlet conditions* are those where at each vertex is required that the boundary values of the function on each edge are equal to zero. In this case the operator completely decouples into the direct sum of the operators (4.21-4.23) with Dirichlet conditions on each edge. There is no communication between the edges. The spectrum $\sigma(\mathcal{H})$ is then found as

$$\sigma(\mathcal{H}) = \left\{ \frac{n^2 \pi^2}{l_e^2} \middle| e \in E, \ n \in \mathbb{Z} - 0 \right\}.$$

Bibliography

[1] Douglas R. Hofstadter. Energy levels and wave functions of Bloch electrons in rational and irrational magnetic fields. *Phys. Rev. B*, 14:2239, 1976.

[2] Julien Vidal, Remy Mosseri, and Benoit Douçot. Aharonov-Bohm cages in two-dimensional structures. *Phys. Rev. Lett.*, 81:5888, 1998.

[3] P.W. Anderson. Absence of diffusion in certain random lattices. *Phys. Rev.*, 109:1492, 1958.

[4] Julien Vidal, Patrick Butaud, Benoit Douçot, and Remy Mosseri. Disorder and interactions in Aharonov-Bohm cages. *Phys. Rev. B*, 64:155306, 2001.

[5] Julien Vidal, Benoit Douçot, Remy Mosseri, and Patrick Butaud. Interaction induced delocalization for two particles in a periodic potential. *Phys. Rev. Lett.*, 85:3906, 2000.

[6] Julien Vidal, Gilles Montambaux, and Benoit Douçot. Transmission through quantum networks. *Phys. Rev. B*, 62:R16294, 2000.

[7] C. C. Abilio, P. Butaud, Th. Fournier, B. Pannetier, J. Vidal, S. Tedesco, and B. Dalzotto. Magnetic field induced localization in a two-dimensional superconducting wire network. *Phys. Rev. Lett.*, 83:5102, 1999.

[8] Cécile Naud, Giancarlo Faini, and Dominique Mailly. Aharonov-Bohm cages in 2D normal metal networks. *Phys. Rev. Lett.*, 86:5104, 2001.

[9] Y. Aharonov and A. Casher. Topological quantum effects for neutral particles. *Phys. Rev. Lett.*, 53:319, 1984.

[10] Harsh Mathur and A. Douglas Stone. Quantum transport and the electronic Aharonov-Casher effect. *Phys. Rev. Lett.*, 68:2964, 1992.

[11] A. V. Balatsky and B. L. Altshuler. Persistent spin and mass currents and Aharonov-Casher effect. *Phys. Rev. Lett.*, 70:1678, 1993.

[12] A. G. Aronov and Y. B. Lyanda-Geller. Spin-orbit Berry phase in conducting rings. *Phys. Rev. Lett.*, 70:343, 1993.

[13] Janine Splettstößer, Michele Governale, and Ulrich Zülicke. Persistent current in ballistic mesoscopic rings with rashba spin-orbit coupling. *Phys. Rev. B*, 68:165341, 2003.

[14] Diego Frustaglia and Klaus Richter. Spin interference effects in ring conductors subject to rashba coupling. *Phys. Rev. B*, 69:235310, 2004.

[15] Dario Bercioux, Michele Governale, Vittorio Cataudella, and Vincenzo Marigliano Ramaglia. Rashba-effect-induced localization in quantum networks. *Phys. Rev. Lett.*, 93:056802, 2004.

[16] J. Nitta, T. Akazaki, H. Takayanagi, and T. Enoki. Gate control of spin-orbit interaction in an inverted $In_{0.53}Ga_{0.47}As/In_{0.52}Al_{0.48}As$ heterostructure. *Phys. Rev. Lett.*, 78:1335, 1997.

[17] Th. Schäpers, G. Engels, J. Lange, Th. Klocke, M. Hollfelder, and H. Lüth. Effect of the heterointerface on the spin splitting in modulation doped $In_xGa_{1-x}As/InP$ quantum wells for B $\rightarrow$ 0. *J. App. Phys.*, 83:4324, 1998.

[18] D. Grundler. Large Rashba splitting in InAs quantum wells due to electron wave function penetration into the barrier layers. *Phys. Rev. Lett.*, 84:6074, 2000.

[19] J. B. Miller, D. M. Zumbühl, C. M. Marcus, Y. B. Lyanda-Geller, D. Goldhaber-Gordon, K. Campman, and A. C. Gossard. Gate-controlled spin-orbit quantum interference effects in lateral transport. *Phys. Rev. Lett.*, 90:076807, 2003.

[20] Tsampikos Kottos and Uzy Smilansky. Periodic orbit theory and spectral statistics for quantum graphs. *Annals of Physics (San Diego)*, 274:76, 1999.

[21] Yoseph Imry and Rolf Landauer. Conductance viewed as transmission. *Rev. Mod. Phys.*, 71:S306, 1999.

[22] M. Büttiker. Four-terminal phase-coherent conductance. *Phys. Rev. Lett.*, 57:1761, 1986.

[23] B. L. Al'tshuler, A. G. Aronov, and B. Z. Spivak. The Aharonov–Bohm effect in disordered conductors. *JETP Lett.*, 33:94, 1981.

[24] Y. Aharonov and D. Bohm. Significance of electromagnetic potentials in the quantum theory. *Phys. Rev.*, 115:485, 1959.

[25] P. Kuchment. Quantum graphs: I. Some basic structures. *Waves Random Media*, 14:107, 2004.

[26] M.J. Richardson and N.L. Balasaz. In the network model of molecules and solids. *Ann. Phys. (N.Y.)*, 73:308, 1971.

[27] Tsampikos Kottos and Uzy Smilansky. Quantum chaos on graphs. *Phys. Rev. Lett.*, 79:4794, 1997.

[28] Tsampikos Kottos and Uzy Smilansky. Periodic orbit theory and spectral statistics for quantum graphs. *Annals of Physics (San Diego)*, 274:76, 1999.

[29] Tsampikos Kottos and Uzy Smilansky. Chaotic scattering on graphs. *Phys. Rev. Lett.*, 85:968, 2000.

[30] V Kostrykin and R Schrader. Kirchhoff's rule for quantum wires. *J. Phys. A: Math. Gen.*, 32:595, 1999.

[31] P. Exner and R. Gawlista. Band spectra of rectangular graph superlattices. *Phys. Rev. B*, 53:7275, 1996.

[32] C. Texier and G. Montambaux. Scattering theory on graphs. *J. Phys. A: Math. Gen.*, 34:10307, 2001.

[33] Y. Avishai, Y. Hatsugai, and M. Kohmoto. Localization problem of a two-dimensional lattice in a random magnetic field. *Phys. Rev. B*, 47:9561, 1993.

[34] Tsuneyoshi Nakayama, Kousuke Yakubo, and Raymond L. Orbach. Dynamical properties of fractal networks: Scaling, numerical simulations, and physical realizations. *Rev. Mod. Phys.*, 66:381, 1994.

Conclusions

Summary

In the present work it has been studied quantum transport in mesoscopic systems, with special interest in the effect due to Rashba spin-orbit interaction. In particular two main aspects related to the Rashba effect have been considered. The first one takes account of the main problems of the spintronics: the realization of an electronic device based on the spin properties of the carriers. The second one is related to the property of Rashba effect to be viewed as an effective magnetic field and, consequently, it is interesting to study the interference phenomena stemming from this.

On the way for a proposal of an electronic device based on the spin properties of the carriers, it has been studied the phenomenon of the spin-double refraction. This occurs in two-dimensional electron gas when carriers impinge upon an interface separating the gas in two part. In the first half there is a free electron gas, in the second half the carriers are subjected to the Rashba effect. This spin-orbit interaction lifts the spin degeneracy and transforms the Fermi contour from one to two concentric circles. This effect is crucial to have spin-double refraction. In fact when the carrier impinge upon the interface from the free side, the momentum parallel to the interface has to be conserved, therefore in the Rashba effect side the carrier emerges as a superposition of two wave functions with different momentum and propagation direction. The behavior of carrier spin in such scattering events is analogous to the polarization of the light in a biaxial crystal: the incident ray splits, within the crystal, in two rays (ordinary and extraordinary) whose polarizations are orthogonal. As in the optic, the two components have limit angle of propagation over they become vanishing waves. This phenomenon gives rise to transmission probabilities different for injection with spin up or spin down carriers. Furthermore, it has been shown that in the case of normal incidence the transmission coefficients go to the same spin dependence as expected from literature. The results for the scattering of a carrier in a pure spin state has been used to investigate the transmission of an unpolarized statistical mixture of spin up and spin down. It has been shown that in this situation, with an injection out of normal incidence, it is observed a spin polarization. Furthermore, it has been studied the effect of an injection through all the allowable angles. It has been shown as, also in this situation,

a partial spin polarization is observed for injection of carriers both in pure spin state and in unpolarized state.

The property of the spin-double refraction has been used for a proposal of spin-field effect transistor. This is realized in a two-dimensional electron gas where a central region with the Rashba spin-orbit interaction divides the gas in three zone. The external one are the source and the drain. The new feature of this device is that it works with unpolarized electrons, therefore source and drain can be n^+-semiconductors. It has been shown how the presence of the two interfaces gives rice to the halving of the transmission of the system and this a clear signature of the spin-double refraction phenomenon. Moreover it has been shown how the system allows both a oscillating current modulation and the polarization of spin-unpolarized injected carriers. Furthermore, it has been studied the effect of the thermal average on the output current and polarization and it has been shown that the effect survive also in the limit of finite temperature. It is important to stress that this proposal is different from the original one of Datta and Das in which the current modulation stems out from the precession within the region with Rashba effect. Instead it has been proposed to use the spin rotation that appears when an carrier beam goes through the interfaces with a incident angle out of the normal. Such angle could be realized by using an adiabatic quantum point contact as source in which the constriction axis forms the previous angle with the interface.

The second part of the thesis has been motivated by several articles in literature where it is shown that in bipartite two-dimensional structures containing nodes with different connectivity, for example the $\mathcal{T}_3$ lattice, it is possible to obtain a electron localization due to the interplay between an external magnetic field and the geometry of the lattice. As in the Aharonov-Bohm effect the magnetic field plays the role of phase generator for the electron wave function. In the thesis it has been proposed to use the Rashba effect as phase generator, and to observe the interplay between the Aharonov-Casher effect, due the Rashba effect, and the geometry of the lattice. It has been studied the simplest form of bipartite lattice containing nodes with different connectivity. This is a particular quantum network extending in only one-dimension, that is a chain of square loops connected at one vertex. It has been presented a phenomenon of localization induced by the Rashba effect in this chain. The analysis has been carried out studying both the spectral and the linear transport properties. In the former case it has been observed that for critical values of the Rashba spin-orbit interaction the spectrum of an infinite chain is reduced to non-dispersive bands. In the latter it has been considered finite chain attached to semi-infinite leads and for the same critical values it has been observed that the conductance of the system is

suppressed. Furthermore is has been shown that this localization effect is robust with respect to the disorder, where disorder is generated as random fluctuations of the wire length. In the case of a linear chain without bipartite structure, it has been observed in the disordered linear transport properties a phenomenon similar to the Aronov-Altshuler-Spivak effect but induced by the Rashba effect. The phase generated by the Rashba effect is related to an $SU(2)$ group, as consequence it has been shown that the localization is not achieved in all the bipartite structure but only in structures fulfilling particular geometrical conditions. As consequence, it has been observed the in the case of the $\mathcal{T}_3$ lattice, localization is not achieved with the Rashba effect. Finally, it has been studied several two-dimensional structures in presence of Rashba effect and magnetic field and it has been shown that in particular case, the interplay between Rashba effect and magnetic field, can completely destroy the localization effect.

Future perspectives

In the case of the proposal for a spin-field effect transistor it has been considered the effect of the Rashba spin-orbit interaction. The semiconductor heterostructures that present the bigger values of the Rashba effect are realized in InAs/AlGaAs. It has been shown that in this heterostructures also the Dresselhaus effect plays a relevant role and its strength can reach one halt of Rashba strength. Therefore it is important to take into account the effect of anisotropy in the Fermi contour induced by the Dresselhaus effect. Preliminary results show that in the case of the normal incidence on single interface, with the Rashba effect in one side and the Dresselhaus effect everywhere, gives different transmissions for the two orthogonal incident spin states. Therefore the inclusion of the Dresselhaus effect should even enhance the polarization effects that it has been found with the only Rashba effect.

Quantum networks are simplified version of the real world. It this optic they have been used the study the chaos problem. In fact, it has been shown in literature, the transition the a chaotic distribution of the eigenvalues induced by a magnetic field in a small quantum network. This kind of transition due to a unitary transformation is well know in literature. Now the research is oriented to study the possible transition to a chaotic behavior due to a symplettic transformation. Preliminary results show that the Rashba effect can induce this kind of chaotic transition in a quantum network.

Acknowledgments

I wish to thank my supervisors Prof. Vittorio Cataudella and Prof. Vincenzo Marigliano Ramaglia for their trust and support during these years. I am indebted with Prof. Arturo Tagliacozzo for his advice in improving this work. I wish to thank also the other members of the group Dr. G. De Filippis and Dr. C.A. Perroni.

I have benefited of useful discussions and friendly collaborations with the other members of the *aula dottorandi* of the Dipartimento di Fisica, in particular, with Dr. Procolo Lucignano, Dr. Carlo Manzo, Dr. Claudio Cacciapuoti and Dr. Alessandro Zampini.

I am specially indebted with Dr. Michele Governale and Prof. *Saro* Fazio, which provided me their support during the period I spent as guest student at the Scuola Normale Superiore of Pisa.

Furthermore, I wish to thank *all* my parents for their patience and Dr. Diego Frustaglia for the fruitful discussions about physics and *life*. Finally I wish to tank two *special* person, the first one is Guido because he is for me a model of generosity, and the second one is Alessandra for her presence in my life.